Investigating the Impact of 5′-Methylthioadenosine Accumulation in *Arabidopsis thaliana*

by

Benjamin Jean-Marie Tremblay

A thesis
presented to the University of Waterloo
in fulfillment of the
thesis requirement for the degree of
Master of Science
in
Biology

Waterloo, Ontario, Canada, 2019

Author's Declaration

I hereby declare that I am the sole author of this thesis. This is a true copy of the thesis, including any required final revisions, as accepted by my examiners.

I understand that my thesis may be made electronically available to the public.

Abstract

Some reactions which use the activated form of methionine (Met), *S*-adenosylmethionine (SAM), as a substrate produce the by-product methylthioadenosine (MTA). In the plant *Arabidopsis thaliana* (Arabidopsis), these reactions include the biosynthesis of nicotianamine (NA), 1-aminocyclopropane-1-carboxylic acid (ACC; the precursor to ethylene), spermidine (Spd), spermine (Spm), and thermospermine (Tspm). MTA is recycled back to Met in the Met salvage cycle. MTA is converted to methylthioribose (MTR) by MTA nucleosidase (MTN) which is encoded for by two genes, *MTN1* (AT4G38800) and *MTN2* (AT4G34840). The Met salvage cycle is not essential for Arabidopsis grown in sulfur-sufficient conditions. Despite this, the accumulation of MTA is very toxic. The double mutant *mtn1-1mtn2-1* (which has 14.9% residual MTN activity) has a severe pleiotropic phenotype including altered vasculature, delayed bolting, fasciation, interveinal chlorosis, and both male and female sterility. Amazingly, fertility can be restored to *mtn1-1mtn2-1* plants transgenerationally by feeding Spd for two weeks at the seedling stage. This restored fertility is sparse in the first generation, and increases over subsequent generations.

An understanding of the underlying physiological impacts of MTA accumulation and Spd restoration was sought by studying the metabolite profile and transcriptome of unopened buds from wild-type (WT), *mtn1-1mtn2-1* and a later generation of Spd-restored *mtn1-1mtn2-1* (generation 3, or G3). The *mtn1-1mtn2-1* mutant accumulates over ten-times WT levels of MTA in unopened buds, making this an ideal system for the study of the impacts of MTA accumulation. These findings confirmed previous research suggesting that NA biosynthesis is very sensitive to feedback inhibition by MTA. It was also revealed that MTA accumulation in *mtn1-1mtn2-1* unopened buds is accompanied with reduced sulfur assimilation through cysteine (Cys), which results in decreased Met and SAM. Furthermore,

these observations hint at changes in the epigenome of *mtn1-1mtn2-1* plants, which may be partially reversed in G3.

Single mutant *mtn1-1* grow a short root when exposed to high concentrations of MTA exogenously. This phenotype was exploited to perform a suppressor screen and several putative *mtar* (*MTA RESISTANT*) mutants were discovered. A mapping-by-sequencing approach suggests the suppressor mutant *mtar2* has a non-synonymous amino acid substitution in Nitrile Specifier Protein 1 (NSP1; AT3G16400). NSP1 drives the formation of the auxin pre-cursor indole-3-acetonitrile from indole glucosinolates (GLS). This finding implicates reduced auxin biosynthesis as a the key factor in suppressing the short root phenotype of *mtn1-1* seedlings fed high concentrations of exogenous MTA.

The results presented in this thesis come together to build a model which attempts to explain the effects of MTA accumulation. In this model, MTA diverts sulfur assimilation away from Cys and Met towards GLS biosynthesis, and excess GLS leads to increased auxin biosynthesis.

Acknowledgements

I would like to thank first and foremost Dr. Barbara Moffatt for not only taking a gamble and having me as a student, but her continued support throughout the entirety of my time with her. She was always willing to consider new ideas, help out with experiments, discuss troubleshooting difficult experiments, encouraging me to attend conferences, and helping edit this thesis among other things.

Next I would like to thank my committee members. Thank you to Dr. Simon Chuong for always being willing to teach me new techniques, use the equipment in his lab, and help interpret my results. Thank you to Dr. Susan Lolle for letting me use some of her lab equipment and reagents without question during times of need, as well as for the interesting discussions regarding the project. Finally, thank you to Dr. Andrew Doxey for providing many valuable insights to my various bioinformatics projects and always being supportive during the writing of my R package.

I am also grateful to Prof. Dr. Rüdiger Hell from Heidelberg University for allowing me to spend a summer in his lab. I was able to freely use his equipment, and as a result a large portion of the data presented in this thesis was obtained in his lab. I would especially like to thank Dr. Markus Wirtz, who taught me how to use the various HPLC machines and discuss results. He tried hard to make sure I got along with everyone in the lab and that I always had everything I needed. He was always fun to talk to, and contributed greatly to making my overall experience in Germany an enjoyable one. I would also like to thank Dr. Yihan Dong, a post-doc in the Hell lab, who was willing to discuss the project with me over lunch and helped with several experiments.

I would like to thank as well my fellow lab members Maye Saechao, Nimhani Perera, and Cherry Chen. These three were key to my getting first getting used to the lab, and

were always willing to help out and give advice whenever I asked. They were always fun to be around with and talk with. I would also like to thank the previous greenhouse technician Lynn Hoyles, who was always willing to help me with my experiments and teach me how to grow healthier plants.

There are also several other students who spent time in the Moffatt lab as undergrads that I would like to thank. First is John McIntosh Steele, who spent a number of terms helping out in the lab. He was key in performing the MTA root lengths experiment, and contributed greatly to the suppressor screen experiments in Chapter 3. He also tirelessly worked to troubleshoot when the MTA-related experiments stopped working, which I am especially grateful for. Next is Nilanth Yogadasan, who previously volunteered in the lab for a term. He, alongside Dr. Moffatt, worked hard to collect and send me a large number of tissue samples while I was in Germany. Much of the data I collected in Germany was only possible due to their efforts. He also continued working on the suppressor screen alongside John once I left for Germany, finding several new suppressor mutants – two of which we are still actively pursuing today.

In addition to John and Nilanth, there were many undergrads who helped with genotyping and helping to take care of my plants that I am thankful to. They are, in no particular order: Raymond Wei, Fanxi Dong, Connie Tsui, Annika Traa, Matthew Lourenco, Delaney Nash, Kimberly Town, Tariro Munyikwa, Kyle Symonds, Jasmin Zhang, Samuel Salamun and Tanisha Mehta.

Finally, I would like to thank my family for their unconditional support. They never once showed me any doubt concerning my ability to complete my degree, and always supported me in everything I did. I am especially grateful for how they helped me organize my trips to and from Europe during my degree. In addition, my father's help made my stay in Germany much less painful then it could have been. I will always be grateful for

everything they have done and are still doing for me. I am also thankful for the support and understanding shown by my girlfriend Ellen during busy times.

Unfortunately I have a rather poor memory and I am certain there were a number of omissions. So, I would to end by thanking people who helped me and went unmentioned, I will always be grateful to anyone kind enough to lend me a helping hand.

Table of Contents

List of Tables

List of Figures

Abbreviations

4-m I3G 4-methoxy-indol-3-ylmethylglucosinolate.

AA Amino Acid.

ACC 1-aminocyclopropane-1-carboxylic acid.

ACL5 ACAULIS 5 (EC 2.5.1.79).

ACO 1-aminocyclopropane-1-carboxylic acid oxidase (EC 1.14.17.4).

ACS 1-aminocyclopropane-1-carboxylic acid synthase (EC 4.4.1.14).

APS adenosine 5′-phosphosulfate.

ARD acidoreductone dioxygenase.

BP Biological Process.

CBL cystathionine β-lyase (EC 4.4.1.8).

CBL3 Calcineurin B-like 3.

CBS cystathionine β-synthase (EC 4.2.1.22).

CDKN2A Cyclin Dependent Kinase Inhibitor 2A.

CDKN2B Cyclin Dependent Kinase Inhibitor 2B.

CGS cystathionine γ-lyase (EC 4.4.1.1).

Chr Chromosome.

Cys cysteine.

CysGly cysteinyl-glycine.

dcSAM decarboxylated SAM.

eIF5A eukaryotic Initiation Factor 5A.

EMS ethyl-methanesulfonate.

FE Fold Enrichment.

gEC γ-glutamylcysteine.

GLS glucosinolates.

GO Gene Ontology.

GSH glutathione.

Hcy homocysteine.

Het Heterozygous.

Homo Homozygous.

HPLC high-performance liquid chromatography.

I3C indole-3-carbinol.

IAN indole-3-acetonitrile.

ITC isothiocyanate.

Mbb monobromobimane.

Met Methionine.

METS methionine synthase (EC 2.1.1.13).

MTA 5′-methylthioadenosine.

MTAP 5′-methylthioadenosine phosphorylase (EC 2.4.2.28).

MTAR METHYLTHIOADENOSINE RESISTANT.

MTN 5′-methylthioadenosine nucleosidase (EC 3.2.2.16).

MTN1 *METHYLTHIOADENOSINE NUCLEOSIDASE 1*.

MTN2 *METHYLTHIOADENOSINE NUCLEOSIDASE 2*.

MTR methylthioribose.

NA nicotianamine.

NAS nicotianamine synthase (EC 2.5.1.43).

$\mathbf{NO_3^-}$ nitrate.

PA polyamine.

PAPS 3′-phosphoadenylyl sulfate.

PCA principle component analysis.

PI propidium idodide.

PO_4^{3-} phosphate.

PRMT5 PROTEIN ARGININE METHYLTRANSFERASE 5 (EC 2.1.1.3202).

Put Putrescine.

RdDM RNA-directed DNA Methylation.

ROS reactive oxygen species.

RT room temperature.

SAH *S*-adenosylhomocysteine.

SAHH SAH hydrolase (EC 3.3.1.1).

SAM *S*-adenosylmethionine.

SAMDC SAM decarboxylase (EC 4.1.1.50).

SAMS SAM synthetase (EC 2.5.1.6).

SNP Single Nucleotide Polymorphism.

SO_4^{2-} sulfate.

sORF small Open Reading Frame.

Spd Spermidine.

SPDS Spd synthase (EC 2.5.1.16).

Spm Spermine.

SPMS Spm synthase (EC 2.5.1.22).

THF tetrahydrofolate.

Tspm thermospermine.

WGS Whole Genome Sequencing.

WT wild type.

Chapter 1

Introduction

1.1 Universal methionine metabolism

1.1.1 The SAM cycle

Methionine (Met) is a universally essential sulfur-containing proteinogenic amino acid which may also play roles as an anti-oxidant and in gene regulation (Tesseraud et al., 2009). The active form *S*-adenosylmethionine (SAM) of Met is produced after the addition of ATP via SAM synthetase activity (SAMS; EC 2.5.1.6; as part of the SAM cycle; Figure 1.1). SAM is used as a methyl donor in SAM-dependent methyltransferase (EC 2.1.1) reactions including that of proteins, DNA, and lipids (Bhagavan and Ha, 2015). The by-product of these methylation reactions is *S*-adenosylhomocysteine (SAH), which is hydrated by SAH hydrolase (SAHH; EC 3.3.1.1) to form adenosine and homocysteine (Hcy). Finally, Hcy can regain a methyl group from methionine synthase (METS; EC 2.1.1.13) using methylated tetrahydrofolate (THF) as donor to finally regenerate Met.

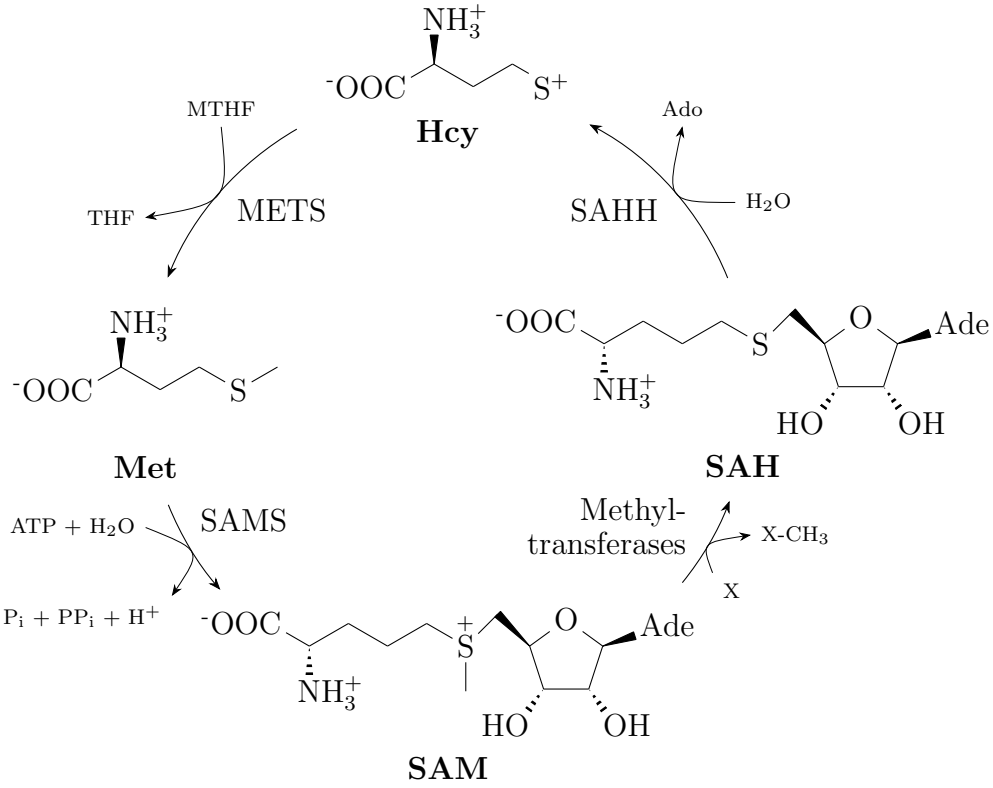

Figure 1.1: The SAM cycle.

The SAM cycle describes the formation of SAM from Met and ATP by SAMS, which is used as a methyl donor by various methyltransferases. The by-product of these reactions, SAH, is regenerated back to Met by the formation of Hcy by SAHH, and finally Met is formed using a methylated THF as methyl donor by METS. *Ade, adenine; Ado, adenosine; Hcy, homocysteine; Met, methionine; METS, methionine synthase; MTHF, methyltetrahydrofolate; SAH, S-adenosylhomocysteine; SAHH, SAH hydrolase; SAM, S-adenosylmethionine; SAMS, SAM synthetase; THF, tetrahydrofolate.*

From this point, one of the major differences between organisms is the trans-sulfuration pathway; the interconversion of Hcy and cysteine (Cys), another sulfur-containing proteinogenic amino acid. In animals, this can only occur in the forward direction, or towards Cys, by first forming cystathionine from Hcy and serine via cystathionine β-synthase (CBS; EC 4.2.1.22), and finally to Cys via cystathionine γ-lyase (CGS; EC 4.4.1.1) (Finkelstein and Martin, 2000). In microorganisms and plants, the reverse direction is also possible via cystathionine β-lyase (CBL; EC 4.4.1.8), allowing for *de novo* Met biosynthesis (Ferla and Patrick, 2014; Ravanel et al., 1998). The lack of this enzyme in non-plant higher eukaryotes makes Met a dietary necessity (Womack and Rose, 1941). Met contains a sulfur atom, and as such, under sulfur limiting conditions salvage can be critical even to those capable of *de novo* Met biosynthesis (Sekowska et al., 2000a; Thomas and Surdin-Kerjan, 1997).

1.1.2 The methionine salvage cycle

As described previously, SAM is used as a methyl donor in methyltransferase reactions. Additionally, SAM is also used in a subset of reactions which, instead of SAH, produce 5′-methylthioadenosine (MTA) as a by-product. One of these reactions, nearly ubiquitous in all organisms, is the biosynthesis of polyamines (PAs). PAs are compounds which have critical roles in cell growth (Pegg and McCann, 1982). SAM is first decarboxylated by SAM decarboxylase (SAMDC; EC 4.1.1.50) before it is used by PA synthases as a substrate. Decarboxylation also prevents the SAM molecule from becoming a methyl donor in SAM-dependent methyltranferase reactions, provide a pool SAM which can only be used by PA synthases (Pegg et al., 1998). Spermidine (Spd) and Spermine (Spm) are the two most common PAs which generate MTA as a byproduct, catalyzed by Spd synthase (SPDS; EC 2.5.1.16) and catalyzed by Spm synthase (SPMS; EC 2.5.1.22) respectively.

There are a series of reactions in the Met salvage cycle before Met can be regenerated. The individual elements of this pathway vary greatly among organism: some first act upon MTA using a MTA phosphorylase (MTAP; EC 2.4.2.28), whilst others use a MTA nucleosidase (MTN; EC 3.2.2.16) instead (Albers, 2009). The enzymes further in the pathway have also gained additional functions in certain organisms; for example in humans, acireductone dioxygenase (ADI1) has been linked with mRNA processing (Gotoh et al., 2007), apoptosis, and cell growth (Oram et al., 2007). The Met salvage cycle may also be an important source of oxygen radical scavenging (Sekowska et al., 2000b) via the incorporation of oxygen by acidoreductone dioxygenase (ARD).

1.1.3 PAs: ubiquitous and essential compounds

PAs are nearly ubiquitous compounds essential for cellular proliferation. The most common amongst them are Putrescine (Put), Spd, and Spm (Miller-Fleming et al., 2015; Pegg, 2009). One of their most significant involvements in cellular physiology is in regulating gene expression. They work at the transcriptional level by directly associating with DNA to alter its conformation, associating with chromatin-remodeling enzymes (Childs et al., 2003), and binding to RNA to regulate mRNA elongation (Pegg, 2009; Yoshida et al., 2002). They also work at the translational level by association with ribosomes to influence tRNA binding (Igarashi and Kashiwagi, 2006; Terui et al., 2007; Yoshida et al., 1999), translation of the inefficient initiation codons UUG and GUG (Igarashi and Kashiwagi, 2006, 2010; Yoshida et al., 2001), and translation efficiency of transcripts with $5'$ UTR regions which normally impeded translation (Yueh and Schneider, 1996).

With such a central involvement in gene expression regulation, it is no surprise that PA depletion leads to severe, and at times complete, decrease in cellular proliferation in

both prokaryotes and eukaryotes (Cunningham-Rundles and Maas, 1975; Odenlund et al., 2009; Ray et al., 1999; Xie et al., 1993). PAs have been found to be required for non-gene expression related process; for example, PA-depleted mammalian and yeast cells are more vulnerable to oxidative stress. Previous studies suggest that PAs have a direct role in reactive oxygen species (ROS) scavenging to protect DNA, membranes, and proteins from oxidative damage in a mechanism independent of glutathione (GSH), the most significant ROS scavenger Das and Misra, 2004; Fujisawa and Kadoma, 2005; Ha et al., 1998; Rider et al., 2007; Sava et al., 2006. PAs are also needed to regulate metabolite movement across membranes, where they directly affect the activities of enzymes which transport ions during osmotic (Groppa, 2008) and pH related stresses (Samartzidou et al., 2003; Watson et al., 1992).

Of the PAs, Spd is also required for the hypusination of eukaryotic Initiation Factor 5A (eIF5A), a protein which is also essential for cellular proliferation (Park et al., 1997). Though eIF5A was first identified and named as a translation initiation factor (Benne and Hershey, 1978; Kemper et al., 1976; Schreier et al., 1977), this characterization has been found to be incorrect as it is in fact an elongation factor (Gregio et al., 2009; Henderson and Hershey, 2011; Saini et al., 2009). Yeast cells lacking eIF5A show global ribosome stalling at certain amino acid motifs such as proline stretches, at stop codons and at the $3'$ UTR of mRNA, suggesting that eIF5A plays an essential role in translation elongation and termination (Schuller et al., 2017).

1.2 MTA and MTAP in mammalian systems

1.2.1 Deletion of the MTAP gene in cancers

In humans, approximately 15% of cancers arise as a result from deletions in chromosome 9p21, a region which contains the tumour suppressor genes Cyclin Dependent Kinase Inhibitor 2A (CDKN2A) and Cyclin Dependent Kinase Inhibitor 2B (CDKN2B) (Beroukhim et al., 2010; Schmid et al., 2000). Also in this region is the gene encoding MTAP, which in 80%–90% of these cancers is found to be co-deleted (Schmid et al., 2000; Zhang et al., 1996). Since humans are incapable of *de novo* Met biosynthesis, MTAP is needed to regenerate the Met used for PA biosynthesis. As a potential therapeutic target, the effects of MTAP deletion and the subsequent MTA accumulation have been avidly studied in mammalian model systems.

1.2.2 Determining the effects of MTA accumulation

Mammalian cells with functional MTAP normally accumulate MTA in the sub-micromolar levels (Pegg et al., 1981; Seidenfeld et al., 1980). Negative effects on cellular proliferation are quickly seen when exposed to higher concentrations. Mouse cell lines show a significant decrease in cellular proliferation at 25 µM, and near complete inhibition at 100 µM (Pegg et al., 1981). Human cell lines show a 50% decrease when exposed to 200 µM MTA (Tisdale, 1983). In order for this negative effect to be exploited in MTAP-depleted cells, a great effort has been undertaken to understand the basis for this growth inhibition.

The first of these causes appears to be as a result of feed-back inhibition by MTA on MTA-producing processes. In the case of mammalian systems the documented targets are

Spd and Spm biosynthesis (Chattopadhyay et al., 2005; Hibasami et al., 1980; Kubota et al., 1985; Raina et al., 1984). Nearly complete inhibition of SPDS and SPMS activity can be achieved in human cells exposed to 100 µM MTA. As reviewed earlier, PAs are indispensable to many cellular processes, and as such Spm and Spd (and by extension eIF5A) depletion likely contribute to the reduction in cellular proliferation in the presence of excess MTA. That being said, simply providing these PAs exogenously to cells exposed to MTA does not completely restore regular cellular function, suggesting other factors are also involved (Pegg et al., 1981).

The second possible cause of the negative effects of MTA accumulation on cellular proliferation is the inhibitory effects of MTA on protein methyltransferases. This was first noted as increased MTA levels correlate with a global reduction in asymmetric protein methylation (Blanchet et al., 2005; Henrich et al., 2016; Zappia et al., 1969). More recently, this has been specifically linked to the direct physical inhibition of protein arginine methyltransferase 5 (PRMT5; EC 2.1.1.3202) activity by MTA (Kryukov et al., 2016; Marjon et al., 2016; Mavrakis et al., 2016). Human PRMT5 knockdown cell lines show a decrease in cellular proliferation when exposed to 25 µM MTA (Mavrakis et al., 2016). PRMT5 has been associated with a host of vital cellular functions such as histone methylation, cell cycle, cell growth, translation, and other regulatory pathways (Andreu-Pérez et al., 2011; Chung et al., 2013; Friesen et al., 2001; Hsu et al., 2011; Ren et al., 2010). With the importance of PRMT5 in cell proliferation, reduced PRMT5 activity likely contributes significantly to the reduced cell proliferation effect caused by excess MTA.

1.3 Plant-specific methionine metabolism

1.3.1 *De novo* methionine biosynthesis in plants

In plants, *de novo* Met biosynthesis is tightly linked with sulfur assimilation (Figure 1.2). Sulfur is first be transported into the plant in the form of sulfate, where it is initially converted to adenosine 5′-phosphosulfate (APS). From this point APS can either be converted to 3′-phosphoadenylyl sulfate (PAPS) and used by sulfotransferases (EC 2.8.2) in sulfuration reactions to be directly incorporated into metabolites, or after several more steps converted to Cys. From this point, Cys can be used to generate either GSH, an important regulator of cellular oxidation state, or cystathionine, where it can be used to generate the Met precursor Hcy in the transulfuration pathway. Though both forward and reverse transulfuration reactions are theoretically possible, evidence for the reverse reaction (towards the biosynthesis of Cys) is limited in comparison (Hildebrandt et al., 2015).

Sulfate taken into plant cells is stored in vacuoles and subsequently transported into chloroplasts for the pathways shown in Figure 1.2 to occur (Gigolashvili and Kopriva, 2014). SAM is also produced in chloroplasts, after which it is transported into the cytoplasm (Gigolashvili and Kopriva, 2014). Met and SAM regeneration (Figures 1.1, 1.5) then occur in the cytoplasm (Gigolashvili and Kopriva, 2014).

1.3.2 Methionine salvage in plants

There are various MTA-producing reactions which feed into the Met salvage cycle. These processes can be classified as SAM-utilizing (Figure 1.3) and decarboxylated SAM (dcSAM)-utilizing reactions (Figure 1.4). Of the former class are two MTA-generating enzymes:

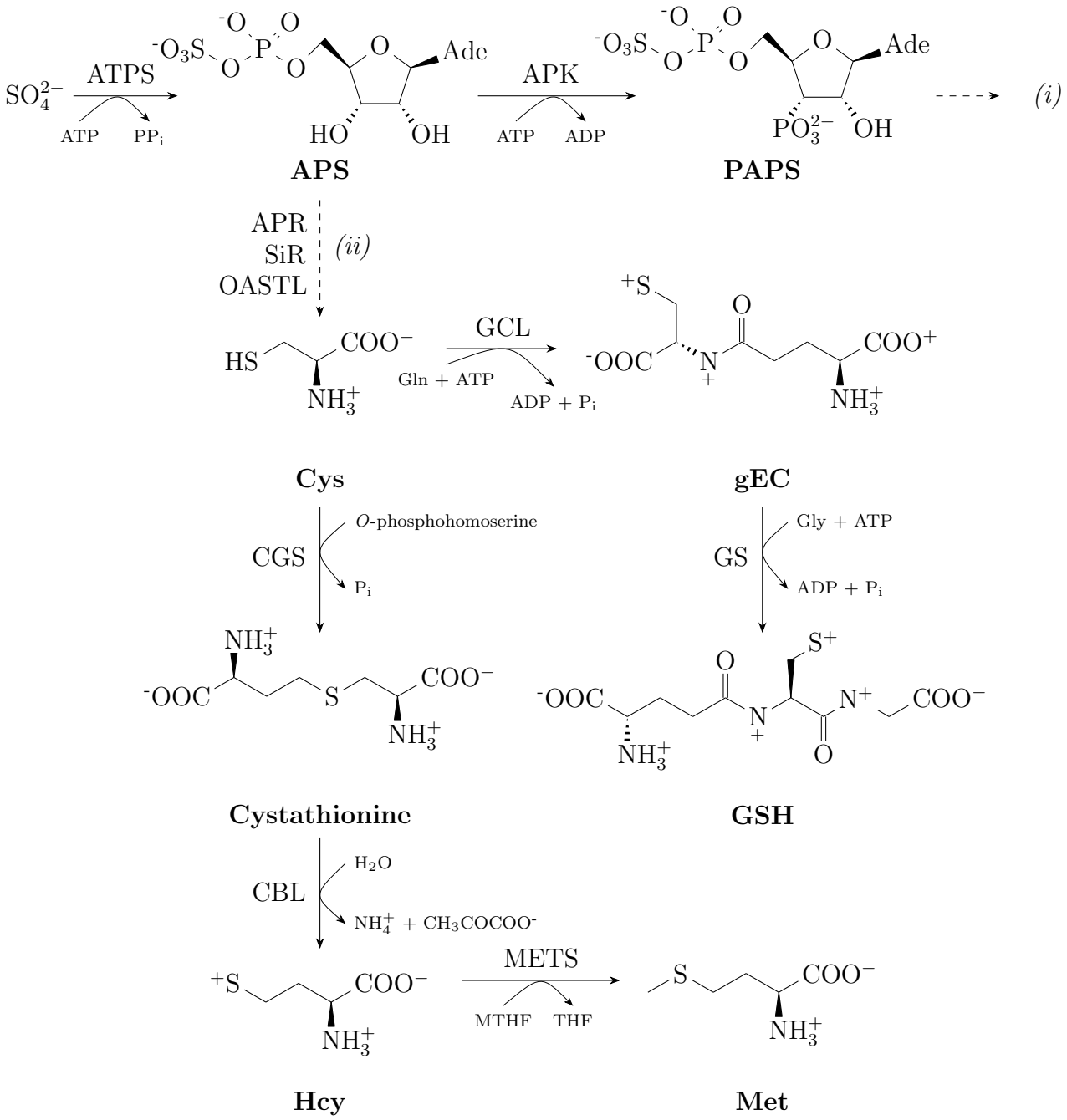

Figure 1.2: Plant sulfur assimilation and methionine biosynthesis.

Figure 1.2: Plant sulfur assimilation and methionine biosynthesis. (Cont)

Sulfur first enters the plant as sulfate, where it is incorporated into APS. At this point it can be converted to PAPS for use by sulfotransferases *(i)*, or it can be used to generate Cys *(ii)*. Cys can be used for the biosynthesis of GSH or Met. *APS, adenylylsulfate. APK, APS kinase. APR, APS reductase. ATPS, ATP sulfurylase. CBL, cystathionine β-lyase. CGS, cystathionine γ-synthetase. Cys, cysteine. GCL, glutamate-cysteine ligase. gEC, γ-glutamylcysteine. Gly, glycine. GS, glutathione synthetase. GSH, glutathione. Hcy, homocysteine. Met, methionine. METS, Met synthase. MTHF, methyl-THF. OASTL, O-acetylserine thiolyase. PAPS, 3-phospho-5-adenylylsulfate. SiR, sulfite reductase. THF, tetrahydrofolate.*

(i) nicotianamine synthase (NAS; EC 2.5.1.43), producing nicotianamine (NA), and *(ii)* 1-aminocyclopropane-1-carboxylic acid synthase (ACS; EC 4.4.1.14), producing the ethylene precursor 1-aminocyclopropane-1-carboxylic acid (ACC). The MTA-generating enzymes which utilize dcSAM, produce PAs: *(i)* the Spd-producing SPDS, *(ii)* the Spm-producing SPMS, as discussed previously, as well as *(iii)* the thermospermine (Tspm)-producing ACAULIS 5 (ACL5; EC 2.5.1.79). In plants, these PAs play important roles related to moderating growth, reducing oxidative stresses, and promoting vascular development (Tiburcio et al., 2014).

The Met salvage cycle in plants (Figure 1.5) is also known as the Yang cycle (see Figure 1.6 for an illustration of how it connects with the SAM cycle and sulfur assimilation). When initially characterized as such, this cycle was believed to be vital for sustaining elevated rates of ethylene biosynthesis during fruit ripening in apple trees (Miyazaki and Yang, 1987). However, a requirement for high sustained ethylene biosynthesis is not present in all plants. For example in Arabidopsis some mutants which cannot complete Met regeneration still have wild type (WT) phenotypes when grown under sulfur-sufficient conditions (Bürstenbinder et al., 2007; Zierer et al., 2016).

With ethylene, NA and PAs all originating from SAM and dcSAM-utilizing reactions,

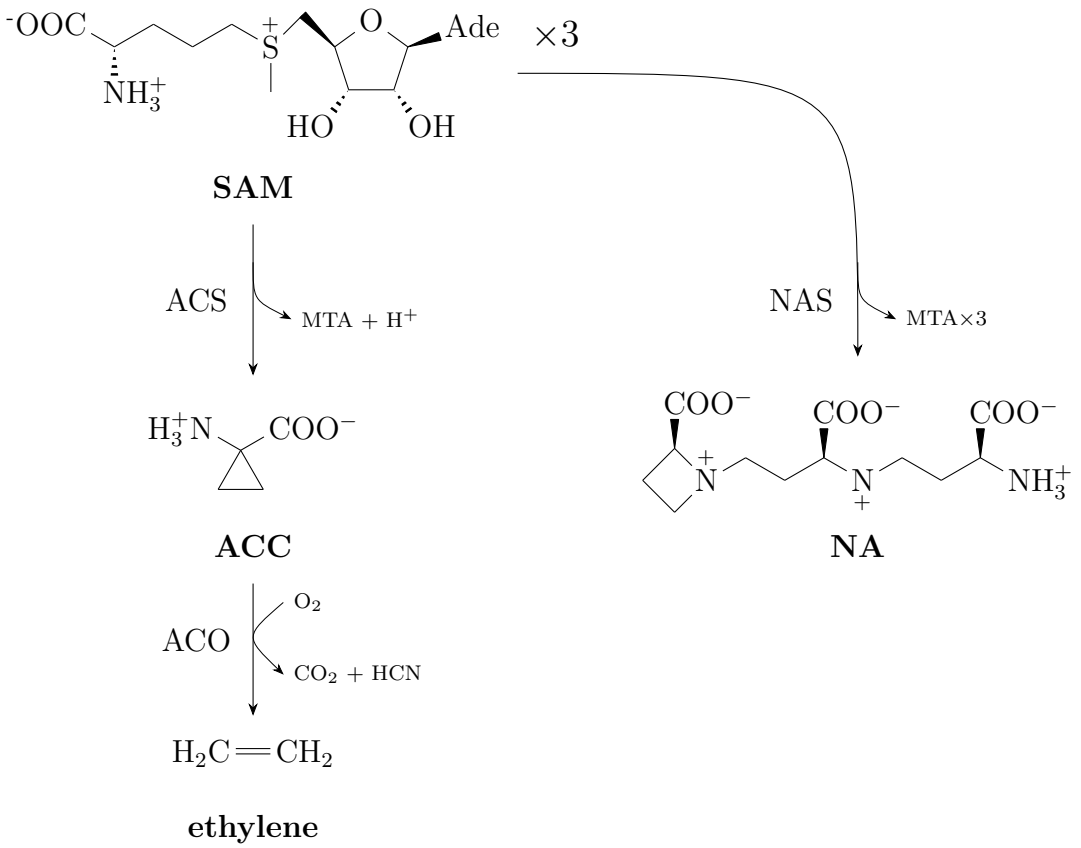

Figure 1.3: Ethylene and NA biosynthesis from SAM.

NAS uses three SAM molecules to form one molecule of the iron chelator NA, producing three MTA molecules as by-product. SAM is also used by ACS to form ACC and an MTA by-product, which is oxidized by ACO to form the gaseous phytohormone ethylene. *ACC, 1-aminocyclopropane-1-carboxylic acid; ACO, 1-aminocyclopropane-1-carboxylic acid oxidase; ACS, 1-aminocyclopropane-1-carboxylic acid synthase; NA, nicotianamine; NAS, nicotianamine synthase.*

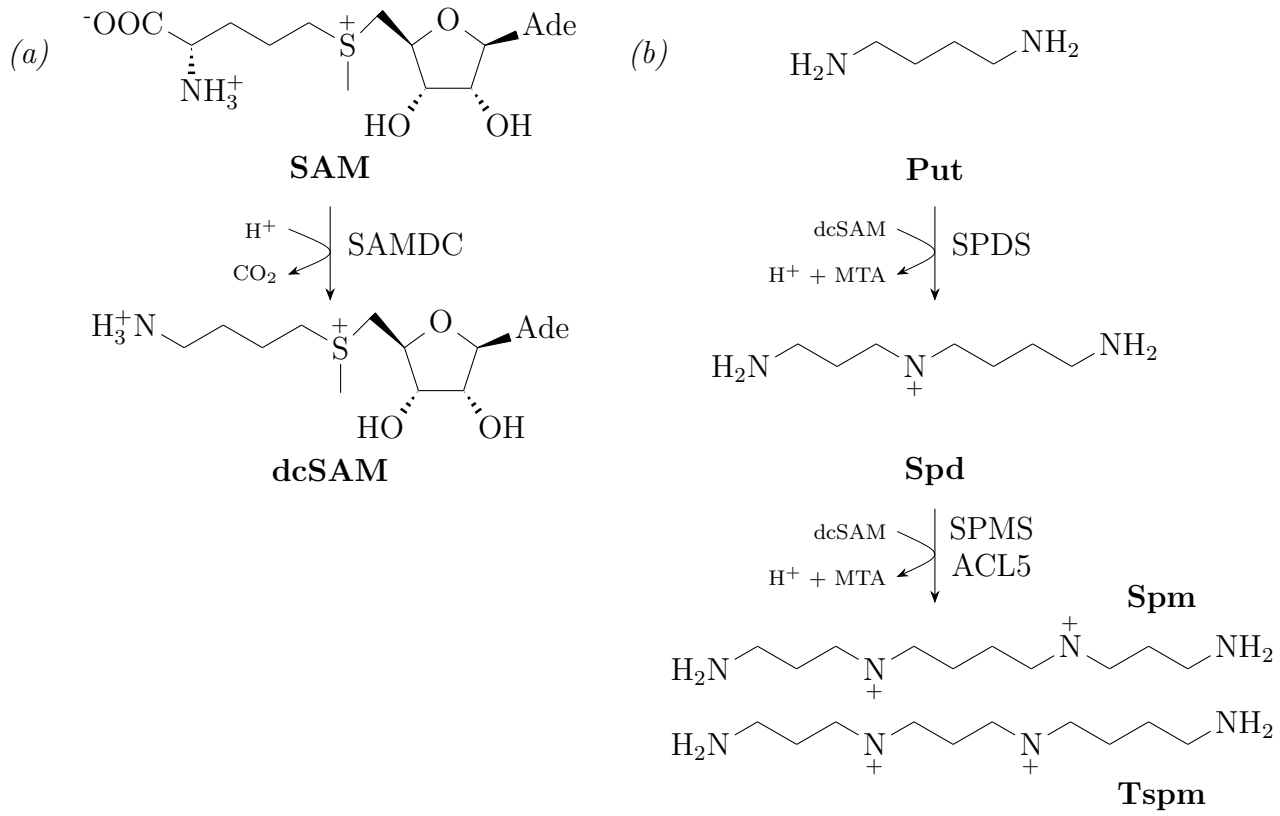

Figure 1.4: PA biosynthesis from dcSAM.

SAM is decarboxylated by SAMDC to form dcSAM *(a)*. This makes the transformed SAM molecule available to SPD, SPMS, and ACL5, to produce Spd, Spm, and Tspm (all generating MTA by-products) respectively *(b)*. Spd is generated from the addition of a methyl group from SAM to Put, whereas Spm and Tspm are created from the addition of that SAM methyl group to Spd. *ACL5, ACAULIS 5; dcSAM, decarboxylated S-adenosylmethionine; MTA, methylthioadenosine; Put, putrescine; SAM, S-adenosylmethionine; SAMDC, S-adenosylmethionine decarboxylase; Spd, spermidine; SPDS, spermidine synthase; Spm, spermine; SPMS, spermine synthase; Tspm, thermospermine.*

there is evidence of connecting biosynthetic regulation between these processes, as well as with the Met salvage itself; though this varies between plant species. In the latter case, it has been shown that the expression of some of the genes encoding enzymes in the Met salvage pathway in rice are induced by ethylene, whereas these same genes show no such response in Arabidopsis (Bürstenbinder et al., 2007). In some species, regulatory links between nicotianamine and ethylene biosynthesis have been found (Wu et al., 2011), as well as between ethylene and PA biosynthesis (Gil-Amado and Gomez-Jimenez, 2012; Icekson et al., 1986; Pandey et al., 2000; Sauter et al., 2013).

1.3.3 Plant ethylene, NA, and PAs

The product of ACS is catalyzed by the enzyme 1-aminocyclopropane-1-carboxylic oxidase (ACO; EC 1.14.17.4) to produce the plant hormone ethylene (Figure 1.3). This occurs in the cytosol and at the plasma membrane (de Poel and Straeten, 2014). Ethylene has important roles in plant growth, senescence and stress responses (Dubois et al., 2018). NA biosynthesis catalyzed by NAS (Figure 1.3), occurs in the cytosol and in plastids (Mizuno et al., 2003). NA is secreted from roots to chelate soil-bound iron, which allows it to be absorbed into the plant (Higuchi et al., 1999). In winter squash fruit ACS, and to a lesser extent ACO, have been found to be sensitive to feedback inhibition by MTA (Hyodo and Tanaka, 1986). While one molecule of MTA is produced for every molecule of ethylene, three molecules of MTA are produced for every molecule of NA produced by NAS. Similar to ACS, NAS in barley has also been shown to be sensitive to feedback inhibition by MTA (Herbik, 1997).

The biosynthesis of the PAs Spd, Spm and Tspm each generate one molecule of MTA (Figure 1.4). SPDS is localized predominately in the nucleus, and weakly in chloroplasts

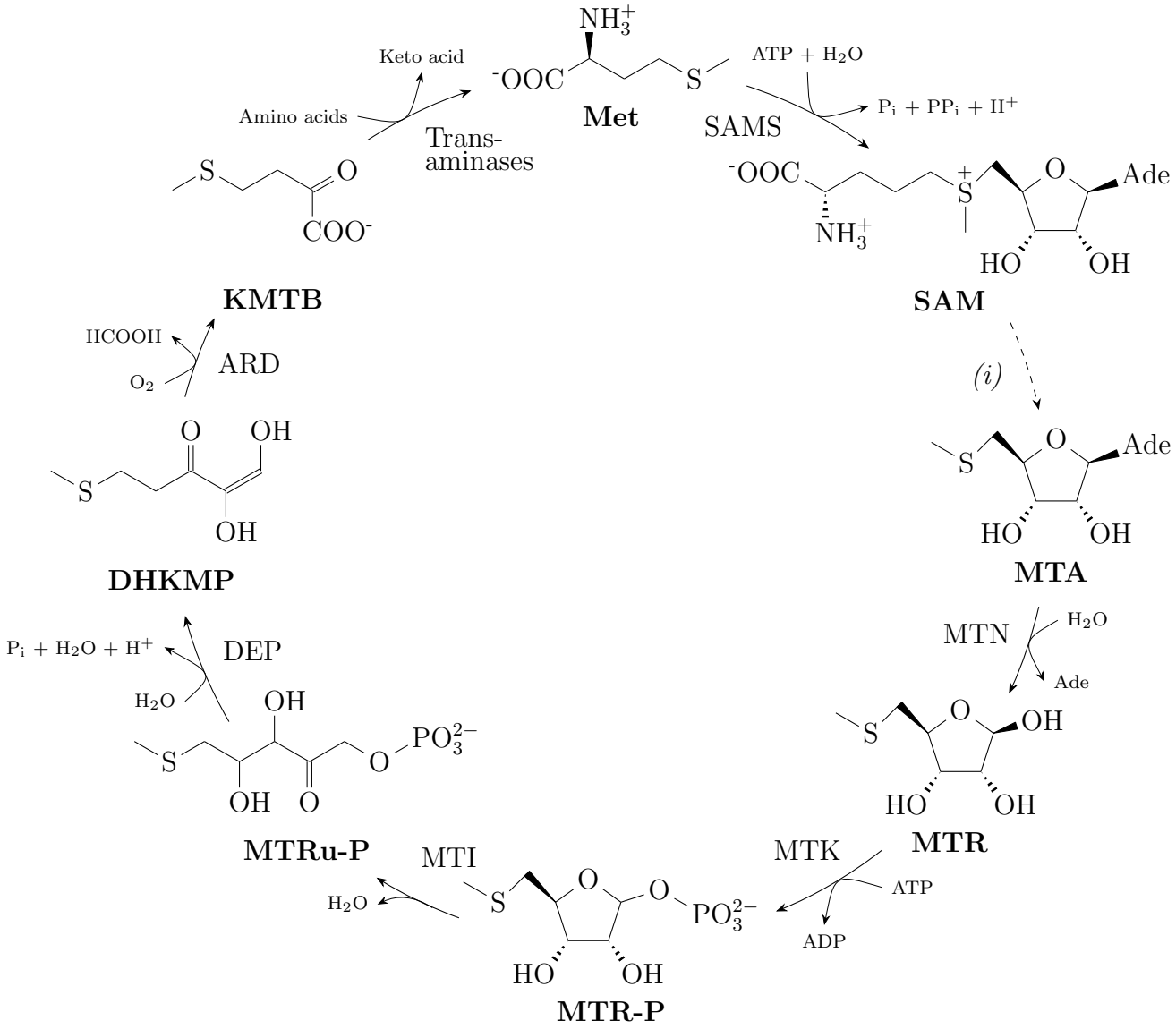

Figure 1.5: Plant methionine salvage reactions.

This series of reactions details the regeneration of Met from SAM-utilizing reactions *(i)* which produce MTA as a by-product instead of SAH. *Ade, adenine. ARD, acireductone dioxygenase. DEP, dehydratase-enolase-phosphatase. DHKMP, acireductone. KMTB, 2-keto-4-methylthiobutyrate. Met, methionine. MTA, methylthioadenosine. MTI, MTR-P isomerase. MTN, MTA nucleosidase. MTK, MTR kinase. MTR, methylthioribose. MTR-P, methylthioribose-1-phosphate. MTRu-P, methylthioribulose-1-phosphate. SAM, S-adenosylmethionine. SAMS, SAM synthetase.*

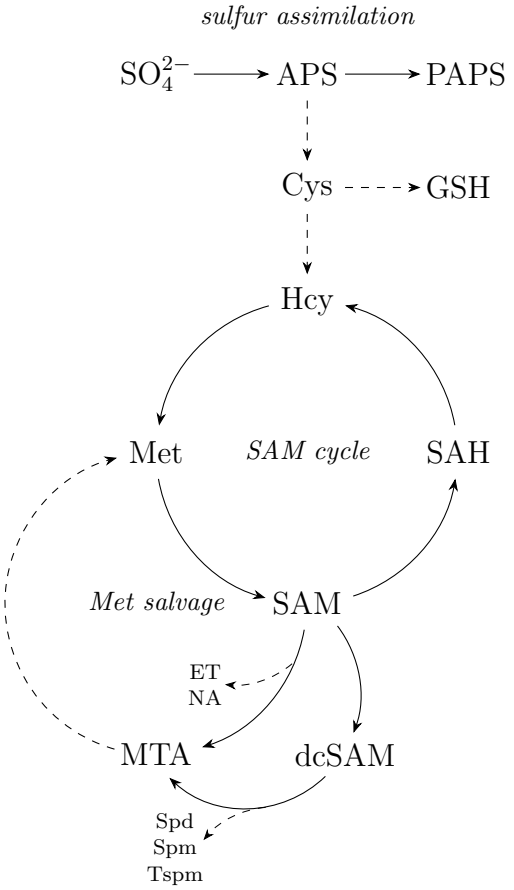

Figure 1.6: Overview of sulfur assimilation, the SAM cycle and Met salvage in Arabidopsis.

Simplified summary figure incorporating key sulfur assimilation steps (Figure 1.2), the SAM cycle (Figure 1.1), and Met salvage (Figure 1.5). Also shown are ethylene and NA biosynthesis from SAM (Figure 1.3), as well as polyamine biosynthesis from dcSAM (Figure 1.4). Dashed arrows indicate hidden steps. Note that the position of Met salvage within the overall pathway is prioritized, resulting in the production of ethylene, NA, Spd, Spm and Tspm to appear as by-products of MTA biosynthesis when in fact the inverse is true. *APS, adenylylsulfate. Cys, cysteine. dcSAM, decarboxylated S-adenosylmethionine. ET, ethylene. GSH, glutathione. Hcy, homocysteine. Met, methionine. NA, nicotianamine. MTA, methylthioadenosine. PAPS, 3-phospho-5-adenylylsulfate. SAH, S-adenosylhomocysteine. SAM, S-adenosylmethionine. Spd, spermidine. Spm, spermine. Tspm, thermospermine.*

(Belda-Palazón et al., 2012). SPMS is localized primarily in the cytosol (Belda-Palazón et al., 2012). The subcellular localization of ACL5 has yet to be described, but its presence in multiple cellular compartments including the cytosol, mitochondria, nucleus, peroxisome, and plasma membrane is predicted (retrieved from the Cell eFP Browser, November 15th, 2018; Winter et al., 2007). Of the three PAs only Spd is essential in plants, being the only PA where depletion leads to embryo arrest (Imai et al., 2004). Both Spm and Tspm on the other hand are not essential, as evidenced by the survival of double mutants lacking SPMS and ACL5 (Yamaguchi et al., 2006). Spm plays a role in some stress responses and Tspm has a vital role in the proper development of plant vasculature (Tiburcio et al., 2014). While there is *in silico* evidence for the physical interaction between SPDS and ACL5 with MTA, there is thus far no experimental work to support this (Waduwara-Jayabahu et al., 2012).

PAs are also conjugated to various PA derivatives by PA oxidases, of which there are five (*PAO1*, *PAO2*, *PAO3*, *PAO4*, and *PAO5*). These conjugates contribute significantly to the total PA pool within some organs in the plant (Imai et al., 2004). They are also believed to have various physiological functions including cell division, cell wall loosening, defence, flowering and sexual differentiation (Facchini et al., 2002; Tiburcio et al., 2014).

Spd is also used in the hypusination of plant eIF5A (Wang et al., 2001). Plants lacking eIF5A have severe developmental defects such as reduced organ size and number, defective sporogenesis, as as well abnormal cell division and growth (Feng et al., 2007). It has also been shown to negatively regulate cytokinin signalling by forming a protein complex with the cytokinin receptor cytokinin response1 (CRE1), which prevents defective protoxylem development in roots by an overabundance of cytokinin signalling (Ren et al., 2013).

1.3.4 Past characterization of plant MTN

In all cases where the kinetics of plant MTN have been measured, the results have been relatively similar. The MTN assay using extract from *Lupinus luteus* seeds was found to have a K_m of 0.41 µM for MTA (Guranowski et al., 1981); recombinant MTN from *Oryza sativa* L. to have a K_m of 2.1 µM (Rzewuski et al., 2007); and recombinant MTN from Arabidopsis to have a K_m of 7.1 µM and a K_m of 3.4 µM for the first and second isoforms (Siu et al., 2011). These enzymes however are not all similar in terms of their ability to hydrolyze SAH. While the MTN from *Lupinus luteus* and the first of the isoforms from Arabidopsis (MTN1) possess no detectable affinity to hydrolyze SAH (Guranowski et al., 1981; Siu et al., 2011), the MTN from *Oryza sativa* L. and the second isoform from Arabidopsis (MTN2) can hydrolyze SAH at 16% and 14% the rate of MTA (Rzewuski et al., 2007; Siu et al., 2011).

Furthermore, plant MTN has been shown to be associated with different regulatory processes. In *Robinia pseudoacacia* L. transcript levels were shown to increase in root cuttings exposed to indole-3-butyric acid (IBA), an assay to promote adventitious root formation (Quan et al., 2014). In *Oryza sativa* L., transcript levels and activity rates of MTN were shown to increase during submergence, a process which enhances ethylene production (Rzewuski et al., 2007). In Arabidopsis, MTN activity was shown to be induced in seedlings which were grown on media containing 500 µM MTA as a sulfur source and on sulfur-deficient media (Bürstenbinder et al., 2010).

MTN has phloem-specific expression in both *Plantago* and Arabidopsis, alongside other Yang cycle-related genes (Pommerrenig et al., 2011). In Arabidopsis *METHYLTHIOADENOSINE NUCLEOSIDASE 1 (MTN1)* is transcribed in all tissues, with the highest expression in flowers, followed by roots, leaves, and stems (Oh et al., 2008). Transcripts of

METHYLTHIOADENOSINE NUCLEOSIDASE 2 (*MTN2)* on the other hand have the highest abundance in pollen grains, with low levels of expression in all other tissues (Ok et al., 2015).

From *in vitro* assays of Arabidopsis, it was observed that MTN activity was sensitive to inhibition in a calcium-dependent manner by Calcineurin B-like 3 (CBL3), a calcium sensor which activates in response to calcium released during periods of stress, allowing for downstream signalling (Oh et al., 2008; Ok et al., 2015). It was shown that these proteins associate in a manner dependent on calcium *in vivo* (Oh et al., 2008; Ok et al., 2015). This association occurs mainly at the plasma membrane of plant cells (Oh et al., 2008; Ok et al., 2015). Currently there is no proposed physiological benefit for CBL3 inhibiting MTN activity during periods of stress. In fact, this finding contradicts a previous study which discussed that Arabidopsis plants can be made more susceptible to pathogen infection by inhibiting MTN activity, thus reducing production of ethylene and decreasing ethylene-induced stress response (Washington et al., 2016).

1.3.5 Arabidopsis MTN-deficient mutants

Arabidopsis has two isoforms of MTN, *MTN1* and *MTN2*. These are responsible for approximately 80% and 20%, respectively, of the overall MTN activity in unopened buds (Bürstenbinder et al., 2010). Under sulfur-suficient conditions, only a fraction of the total amount of MTN activity is required; this can be seen in the fact that both *mtn1-1* and *mtn2-1* single mutants exhibit WT phenotypes, seemingly unaffected by the loss in MTN activity (Bürstenbinder et al., 2010). However when seedlings of these mutants are exposed to 500 µM MTA as a sulfur source, changes in the phenotype can be seen (Bürstenbinder et al., 2010). This includes accumulation of SAM, dcSAM, Put, and Spm, as well as

decreased root and shoot tissue growth (Bürstenbinder et al., 2010). These changes are likely due to the mutants' inability to properly replenish the plants' supply of sulfur, resulting in severe growth rate reduction.

In the double mutant *mtn1-1mtn2-1* however, phenotypic changes become apparent even under sulfur-suficient conditions. This mutant is both male and female sterile, and shows a number of abnormal phenotypes such as delayed bolting, increased vasculature, and interveinal chlorosis (Waduwara-Jayabahu et al., 2012). Whereas the single mutants show no MTA accumulation under sulfur-suficient conditions, a large accumulation of MTA can be detected (Waduwara-Jayabahu et al., 2012) in the double mutant; this accumulation is instead likely the causal factor of the mutant phenotype. Since ACS and NAS are sensitive to feedback inhibition by MTA (Herbik, 1997; Hyodo and Tanaka, 1986), and plant SPDS and ACL5 have been shown *in silico* to be sensitive to feedback inhibition by MTA, it has been proposed that the mutant phenotype seen in the *mtn1-1mtn2-1* plant is likely due to the feedback inhibition of MTA-producing processes (Waduwara-Jayabahu et al., 2012).

The evidence for this is however not conclusive, as while NA levels decrease significantly no changes in Spd and Spm are seen (Waduwara-Jayabahu et al., 2012). Even when the single mutants are externally exposed to high levels of MTA no decrease in Spd and Spm are detected (Bürstenbinder et al., 2010). This suggests that while perhaps some of the MTA-producing enzymes undergoing feedback inhibition under high MTA *in vivo*, not all are (ethylene and Tspm have not been quantified in the *mtn1-1mtn2-1* mutant). While the interveinal chlorosis phenotype clearly supports the decrease in NA levels (Waduwara-Jayabahu et al., 2012), this leaves open possible explanations for the other detected abnormal phenotypes. While Arabidopsis also has its own PRMT5, at this point it is unknown if it has the same sensitivity to MTA as seen in the human PRMT5 (see above).

One interesting aspect of the *mtn1-1mtn2-1* phenotype lies in the male and female

sterility. It was discovered that this could be partially reversed by the application of 100 µM Spd in the media on which mutant seedlings germinate and grow for the first two weeks (Waduwara-Jayabahu et al., 2012). Furthermore, this fertility is maintained transgenerationally, suggesting an epigenetic mechanism to be at play, as the plant maintains its fertility despite the lack of MTN activity and even after any Spd is made available (exogenously) (Waduwara-Jayabahu et al., 2012). While most of the abnormal phenotypes are still present in the restored line, those related to chlorosis, flowering time, and vascular development show recovery towards WT (Waduwara-Jayabahu, 2011).

1.4 Arabidopsis as a model organism

This thesis focuses on the study of plant MTN. The plant of choice for this effort was Arabidopsis; not only are there available mutant lines which have been previously studied (Bürstenbinder et al., 2010; Waduwara-Jayabahu, 2011; Waduwara-Jayabahu et al., 2012), Arabidopsis itself offers many advantages as a model system. Currently this is due to several reasons: there is a vast amount of Arabidopsis-related literature already, it has a comparatively small genome which can be relatively easily genetically engineered, it is small in size and has a short generation time, it both can self-fertilize and be used for out-crossing, and has large seed yields (Koornneef and Meinke, 2010; Meinke et al., 1998; Norman and Benfey, 2009).

1.5 Research Objectives

The first four research objectives focus on refining our current understanding of MTA toxicity. These are investigated in Chapter 2. The last research objective seeks to discover previously unknown pathways affected by MTA. This is investigated in Chapter 3. The research objectives are:

1. Increase our understanding of the pathways affected by MTA accumulation in MTN-deficient mutants.
2. Determine which pathways affected by MTA accumulation in *mtn1-1mtn2-1* are restored in G3.
3. Investigate the heritable epigenome of *mtn1-1mtn2-1* plants.
4. Investigate whether Arabidopsis PRMT5 activity is affected by MTA accumulation in MTN-deficient mutants.
5. Use a forward genetics approach to identify which pathways significantly contribute to the mutant phenotypes.

Chapter 2

Methylthioadenosine accumulation in Arabidopsis inflorescences alters the transcriptome and drives sulfur assimilation away from cysteine and methionine biosynthesis

2.1 Introduction

In Arabidopsis, Met biosynthesis occurs *de novo* via the transsulfuration pathway, using the sulfur-containing amino acid Cys as a precursor. Met is converted to the active methyl donor SAM by SAMS, using ATP as a cofactor. Methyltransferases use SAM as a substrate in methylation reactions, leaving behind the byproduct SAH. SAH is hydrolyzed to the

Met precursor Hcy, allowing for the regeneration of Met. This cycle is known as the SAM cycle. In Arabidopsis SAM can also be used by an alternate set of reactions, which include the biosynthesis of NA and the ethylene precursor ACC. SAM can also be decarboxylated, which in Arabidopsis allows it to be used for the biosynthesis of the PAs Spd, Spm and Tspm. All of these alternate SAM-utilizing reactions produce MTA as a byproduct. Similar to SAH, Met is regenerated from MTA. This occurs via the methionine salvage cycle, where MTA goes through a number of transformations before Met is formed.

All of the metabolites produced by these alternate SAM-utilizing reactions have important roles in plant physiology. NA acts as an iron chelator to dissolve soil-bound iron for transport into the root system (Higuchi et al., 1999). Ethylene is a gaseous plant hormone involved in plant development and stress responses (Dubois et al., 2018). Among the three PAs, Spd is the most significant, being the only essential PA: SPDS-knockout Arabidopsis are embryo lethal (Imai et al., 2004). Spd has various roles including regulation of gene expression, growth, ROS scavenging, and stress responses (Tiburcio et al., 2014). Spd is also used for the hypusination of eIF5A, a factor involved in translation elongation and termination (Schuller et al., 2017). Spm is believed to play a role in stress responses, but SPMS-knockout Arabidopsis grown in control conditions are otherwise unaffected (Yamaguchi et al., 2006). Tspm has a key role in vascular development, with ACL5-knockout Arabidopsis exhibiting a severe dwarf phenotype with thicker veins (Clay and Nelson, 2005; Imai et al., 2006).

Under low-sulfur conditions in Arabidopsis, the Met salvage cycle is crucial for the maintenance of the Met pool (Bürstenbinder et al., 2007; Zierer et al., 2016). Conversely under sulfur-sufficient conditions the Met salvage cycle is non-essential, evidenced as even knockout mutants of Met salvage cycle enzymes exhibit no mutant phenotypes (Bürstenbinder et al., 2007; Zierer et al., 2016). There is only one exception to this: MTA

accumulation in Arabidopsis lacking the enzyme MTN (which catalyzes the formation of methylthioribose (MTR) from MTA) is very toxic (Bürstenbinder et al., 2010; Waduwara-Jayabahu et al., 2012). The exact reason for this toxicity is not known, but previous studies have suggested the feedback inhibition by MTA of the alternate SAM-utilizing reactions to be a major culprit (Bürstenbinder et al., 2010; Waduwara-Jayabahu et al., 2012).

There is *in vitro* evidence of the sensitivity of NAS and ACS enzymes to MTA (Herbik, 1997; Hyodo and Tanaka, 1986), and *in silico* evidence of an interaction between MTA and the PA biosynthesis enzymes SPDS and ACL5 (Waduwara-Jayabahu et al., 2012). The corresponding *in vivo* evidence is mixed however. Reductions in NA levels in the male and female sterile MTN-deficient double mutant *mtn1-1mtn2-1* have been shown (Waduwara-Jayabahu et al., 2012), but not for ethylene, Spd and Spm (Waduwara-Jayabahu et al., 2012; Washington et al., 2016). Although Tspm has not been measured, there is an obvious lack of a severe dwarfism phenotype in *mtn1-1mtn2-1* mutants (Waduwara-Jayabahu et al., 2012) normally seen in *acl5* mutants (Clay and Nelson, 2005).

Interestingly, Waduwara-Jayabahu et al. (2012) found that fertility in *mtn1-1mtn2-1* plants could be restored by feeding Spd at the seedling stage. Furthermore this restoration is maintained transgenerationally, suggesting the mechanism driving restoration to be epigenetic (Waduwara-Jayabahu et al., 2012). This epigenetic mechanism likely involves changes in DNA methylation, which are inheritable (Budhavarapu et al., 2013). Fertility restoration in the first generation is limited to the occasional individual branches, though fertility increases over subsequent generations (Waduwara-Jayabahu et al., 2012).

The goal of this study was three fold. First, investigate which alternate SAM-utilizing biosynthesis pathways are affected by MTA accumulation in MTN-deficient mutants. Second, identify potentially unknown pathways affected by MTA. Third, identify which MTA-affected pathways in *mtn1-1mtn2-1* plants are altered by Spd restoration. This was done by

combining metabolite measurements of key MTA-related metabolites and RNAseq analyses. The results of these experiments helped clarify the impact of MTA accumulation on NA and PA biosynthesis and revealed a new previously unappreciated relationship between sulfur assimilation and MTA.

2.2 Materials and methods

2.2.1 Plant materials and growth conditions

Germination and seedling growth

Arabidopsis thaliana (Col-0 ecotype) seeds were surface sterilized using chlorine gas generated by mixing 100 mL bleach and 4 mL hydrochloric acid in a sterilization chamber. Seeds were left in the chamber for a minimum of 1 h (Lindsey et al., 2017). Sterilized seeds were then sown on half-strength MS media with 0.8 % (w/v) agar and 1 % (w/v) sucrose (Murashige and Skoog, 1962). For treatment-related seedling experiments, supplements were added directly to the molten medium (chemicals were obtained from Sigma-Aldrich Canada Co., Oakville, ON, Canada). After stratification in the dark at 4 °C for 2 d, seeds plated on media were placed in a growth chamber (TC7, Conviron, Winnipeg, Canada) with continuous light from fluorescent bulbs set to 100 µE m^{-2} s^{-1} for 14 d.

Adult plant growth

Seedlings were transplanted into individual pots of soil with equal amounts Sunshine LC1 mix and Sunshine LG3 germination mix (SunGro Horticulture Inc., Washington, USA). Plants were maintained in growth chambers with a 16 h daily light cycle from fluorescent bulbs with light levels set to ∼150 µE m^{-2} s^{-1}. The plants were watered every two or three days and fertilized weekly using 1.5 g L^{-1} of a 20:20:20 (N:P:K) fertilizer mix (Plant Products Co. Ltd., Brampton, Canada).

Plant lines

Aside from WT plants, mutant plants containing the following T-DNA insertions at the *MTN1* and *MTN2* loci (obtained from the Arabidopsis Biological Resource Center, Ohio State University, USA) were also studied: SALK_085385 (*mtn1-1*), SALK_071127 (*mtn2-1*), and SALK_022510 (*mtn2-5*). From these, the double mutants *mtn1-1mtn2-1* and *mtn1-1mtn2-5* were generated (Waduwara-Jayabahu et al., 2012). The following transgenes were introgressed into the *mtn1-1mtn2-1* mutant: pCYCB1;1-GFP (Ubeda-Tomás et al., 2009) and roGFP2 (Schwarzländer et al., 2008). Transgenic plant lines were genotyped with PCR as described by Bürstenbinder et al. (2010) and Waduwara-Jayabahu et al. (2012), using the primers listed in Table 2.1.

2.2.2 Confocal microscopy

Seedlings used for confocal microscopy analyses were grown vertically for 5 d as described in subsection 2.2.1. GFP-expressing roots were pre-stained with 100 mg L^{-1} propidium idodide (PI) for 30 s. Plant samples were imaged using a Zeiss 700 confocal microscope (Carl Zeiss Inc., Toronto, Canada) with a plan-apochromat 20x/0.8 objective. The following solid state lasers were used for excitation: 405 nm for the oxidized form of roGFP2; and 488 nm for GFP, the reduced form of roGFP2, and PI. GFP and PI fluorescence was separated using a 555 nm single-pass filter and a 560 nm long-pass filter, respectively. Fluorescence from the oxidized and reduced forms of roGFP2 was separated by setting the variable secondary dichroic splitter to 492 nm.

Table 2.1: Primers used for genotyping.

Primer name	Sequence (5′ to 3′)
*mtn1-1*F	TGACGGAGACCAACTCCATAC
*mtn1-1*R	GAGGCTCTTCCTTTGGTCAAC
*mtn2-1*F	CCTTGCTTACGTGGCATAAAC
*mtn2-1*R	GGAAAGGGCAAAAATATATGG
*mtn2-5*F	ACTGTGCCAACACTCTCAACC
*mtn2-5*R	AAGATTTCCGCTTCCTGAAAG
LBb1.3	ATTTTGCCGATTTCGGAAC
AT3TE60430F	TAAATTGCCCTGCTGCTTCT
AT3TE60430R	AGCGCTCATCCCTCACTCTA
AT1G67105F	ACGAGTTGGAGTTAAGTGGTT
AT1G67105R	CAATTTTGCAGTTGTGTTTGTGT

2.2.3 Chop PCR

Genomic DNA was extracted from ∼50 mg pools of unopened floral buds (buds) using a DNeasy Plant Mini Kit (Qiagen Inc., Toronto, ON, Canada). 500 ng genomic DNA was digested overnight with 20 units of the restriction enzyme McrBc (New England Biolabs, Whitby, ON, Canada) in a 50 µL reaction volume at 37 °C, and inactivated by incubation at 65 °C for 20 min. An undigested control using 2 µL glycerol instead of McrBc was performed simultaneously. Digested and undigested DNA was amplified with PCR using the following program: 5 min at 94 °C; followed by 35 cycles of 94 °C for 30 s, 58 °C for 30 s, and 72 °C for 1 min; and a final 10 min at 72 °C.

2.2.4 HPLC metabolite measurements

Sample collection and extraction

Seedlings (14 d) and unopened buds were collected and flash frozen using liquid nitrogen, then weighed to ∼100 mg in 1.5 mL microcentrifuge tubes. The plant material was ground to a fine powder using a homogenizer and stored indefinitely at −80 °C. To extract, 1 mL of 0.1 M HCl was added to the tubes, and vortexed every ∼30 s for 15 min. The tubes were subsequently centrifuged at 16 000 RCF, 4 °C, for 5 min. The supernatants were transferred to new tubes and stored indefinitely at −80 °C.

Derivatisation and quantification of thiols

The thiol-containing compounds were measured as described by Wirtz et al. (2004). The thiol-containing compounds Cys and GSH were first reduced by mixing 10 µL of sample

extract with 190 µL of water, 20 µL of 1 M tris (pH 8.3), 10 µL of 10 mM DTT, and 25 µL of 0.08 M NaOH. This mixture was incubated in the dark at room temperature (RT) for 1 h. The reduced thiols were derivatized by adding 25 µL of 10 mM (dissolved in acetonitrile) of the fluorescent conjugate monobromobimane (Mbb) and mixing by inversion, before incubating in the dark at RT for 15 min. Derivatization was halted by the addition of 705 µL acetic acid (5 %). To remove any precipitates, tubes were centrifuged at 16 000 RCF, 4 °C, for 45 min. The prepared samples were either stored at −80 °C for later use or 900 µL of the sample transferred into high-performance liquid chromatography (HPLC) vials for immediate quantification.

HPLC vials loaded with derivatised sample extracts were loaded into a Waters 717plus Autosampler (Waters GmbH, Eschborn, Germany) and 10 µL of the sample injected by a Waters 600E pump (Waters GmbH, Eschborn, Germany) through a Nova-Pak C18 (60 Å, 4 µm, 4.6 mm × 250 mm) column (Waters GmbH, Eschborn, Germany) kept at a constant 37 °C. The flow-through was pumped into a Jasco 920 Intelligent Fluorescent Detector (Jasco Deutschland GmbH, Pfungstadt, Germany) set to 380 nm excitation, 480 nm emission, FST response, Norm mode, gain of 1000, and attenuation of 1. Thiols were eluted from the column using gradient amounts of buffer A (100 mM potassium acetate, pH 5.3 with acetic acid) and buffer B (100 % methanol) in the following program: 12.5 min of 91 % buffer A and 9 % buffer B; 3 min of 100 % buffer B; and 8.5 min of 91 % buffer A and 9 % buffer B. Absolute quantification was performed using Empower Pro (Waters GmbH, Eschborn, Germany) after generating standard curves from 1, 5, and 10 pmol amounts of Cys, γ-glutamylcysteine (gEC), cysteinyl-glycine (CysGly), and GSH.

Derivatisation and quantification of adenosines

Adenosine-containing compounds were measured as described by Rzewuski et al. (2007). The derivatisation of adenosine-containing compounds SAM, SAH, and MTA was performed by mixing 300 µL of the sample extract with 620 µL CP-buffer (620 mM citric acid-1-hydrate, 760 mM di-sodium hydrogen phosphate di-hydrate, pH 4 with NaOH) and 80 µL chloroacetaldehyde (45 %). This mixture was incubated at 80 °C for 10 min and subsequently cooled on ice until the sample reached RT. The samples were centrifuged at 16 000 RCF, 20 °C, for 45 min. The supernatants were transferred to HPLC vials for immediate use.

Quantification was performed as described above, with the following modifications. The detector emission was set to 280 nm, and excitation to 410 nm. The adenosines were selectively eluted from the column using varying gradient amounts of buffer A (50 mM tri-sodium phosphate dodecahydrate, 10 mM sodium 1-heptanesulfonic acid, 4 % acetonitrile, pH 3.2 with phosphoric acid) and buffer B (100 % acetonitrile) in the following program: 5 min of 100 % buffer A; 15 min of 85 % buffer A and 15 % buffer B; 10 min of 10 % buffer A and 90 % buffer B; and 20 min of 100 % buffer A. Absolute quantification was performed using Empower Pro (Waters GmbH, Eschborn, Germany) after generating standard curves from 1, 5, and 10 pmol amounts of SAM, SAH, and MTA.

Derivatisation and quantification of nicotianamine

The metabolite NA was measured as described by Klatte et al. (2009). The derivatisation of NA was performed by first mixing 25 µL of the sample extract with 75 µL of a 0.5 M borate buffer (pH 7.7 with NaOH and added 5 mM EDTA). This mixture was derivatised by adding 50 µL of 12 mM FMOC-Cl (9-fluorenylmethyl chloroformate 9-fluorenylmothoxycarbonyl chloride; dissolved in acetone), vortexing, and incubating for 45 s at RT. Subsequently, the

reaction was deactivated by the addition of 50 µL ADAM (adamantan-1-amine amantadine hydrochloride; dissolved in 75 % acetone) and incubating for 45 s at RT. The samples were centrifuged at 16 000 RCF, 4 °C, for 20 min and the supernatants transferred to new tubes. The centrifugation was repeated for 40 min and 100 µL of the supernatants transferred to HPLC vials for immediate quantification.

Quantification was performed as described above, with the following modifications. The samples were passed through a Phenomenex C18 (4 mm × 3 mm) column (Phenomenex Inc., Aschaffenburg, Germany) and eluted using two buffers containing 50 mM Na-acetate buffer (ph 4.2) and acetonitrile: buffer A (80 % Na-acetate buffer and 20 % acetonitrile) and buffer B (20 % Na-acetate buffer and 80 % acetonitrile). The elution program was as follows: 15 min of 100 % buffer A; 5 min of 80 % buffer A and 20 % buffer B; 3 min of 100 % buffer B; and 7 min of 100 % buffer A. The flow-through passed through the detector with the following settings: 263 nm excitation, 313 nm emission, and gain of 100. Absolute quantification was performed using Empower Pro (Waters GmbH, Eschborn, Germany) after generating a standard curve from 1, 2, 4, and 8 pmol amounts of NA.

Derivatisation and quantification of amino acids and polyamines

Amino acids and polyamines were measured as described by Heeg et al. (2008). The amino acids alanine, arginine, asparagine, aspartic acid, glutamine, glutamic acid, glycine, histidine, isoleucine, lysine, Met, phenylalanine, proline, serine, threonine, tyrosine, valine, and the polyamines Put, Spd were derivatised in the following manner. First, 5 µL of sample was combined with 35 µL of 0.2 M boric acid buffer (pH 8.8 with NaOH). To this mixture was applied 20 µL of a AccQ Taq reagent (3 mg mL^{-1} in acetonitrile; Waters GmbH, Eschborn, Germany) and incubated at RT for 5 min. Following this samples were incubated at 55 °C for 10 min, and afterwards 440 µL of water was added. The samples were centrifuged at

16 000 RCF, 4 °C, for 15 min. The samples were either stored at −80 °C for later use or transferred into HPLC vials for immediate use.

HPLC vials were loaded into a Acquity H-class UPLC with Acquity FLR-Detector (Waters GmbH, Eschborn, Germany). 2 µL of sample was injected and pumped through a Acquity BEH C18 (1.7 µm, 150 mm × 2.1 mm) column (Waters GmbH, Eschborn, Germany) kept at 42 °C. Metabolites were eluted from the column by varying gradient of a buffer A (140 mM sodium acetate, 7 mM tri-ethanolamine, pH 6.3 with NaOH) and a buffer B (100 % acetonitrile). The elution program was as follows: 7 min of 92 % buffer A and 8 % buffer B; 0.3 min of 91 % buffer A and 9 % buffer B; 5 min of 85 % buffer A and 15 % buffer B; 4.1 min of 82 % buffer A and 18 % buffer B; 2.3 min of 60 % buffer A and 40 % buffer B; 3 min of 20 % buffer A and 80 % buffer B; and 2.5 min of 92 % buffer A and 8 % of buffer B. The elutes were passed through the detector with the following settings: excitation of 250 nm, emission of 395 nm, data rate of 10 pts s^{-1}, and gain of 20. Absolute quantification was performed using Empower Pro (Waters GmbH, Eschborn, Germany) after generating a standard curve from 5, 10, 25, and 50 pmol amounts of all the standard amino acids, and the polyamines Put, Spd, and Spm.

Quantification of anions

Anions were measured as described by Wirtz and Hell (2007). To quantify the anions nitrate (NO_3^-), phosphate (PO_4^{3-}), and sulfate (SO_4^{2-}), sample extracts were diluted ten-fold with water and centrifuged at 16 000 RCF, 4 °C, for 45 min. The supernatants were transferred into Dionex vials (Thermo Fisher Scientific GmbH, Dreieich, Germany) and loaded into a Dionex AS-50 autosampler (Thermo Fisher Scientific GmbH, Dreieich, Germany). A Dionex ICS-1000 pump/detector (Thermo Fisher Scientific GmbH, Dreieich, Germany) was used to inject 25 µL of the sample through a Ion-PAC AS 9HC 2x250 mm column (Thermo Fisher

Scientific GmbH, Dreieich, Germany). Anions were eluted using a 0.3 mL min^{-1} isocratic run gradient. Absolute quantification was performed by generating standard curves using Chromeleon (Thermo Fisher GmbH, Dreieich, Germany) after 1, 5, and 10 nmol amounts of NO_3^-, PO_4^{3-}, and SO_4^{2-}.

2.2.5 RNA sequencing

Sample collection and RNA extraction

Unopened buds from adult plants were collected and pooled to ∼50 mg in 1.5 mL microcentrifuge tubes and frozen in liquid nitrogen. The tissue was ground to a fine powder with a homogenizer and RNA extracted with an RNeasy Plant Mini Kit (Qiagen Inc., Toronto, ON, Canada). RNA was DNase-treated with a RNase-Free DNase Set (Qiagen Inc., Toronto, ON, Canada). RNA integrity was confirmed using an Agilent 2100 Bioanalyzer System (Agilent Technologies Inc., Mississauga, ON, Canada) at the Farncombe Metagenomics Facility, McMaster University, Canada.

Sequencing and transcript quantification

For RNA sequencing, mRNA 250–300 bp insert cDNA library preparation was performed by Novogene Corporation (Sacramento, CA, USA) and sequenced on a NovaSeq 6000 platform (Illumina Inc., San Diego, CA, USA) with paired-end 150 bp sequencing strategy and 20 M reads per sample. FastQ files were quality filtered and adapter-trimmed using Trim Galore! v0.4.5 (Krueger, 2012), then mapped onto the TAIR10 release of the *Arabidopsis thaliana* genome (Lamesch et al., 2012) with STAR v2.5.4b (Dobin et al., 2013). The resulting SAM files were sorted and converted to BAM with SAMtools v1.3.1 (Li et al., 2009).

Transcript quantification based on the Araport11 genome annotations (Cheng et al., 2017) was performed with StringTie v1.3.4d (Pertea et al., 2015).

2.2.6 Data analysis

All statistical analysis in this chapter was performed within the R language (R Core Team, 2018). One way ANOVA tests, Tukey's honest significant difference (HSD) tests, principle component analysis (PCA), and Fisher's Exact Test analyses were done using the base R package stats (R Core Team, 2018). The R package edgeR (Robinson et al., 2010) was used to analyze gene expression levels and perform pairwise comparisons; as well as perform statistical contrasts as described by Lun et al. (2016). Clustering analysis was done using the R package WGCNA (Langfelder and Horvath, 2008, 2012).

2.3 Results

2.3.1 Metabolite analysis

Overview of metabolite measurements of MTN-deficient mutants

The impact of MTN-deficiency on neighbouring Met-related pathways (Figures 1.1–1.5) was examined, as well as how these possible effects were changed in the restored generations. Since there are extensive data on *mtn1-1mtn2-1* mutant seedlings (Bürstenbinder et al., 2010; Waduwara-Jayabahu, 2011; Waduwara-Jayabahu et al., 2012), it was an obvious choice to extend this knowledge base with a metabolite analysis of seedlings. However, a major focus of this research concerns the Spd restoration of fertility (which is intrinsically linked to the reproductive tissues of the plant), examining the metabolite profile of buds was also determined to be a priority.

Metabolites were monitored in WT, *mtn1-1mtn2-5*, *mtn1-1mtn2-1*, G2, and G3 genotypes, and compared under control conditions and after treatment with 100 µM Spd, in both seedlings (14 d) and unopened buds. The *mtn1-1mtn2-1* genotype was separated based on the parent genotype (both $\frac{\text{MTN1}}{mtn1\text{-}1} \cdot \frac{mtn2\text{-}1}{mtn2\text{-}1}$ and $\frac{mtn1\text{-}1}{mtn1\text{-}1} \cdot \frac{\text{MTN2}}{mtn2\text{-}1}$ are possible) in order to factor out any possible effects of embryonic exposure to differential levels of maternal MTN. A total of 29 different metabolites were measured using HPLC, with three to five replicates per sample. In order to visualize the overall profile separation between genotypes and treatments, the data were collated and PCA performed on a per tissue basis (Figure 2.1).

As seen in Figure 2.1, it is apparent that the treatment conditions do not cluster discretely within genotypes. For example this can also be seen consistently in the individual metabolite

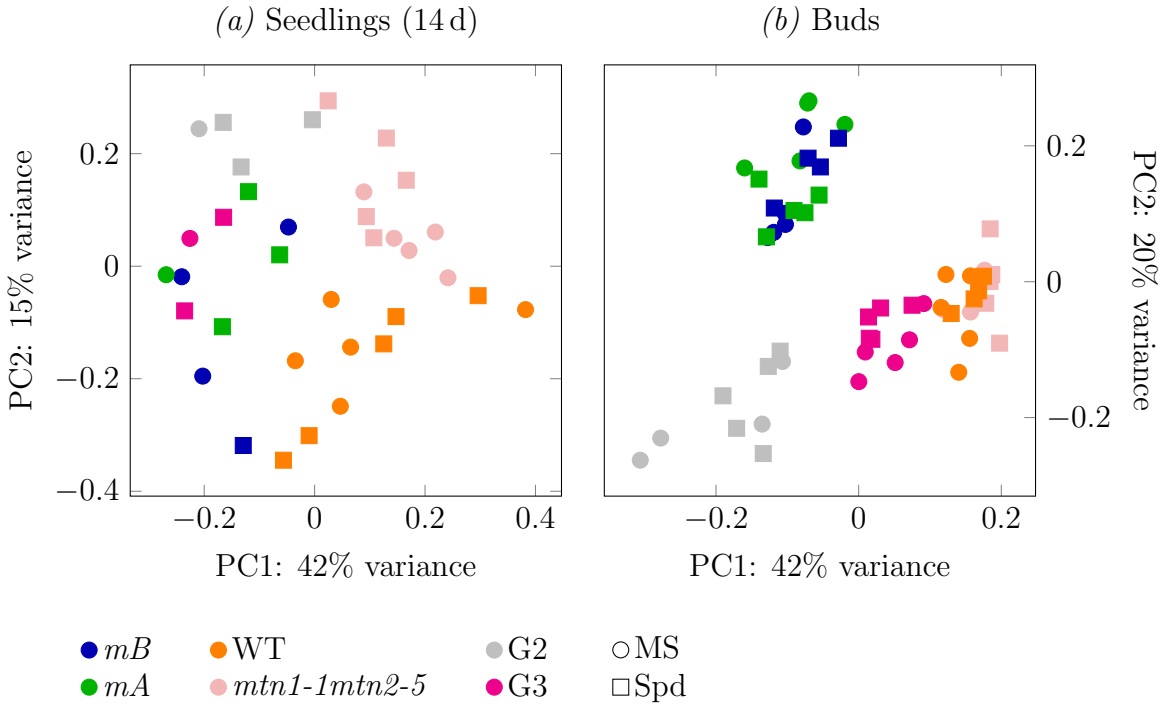

Figure 2.1: PCA of metabolite measurements.

All HPLC metabolite measurements were summarised in a PCA. The PCA in *(a)* is comprised of measurements from 14 d seedlings, and the PCA in *(b)* for unopened buds. Measurements were grouped based on genotype and treatment. For the *mtn1-1mtn2-1* genotype, measurements were divided based on the genotype of the parent plant: *mA* for having a parent with a WT copy of MTN1, and *mB* for having a parent with a WT copy of MTN2.

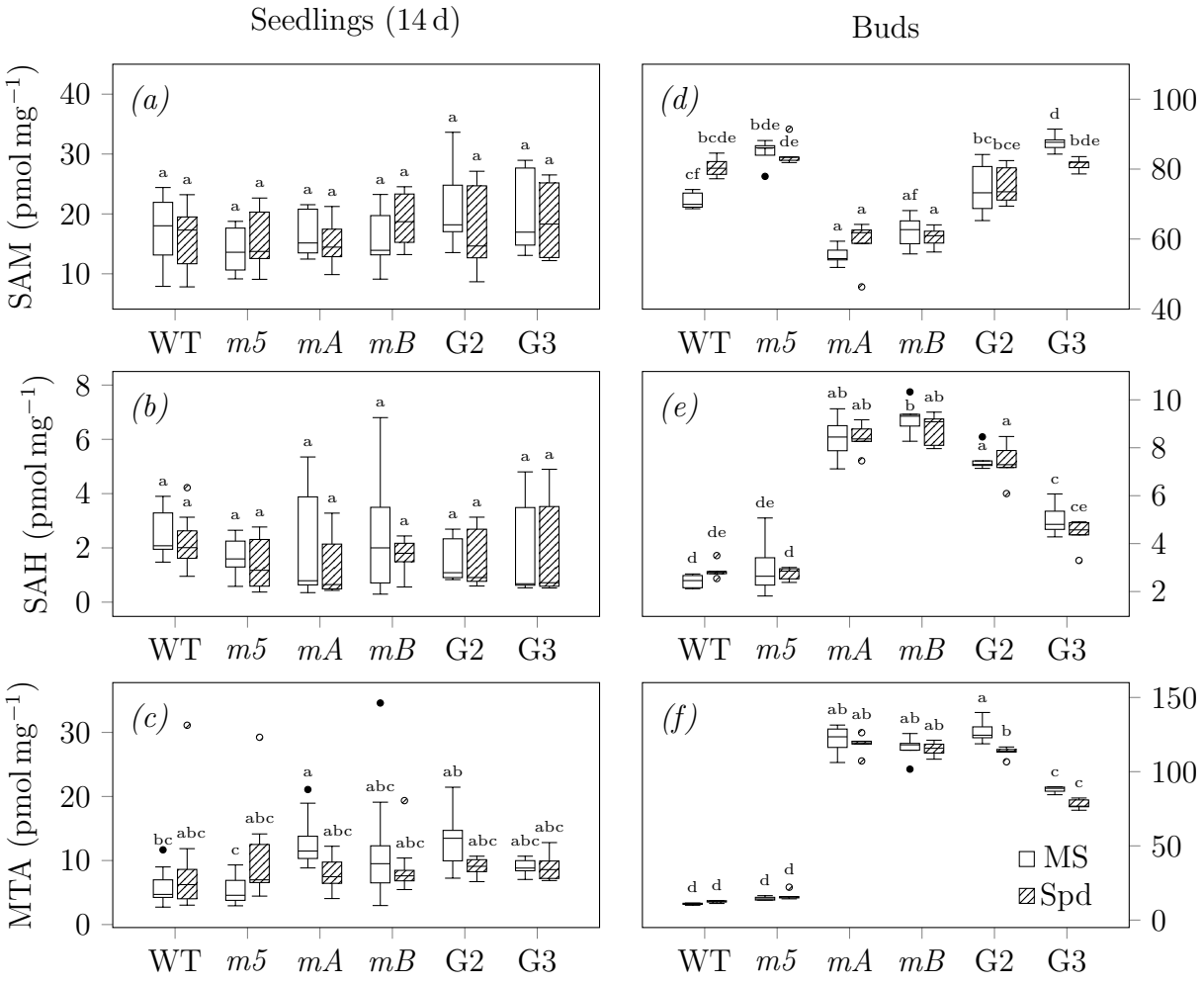

Figure 2.2: SAM, SAH, and MTA metabolite measurements.

HPLC metabolite measurements of 14 d seedlings (*a–c*) and unopened buds (*d–f*) for *S*-adenosylmethionine (SAM), *S*-adenosylhomocysteine (SAH), and methylthioadenosine (MTA). Measurements were grouped based on genotype and treatment. Letters represent significant difference from a Tukey's HSD post-hoc test after a one-way ANOVA ($p < 0.05$), $n = 5$. Boxes which do no share any common letters are significantly different. *m5, mtn1-1mtn2-5. mA, mtn1-1mtn2-1* (parent with a WT copy of MTN1). *mB, mtn1-1mtn2-1* (parent with a WT copy of MTN2).

measurements in Figures 2.2-2.5. Furthermore the discrete clustering of genotypes between the first two principle components of each tissue differs greatly. Although there is a loose clustering in the seedling data between WT and *mtn1-1mtn2-5*, the *mtn1-1mtn2-1*, G2, and G3 genotypes are nearly intermingled (Figure 2.1*a*). This observation is more or less consistent with previous seedling data of both the single mutants *mtn1-1* and *mtn2-1* (Bürstenbinder et al., 2010), as well as leaf tissue measurements of the double mutant *mtn1-1mtn2-1* (Waduwara-Jayabahu et al., 2012). There, only small differences were observed relative to WT. Interestingly, the levels of metabolites of buds cluster very distinctly (Figure 2.1*b*). This is consistent with the strong significant decreases observed between metabolite levels of WT and *mtn1-1mtn2-1* inflorescences recorded previously (Waduwara-Jayabahu et al., 2012).

Metabolite analysis of *mtn1-1mtn2-1*

Looking at the metabolite levels of *mtn1-1mtn2-1* seedlings grown with or without Spd (Figures 2.2*a–c*, 2.3*a–c*, 2.4*a–c*, 2.5*a–c*), a few general observations can be made regarding these: *(i)* they are not significantly affected by the treatment; *(ii)* they are not significantly affected by the genotype of the parent plant; and *(iii)* the absolute difference of metabolites in non-WT samples relative to WT is not more than two fold.

NA is the only metabolite significantly different in *mtn1-1mtn2-1* relative to WT (Figure 2.3*a*). The NA result is consistent with the strong NA-driven chlorosis observed previously (Waduwara-Jayabahu et al., 2012). Though the other metabolites do not appear to be significantly different relative to WT, it is important to note that this does not necessarily mean the other metabolites are not relevant to the phenotype of *mtn1-1mtn2-1*.

Looking at the metabolite results for *mtn1-1mtn2-1* buds, the only metabolites which

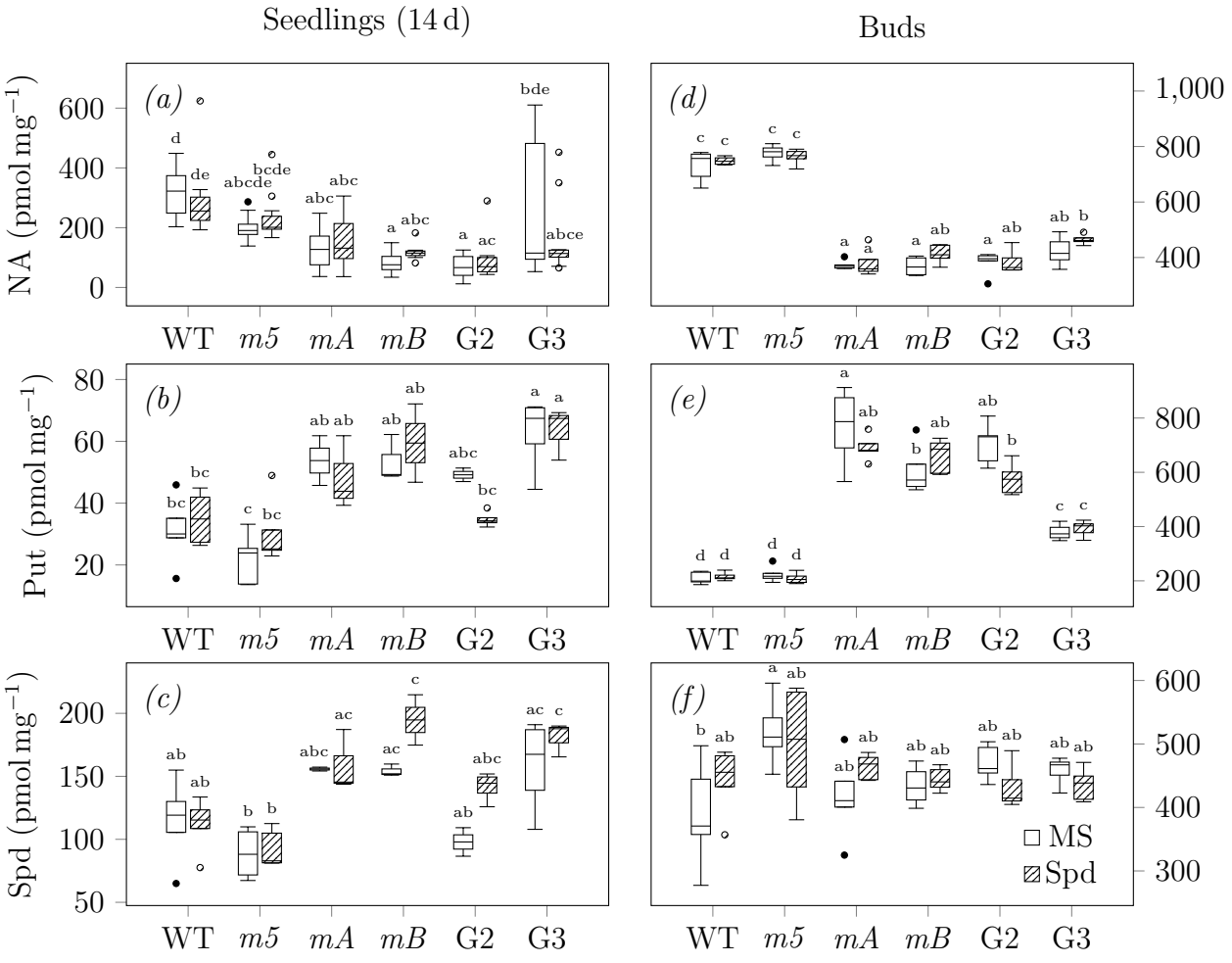

Figure 2.3: NA, Put and Spd metabolite measurements.

HPLC metabolite measurements of 14 d seedlings (*a–c*) and unopened buds (*d–f*) for nicotianamine (NA), putrescine (Put), and spermidine (Spd). Measurements were grouped based on genotype and treatment. Letters represent significant differenceTukey's a Tukey's HSD post-hoc test after a one-way ANOVA ($p < 0.05$), $n = 5$. Boxes which do no share any common letters are significantly different. *m5, mtn1-1mtn2-5. mA, mtn1-1mtn2-1* (parent with a WT copy of MTN1). *mB, mtn1-1mtn2-1* (parent with a WT copy of MTN2).

do not show any consistent significant changes compared to WT are Spd (Figure 2.3*f*), GSH (Figure 2.4*e*), and the anions shown in Figure 2.5*d-f*. Of the metabolites which are consistently significantly different, SAM (Figure 2.2*d*), NA (Figure 2.3*d*), Cys (Figure 2.4*d*), and Met (Figure 2.4*f*) are lower than WT. On the other hand, SAH (Figure 2.2*e*), MTA (Figure 2.2*f*) and Put (Figure 2.3*e*) are higher than WT. From these results the increased levels of MTA and Put, and the decreased levels of NA are consistent with previous measurements of *mtn1-1mtn2-1* inflorescences (Waduwara-Jayabahu et al., 2012). Spd was also measured by Waduwara-Jayabahu et al. (2012) and a slight but not significant decrease was observed, which is not in agreement with the WT-levels observed here (Figure 2.3*f*).

Metabolite analysis of *mtn1-1mtn2-5*

Consistent with the seedling data of *mtn1-1mtn2-1*, there is a large amount of variation in the metabolite levels of *mtn1-1mtn2-5* seedlings. For buds however, where large differences between *mtn1-1mtn2-1* and WT were observed, in contrast the *mtn1-1mtn2-5* samples are much more closely aligned with the WT samples. Though previous data on this genotype are much sparser than *mtn1-1mtn2-1*, it has been considered as a moderate form of the MTN-deficient phenotype (Waduwara-Jayabahu, 2011). Of course, on one hand, it is logical for the metabolite profile of this genotype to be more so similar to that of WT: unlike *mtn1-1mtn2-1*, these plants are completely fertile (Waduwara-Jayabahu, 2011).

Metabolite analysis of G2 and G3

Measuring these metabolites in *mtn1-1mtn2-1* plants having been fertility-restored by Spd provided an opportunity to observe which processes likely remain unchanged. Due to

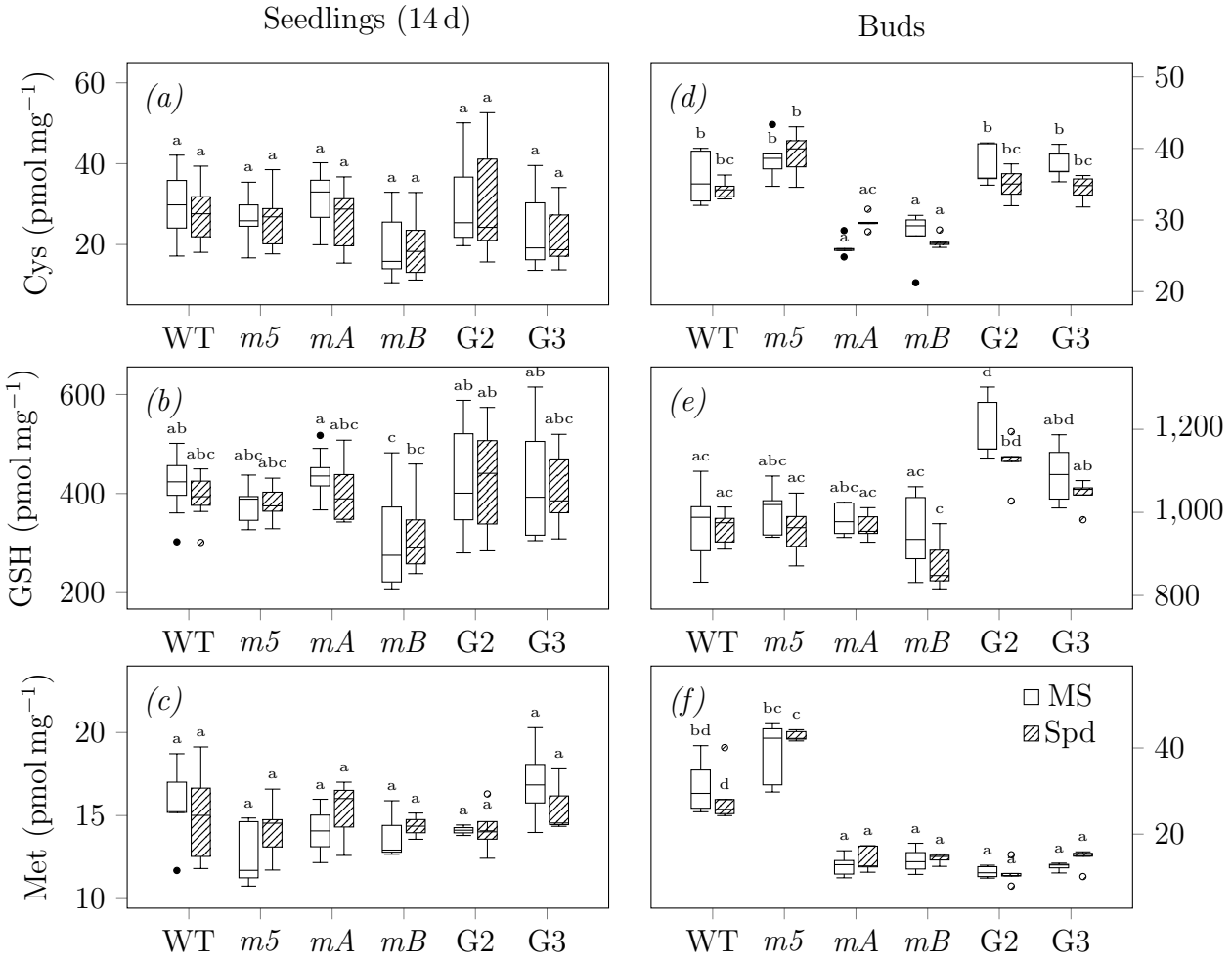

Figure 2.4: Cys, GSH and Met metabolite measurements.

HPLC metabolite measurements of 14 d seedlings (*a–c*) and unopened buds (*d–f*) for cysteine (Cys), glutathione (GSH), and methionine (Met). Measurements were grouped based on genotype and treatment. Letters represent significant difference from a Tukey's HSD post-hoc test after a one-way ANOVA ($p < 0.05$), $n = 5$. Boxes which do no share any common letters are significantly different. *m5, mtn1-1mtn2-5. mA, mtn1-1mtn2-1* (parent with a WT copy of MTN1). *mB, mtn1-1mtn2-1* (parent with a WT copy of MTN2).

variation in the data, the metabolite profiles of seedlings is likely not very informative in this regard. The exception to this in seedlings is NA levels which show no recovery (Figure 2.3*a*). The metabolite profiles of G2 and G3 unopened buds are much more revealing. For G2 buds, the levels of SAH (Figure 2.2*e*), MTA (Figure 2.2*f*), NA (Figure 2.3*d*), Put (Figure 2.3*e*), and Met (Figure 2.4*f*) remain both significantly different compared to WT and similar to *mtn1-1mtn2-1*. Interestingly in G3 buds, SAH (Figure 2.2*e*), MTA (Figure 2.2*f*) and Put (Figure 2.3*e*) are in fact significantly different from *mtn1-1mtn2-1*, moving towards (but not quite at) WT levels. This is consistent with previous observations that the degree of restoration improves over subsequent generations (Waduwara-Jayabahu, 2011).

The metabolites which begin to show recovery even in G2 buds are SAM (Figure 2.2*d*) and Cys (Figure 2.4*d*). Of these, SAM (Figure 2.2*d*) continues to increase further in G3 buds — to the point of surpassing WT levels. One metabolite which is present at WT levels in *mtn1-1mtn2-1* buds is GSH (Figure 2.4*e*); yet despite this GSH levels increase significantly in G2, and begin to decrease back to WT levels in G3. Possibly this bump in G2 buds is as a result of the increase in Cys levels (Figure 2.4*d*), as GSH production is dependent on Cys as a precursor (Figure 1.2); and the subsequent decrease in G3 a result of the generational improvement of the restoration phenotype.

Intriguingly, while SAM (Figure 2.2*d*), SAH (Figure 2.2*e*), MTA (Figure 2.2*f*) and Cys (Figure 2.4*d*) show recovery, Met (Figure 2.4*f*) levels only remain similar to those in *mtn1-1mtn2-1*.

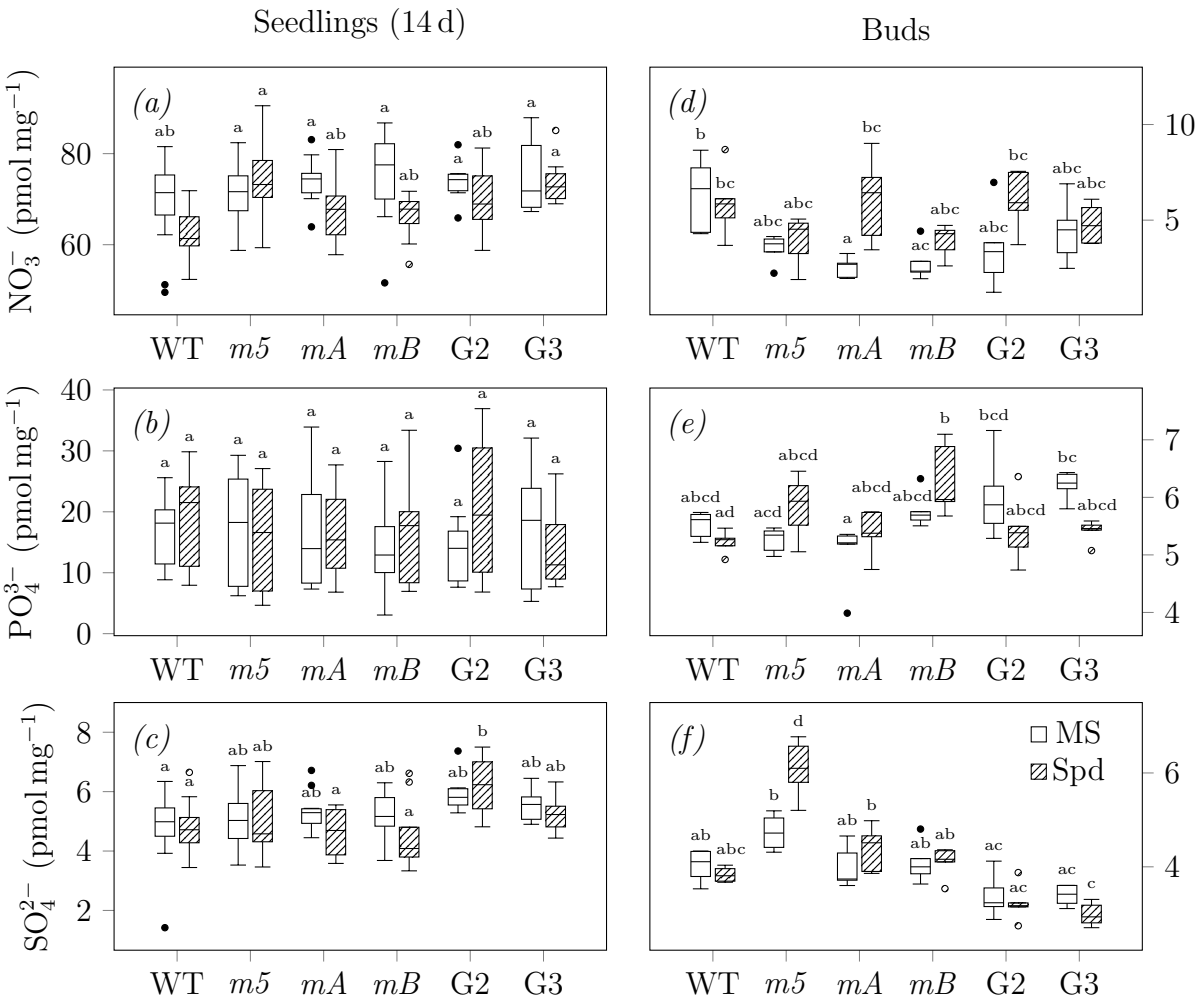

Figure 2.5: NO_3^-, PO_4^{3-} and SO_4^{2-} metabolite measurements.

HPLC metabolite measurements of 14 d seedlings (*a–c*) and unopened buds (*d–f*) for nitrate (NO_3^-), phosphate (PO_4^{3-}), and sulfate (SO_4^{2-}). Measurements were grouped based on genotype and treatment. Letters represent significant difference from a Tukey's HSD post-hoc test after a one-way ANOVA ($p < 0.05$), $n = 5$. Boxes which do no share any common letters are significantly different. *m5, mtn1-1mtn2-5. mA, mtn1-1mtn2-1* (parent with a WT copy of MTN1). *mB, mtn1-1mtn2-1* (parent with a WT copy of MTN2).

2.3.2 Transcriptomics analysis

Extending our metabolic understanding of restoration

Using the metabolite data as a foundation, transcriptomic analysis of mutant and restored buds by RNAseq was the next step taken in this research. The choice of an RNAseq experimental approach came from a desire to understand the underlying regulation of the pathways controlling metabolite output. As for the tissue, when comparing the large intra-genotypic variation noted in Figure 2.1 it becomes clear that buds have more potential to offer meaningful results. Finally, in order to simplify and focus the experimental scope, only WT, *mtn1-1mtn2-1*, and G3 were selected.

In order to maximize the impact of the RNAseq results, integrating the final data with the metabolite data presented here was paramount. This could only really be useful for genotypes which showed distinct metabolic profiles; thus *mtn1-1mtn2-5* and G2 genotypes were left out. Seeing as the parent of the *mtn1-1mtn2-1* had little effect on the metabolic profile, only one parent was chosen, $\frac{mtn1\text{-}1}{mtn1\text{-}1} \cdot \frac{\text{MTN2}}{mtn2\text{-}1}$. This parent was selected so that it would provide a maternal environment with the least amount of possible MTN activity (as MTN2 provides less than half of the overall MTN activity; Waduwara-Jayabahu et al., 2012) in case this could affect the phenotype of progeny.

As seen in Figure 2.6, the intra-genotypic variation was quite low. All three genotypes cluster very distinctly as well and both plotted principle components demonstrates interesting relationships between the genotypes. Along the X-axis (PC1), WT is very distinct. Furthermore, G3 actually is plotted further away from WT and quite close to *mtn1-1mtn2-1*. As for the Y-axis (PC2), WT appears to be in between G3 and *mtn1-1mtn2-1*. This could suggest a dual response: on one hand, the Spd-induced changes in G3 cause the

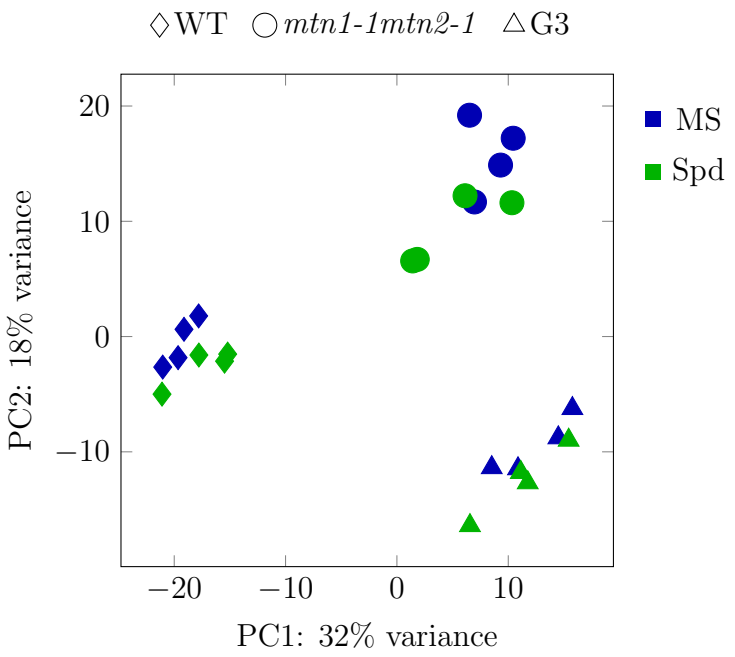

Figure 2.6: PCA from RNAseq data of unopened buds.

Gene expression data from an RNAseq experiment of unopened buds were summarised in a PCA. Each point represents an individual sample. The samples are split evenly between WT, *mtn1-1mtn2-1* and G3 genotypes. Each genotype is split between control (MS) and treated (Spd) samples.

mtn1-1mtn2-1 transcriptional profile to move further away from WT; however on the other hand another distinct subset of the G3 transcriptome has moved away from *mtn1-1mtn2-1* itself, in the direction of the WT transcriptome.

Additionally, it must be noted that the treatments have little impact on the inter-genotype samples. Despite this, an interesting pattern can be seen for all genotypes: the Spd samples almost always cluster towards the bottom right diagonal, suggesting the treatment is having a subtle, but constant, effect on the transcriptomes.

Overview of gene expression differences

Another method to compare the gene expression profiles of the samples is to look at the number of differentially expressed genes, as well as common differentially expressed genes. This can help show, on a large scale, to what extent the treatments and genotypes have affected the transcriptomes away from WT. Looking at Figure 2.7*a*, the Spd treatment is having a very subtle effect on the transcriptomes. When comparing MS and Spd, both WT and *mtn1-1mtn2-1* genotypes have fewer than 100 genes which are above the two-fold differential expression threshold. G3, which appears to be the most affected by Spd, still has less than 200 genes above the threshold. Interestingly, though the effect is obviously subtle, the majority of these genes are up-regulated by Spd. This concerted change is consistent with the modest Spd-induced changes noted in Figure 2.6.

When looking at the inter-genotype comparisons in Figure 2.7*a*, a couple observations are clear: *(i)* MTN-deficiency correlates with relatively more down-regulated genes, and *(ii)* G3 buds have fewer differentially regulated genes relative to WT than when compared to *mtn1-1mtn2-1*. The increased number of down-regulated genes is consistent with Figure 2.7*b*: when looking for differentially expressed genes which are in common between the

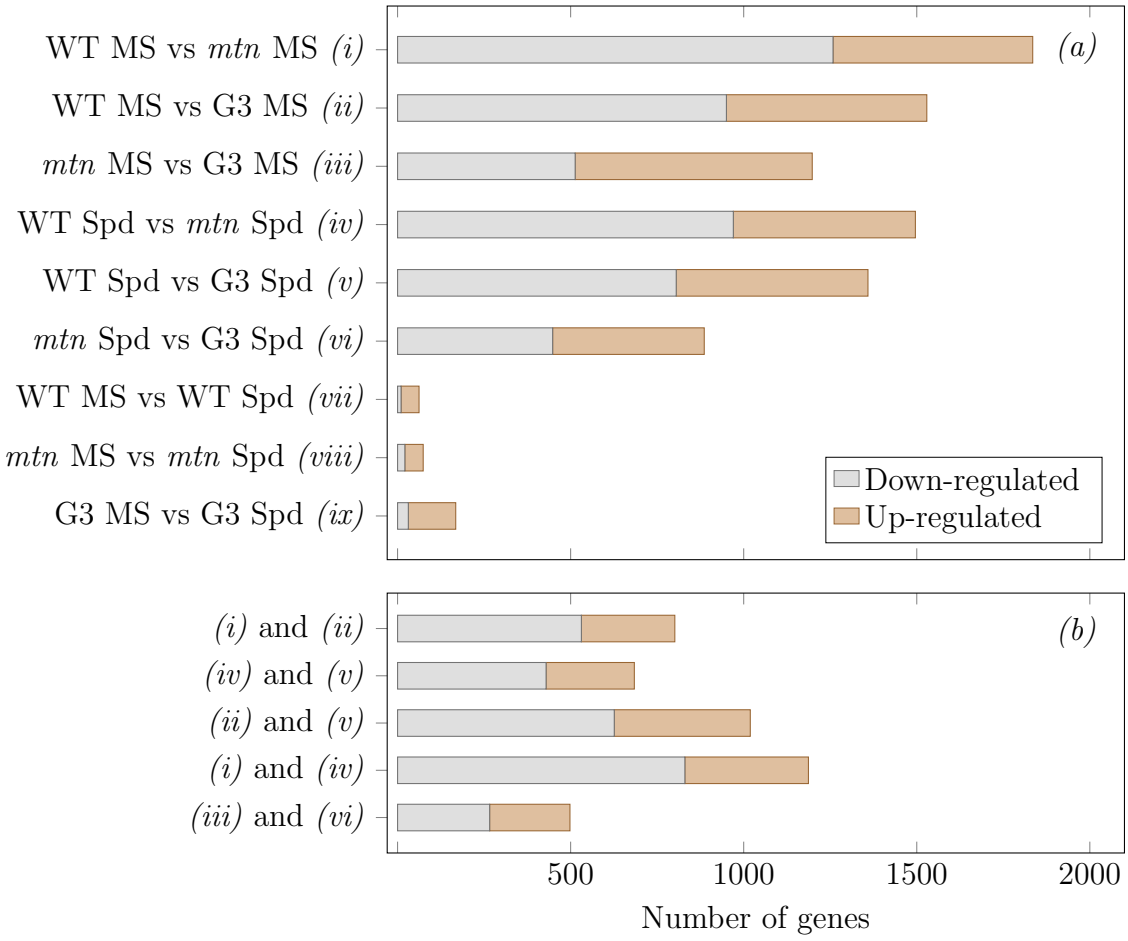

Figure 2.7: Comparisons of differentially expressed genes.

Gene expression differences between genotypes and treatments of an RNAseq experiment are summarised. The number of differentially expressed genes (with a two-fold difference cutoff and Q < 0.1) between WT, *mtn1-1mtn2-1* (*mtn*) and G3 genotypes (separated by treatment) are shown in *(a)*. Commonly differentially expressed genes between comparisons shown in *(a)* are shown in *(b)*.

comparisons in Figure 2.7*a*, the majority are down-regulated. Furthermore the difference between the transcriptomes of G3 and *mtn1-1mtn2-1* can also be seen here, as only 804 genes are in common between the WT—G3 and WT—*mtn1-1mtn2-1* comparisons. This is opposed to the 1529 and 1835 genes which are differentially expressed in G3 and *mtn1-1mtn2-1* relative to WT (MS), respectively.

Using clustering to find biologically relevant gene groups

A gene clustering approach was used in order to explore the impacts of MTN-deficiency and Spd on plant regulatory processes using the RNAseq data. This works by assuming that similarly regulated genes are co-expressed. Using this assumption, one can build co-expression networks and associate functions to genes using a guilt-by-association approach (Carpenter and Sabatini, 2004; Parikshak et al., 2015). Afterwards, by examining the changes in expression of clusters between samples, the effects of phenotypic variation on gene regulation can be deduced. The gene clustering was done using the R package `WGCNA` (Langfelder and Horvath, 2008, 2012). Genes from the RNAseq were assigned into clusters based on relative expression. Clusters of genes which showed no significant gene expression variation between genotypes or treatments were discarded. The remaining clusters were loosely subdivided into four types, shown in Figure 2.8.

Type I gene clusters contain genes that differ in expression across all three genotypes. Two clusters were assigned as type I, clusters A and B. The genes in cluster A were more highly expressed in the G3 samples, had low expression in the WT samples, and the *mtn1-1mtn2-1* samples exhibit expression levels between the two. The inverse was seen in cluster B; WT samples had the highest expression, with G3 the lowest. These were both large clusters, with cluster A having 2535 genes and cluster B with 1406 genes.

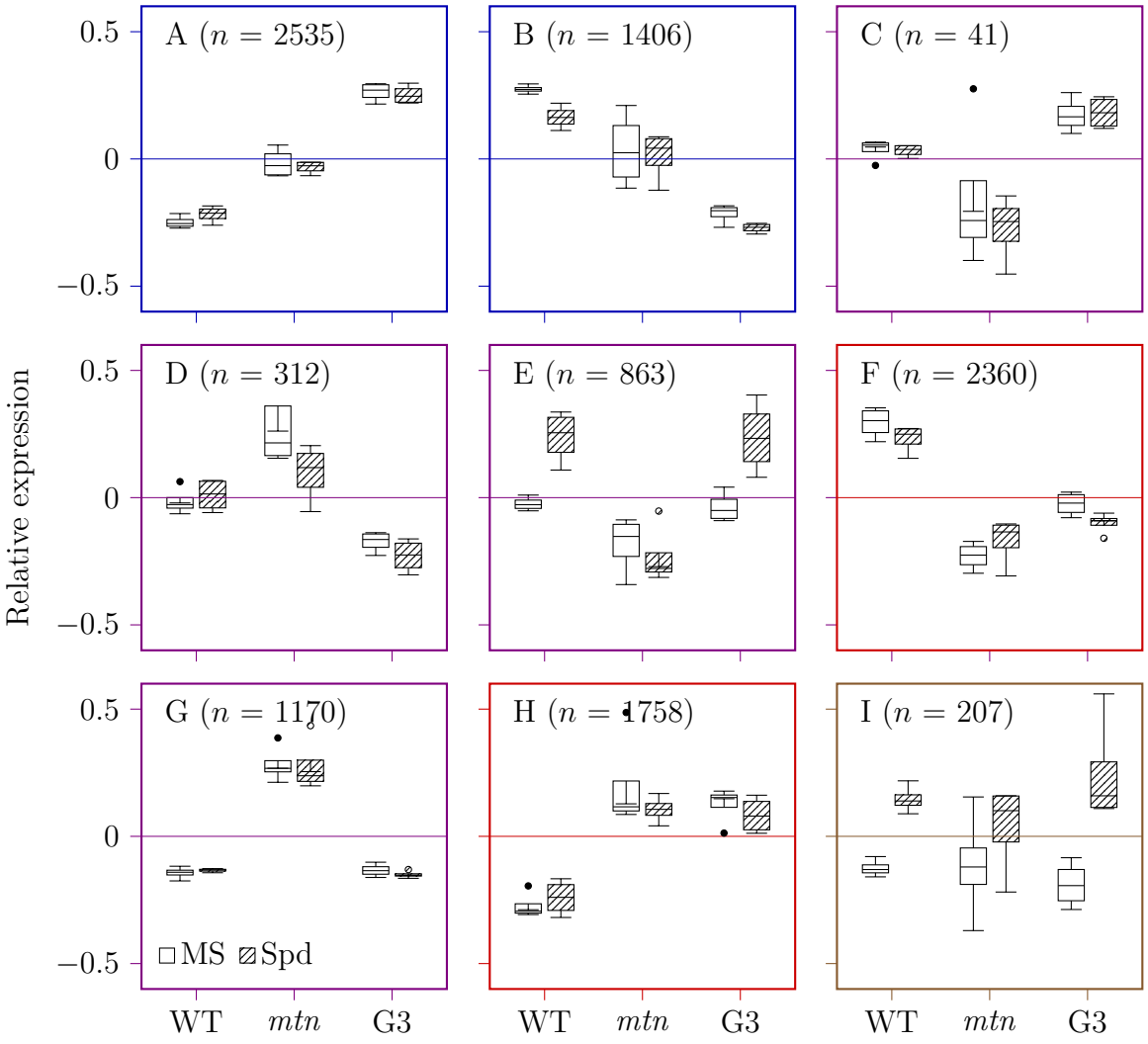

Figure 2.8: Gene expression clusters.

Genes from an RNAseq experiment were clustered based on expression. Clusters which showed sufficient variation between groups are shown. These are represented as the relative expression of the cluster genes between samples. Furthermore clusters were subdivided into types: type I clusters where genes are differently expressed between all genotypes (A, B), type II clusters were genes in WT and G3 samples are similarly expressed (C, D, E, G), type III clusters where *mtn1-1mtn2-1* and G3 samples are similarly expressed (F, H), and type IV clusters where genes are differently expressed between treatments (I).

In type II clusters, the expression level of genes in the WT samples were more similar to the G3 samples rather than the *mtn1-1mtn2-1* samples. The largest number of clusters were assigned as type II clusters: from C to G. The number of genes in these clusters varied quite significantly: C had 41 genes, D had 312, E had 863, and G had 1170. Of these clusters, in C and E the genes in the G3 samples had relatively lower expression; the opposite was true for D and G.

Both type III and IV had the fewest clusters, with F (originally classified as a type II cluster) and H belonging to type III, and I to type IV. Type III represented genes which were similarly expressed between the G3 and *mtn1-1mtn2-1* samples; and type IV represented genes whose expression differed between treatments. For clusters F and H the relative expression level of genes in the WT samples were lower; and for cluster I the relative expression of genes in the Spd-treated samples were higher. Cluster F had 2360 genes and cluster H had 1758 genes, whereas cluster I was a comparably smaller cluster with 207 genes.

Gene ontology analysis of gene expression clusters

To assign functions to the gene clusters in Figure 2.8, Gene Ontology (GO) enrichment was used (The Gene Ontology Consortium et al., 2000), specifically the Biological Process (BP) category of GO. For each cluster, enriched terms were tested for significance using Fisher's Exact Test with a cutoff of $Q < 0.01$. From these several terms with high Fold Enrichment (FE) were selected and shown in Table 2.2. In this table, all clusters (with the exception of cluster C) had significantly enriched terms.

When comparing the enriched terms between clusters, those in A and H have the biggest overlap. Both clusters have the ribosome biogenesis, RNA methylation, and translation

terms. Though these clusters are from different types (A is type I cluster where all genotypes expressed differently, H is type III cluster where *mtn1-1mtn2-1* and G3 samples are similarly expressed), they are similar in that the relative expression of the cluster genes is lower in the WT samples (Figure 2.7). Cluster A has a few additional terms which are not present in H, such as chloroplast organization and sulfur compound metabolic process. The other type III cluster F had a term for nucleotide-sugar biosynthetic process.

The other type I cluster (where all genotypes are differently expressed) with enriched terms, B, has mostly terms related to light and photosynthesis. The only exception is the term myo-inositol hexakisphosphate biosynthesis process. This term is actually among the most highly enriched, with a FE of 11.20.

The clusters D, E, and G generally have different terms despite all being type II clusters (where WT and G3 samples are similarly expressed). Cluster D has two terms with very high FE: proteasome assembly and response to misfolded protein. The term with the highest FE in cluster E is root hair elongation; and for cluster G, proteasome-mediated ubiquitin-dependent protein catabolic process. Considering that this was an RNAseq of buds, the root hair elongation term from cluster E does show that even if these GO terms are significantly enriched, they may not be necessarily accurate. Though these genes may be associated with root development, this does not prevent them from having additional functions relevant to the current tissue.

Finally cluster I has several enriched terms with very high FE: regulation of defence response, regulation of cell death, plant-type hypersensitive response, and protein targeting to membrane. Cluster I is part of the Spd-responsive type IV clusters. Spd in plants has been described as an anti-stressor and is involved in negating cell death (Moschou and Roubelakis-Angelakis, 2013). Though the relative expression of the genes within this cluster is increased in the Spd-treated samples (Figure 2.7), this does not necessarily contradict

the enriched GO terms. These terms can be quite vague; for example the genes represented by the regulation of cell death term are just as likely to be genes which induce cell death as those which suppress cell death.

Comparing treatments via statistical contrast

In Figure 2.6, all Spd-treated samples were slightly moved in the same direction compared to untreated samples. In order to find which genes are driving the consistent changes from Spd, the data was fitted using the generalized linear model approach of `edgeR` (Lun et al., 2016). This analysis allows for the creation of an experimental design in which specified variables (in this case genotypes) are factored out. Seeing as the possible Spd-driven changes seen in Figure 2.6 are quite subtle, the number of genes which drive this concerted movement of Spd-treated samples are accordingly few. These genes are described in Table 2.3. It is immediately apparent that the majority of the differentially expressed genes are up-regulated by Spd, consistent with the effect being across all genotypes.

With this approach a total of 49 genes were found to the significantly differentially regulated by Spd (Table 2.3). Despite this being a low number relative to the inter-genotypic numbers seen in Figure 2.7*a*, some of the fold changes are quite large, ranging from -5.81 ($\log_2$FC) to 5.22 ($\log_2$FC). These are approximately equivalent to 56–fold down-regulated and 37–fold up-regulated, respectively. Perhaps as a result of the size of the gene list (Table 2.3), a GO overrepresentation test of the list as a whole yielded few BP terms. To compensate, for each gene the most descriptive GO BP term was instead selected and included in Table 2.3. From these a few processes can be seen repeatedly: namely terms related to the cell wall and stress. These two terms may in fact be related however; a previous study has shown a link between increased water stress and increased cell wall-bound Spd (Hura et al., 2015).

Table 2.2: Enriched GO terms from gene expression clusters.

Genes from the gene expression clusters were used in a GO enrichment analysis. Those GO terms with Q values lower than 0.1 were included. Only cluster C did not have any significantly enriched GO terms.

Type	Cluster	Select GO BP*	FE†	P-value	Q-value
I	A	RNA modification	3.37	$5.32 \cdot 10^{-31}$	$7.89 \cdot 10^{-28}$
I	A	organophosphate biosynthetic process	2.28	$3.06 \cdot 10^{-30}$	$2.27 \cdot 10^{-27}$
I	A	nucleotide metabolic process	2.50	$5.40 \cdot 10^{-30}$	$2.67 \cdot 10^{-27}$
I	A	RNA methylation	4.11	$3.65 \cdot 10^{-26}$	$4.16 \cdot 10^{-24}$
I	A	ncRNA metabolic process	3.00	$8.51 \cdot 10^{-26}$	$7.01 \cdot 10^{-24}$
I	A	ribosome biogenesis	3.05	$1.92 \cdot 10^{-25}$	$1.50 \cdot 10^{-23}$
I	A	carbohydrate derivative biosynthetic process	2.02	$5.12 \cdot 10^{-19}$	$2.81 \cdot 10^{-17}$
I	A	translation	2.20	$4.16 \cdot 10^{-17}$	$2.20 \cdot 10^{-15}$
I	A	peptide biosynthetic process	2.20	$7.42 \cdot 10^{-17}$	$3.80 \cdot 10^{-15}$
I	A	chloroplast organization	2.95	$1.03 \cdot 10^{-16}$	$5.07 \cdot 10^{-15}$
I	A	sulfur compound metabolic process	1.95	$1.03 \cdot 10^{-14}$	$4.02 \cdot 10^{-13}$
I	A	generation of precursor metabolites and energy	2.01	$3.70 \cdot 10^{-14}$	$1.41 \cdot 10^{-12}$
I	B	myo-inositol hexakisphosphate biosynthetic process	11.20	$3.66 \cdot 10^{-33}$	$2.64 \cdot 10^{-30}$
I	B	alcohol biosynthetic process	7.04	$2.57 \cdot 10^{-27}$	$6.18 \cdot 10^{-25}$
I	B	photosynthesis, light reaction	3.12	$1.29 \cdot 10^{-13}$	$1.86 \cdot 10^{-11}$

Table 2.2 continued

Type	Cluster	Select GO BP*	FE†	P-value	Q-value
I	B	chlorophyll metabolic process	3.75	$1.22 \cdot 10^{-12}$	$1.46 \cdot 10^{-10}$
I	B	response to red light	4.85	$4.28 \cdot 10^{-12}$	$4.41 \cdot 10^{-10}$
I	B	response to blue light	3.65	$1.59 \cdot 10^{-8}$	$7.38 \cdot 10^{-7}$
I	B	cellular response to light stimulus	4.25	$1.41 \cdot 10^{-7}$	$4.96 \cdot 10^{-6}$
II	D	macromolecular complex assembly	5.77	$1.27 \cdot 10^{-22}$	$9.92 \cdot 10^{-20}$
II	D	proteasome assembly	11.17	$6.61 \cdot 10^{-20}$	$9.14 \cdot 10^{-18}$
II	D	response to misfolded protein	11.17	$6.61 \cdot 10^{-20}$	$9.14 \cdot 10^{-18}$
II	D	generation of precursor metabolites and energy	4.70	$4.56 \cdot 10^{-15}$	$2.52 \cdot 10^{-13}$
II	D	cellular metabolic compound salvage	9.02	$2.17 \cdot 10^{-14}$	$1.13 \cdot 10^{-12}$
II	D	response to cadmium ion	4.49	$8.30 \cdot 10^{-11}$	$2.65 \cdot 10^{-9}$
II	E	root hair elongation	4.01	$7.52 \cdot 10^{-9}$	$5.30 \cdot 10^{-6}$
II	E	cell growth	2.22	$9.50 \cdot 10^{-8}$	$4.35 \cdot 10^{-5}$
II	E	steroid metabolic process	3.22	$2.95 \cdot 10^{-7}$	$8.11 \cdot 10^{-5}$
III	F	nucleotide-sugar biosynthetic process	6.70	$7.62 \cdot 10^{-8}$	$1.25 \cdot 10^{-4}$
III	F	monosaccharide metabolic process	1.96	$7.54 \cdot 10^{-7}$	$4.17 \cdot 10^{-4}$
III	F	response to UV	2.06	$3.07 \cdot 10^{-6}$	$1.01 \cdot 10^{-3}$

Table 2.2 continued

Type	Cluster	Select GO BP*	FE†	P-value	Q-value
III	F	pollination	1.79	$2.37 \cdot 10^{-5}$	$5.55 \cdot 10^{-3}$
III	F	reactive oxygen species biosynthetic process	2.59	$9.35 \cdot 10^{-5}$	$7.30 \cdot 10^{-3}$
II	G	small molecule catabolic process	2.05	$6.19 \cdot 10^{-7}$	$8.32 \cdot 10^{-4}$
II	G	proteasome-mediated ubiquitin-dependent protein catabolic process	3.59	$1.33 \cdot 10^{-6}$	$8.77 \cdot 10^{-4}$
II	G	response to misfolded protein	2.98	$2.92 \cdot 10^{-6}$	$8.77 \cdot 10^{-4}$
II	G	DNA metabolic process	1.75	$2.54 \cdot 10^{-5}$	$2.84 \cdot 10^{-3}$
II	G	protein catabolic process	1.99	$3.13 \cdot 10^{-5}$	$3.23 \cdot 10^{-3}$
II	G	cell cycle	1.75	$3.75 \cdot 10^{-5}$	$3.60 \cdot 10^{-3}$
III	H	translation	5.06	$3.74 \cdot 10^{-85}$	$5.63 \cdot 10^{-82}$
III	H	peptide biosynthetic process	5.02	$1.59 \cdot 10^{-84}$	$1.20 \cdot 10^{-81}$
III	H	RNA methylation	6.86	$4.59 \cdot 10^{-48}$	$1.15 \cdot 10^{-45}$
III	H	methylation	3.60	$5.37 \cdot 10^{-39}$	$1.01 \cdot 10^{-36}$
III	H	macromolecule methylation	3.60	$5.37 \cdot 10^{-39}$	$1.01 \cdot 10^{-36}$
III	H	ribosome biogenesis	4.34	$3.97 \cdot 10^{-38}$	$6.63 \cdot 10^{-36}$
IV	I	regulation of defense response	9.79	$9.49 \cdot 10^{-30}$	$7.92 \cdot 10^{-27}$
IV	I	regulation of cell death	11.27	$1.35 \cdot 10^{-27}$	$2.26 \cdot 10^{-25}$
IV	I	plant-type hypersensitive response	11.07	$1.48 \cdot 10^{-26}$	$1.68 \cdot 10^{-24}$

Table 2.2 continued

Type	Cluster	Select GO BP*	FE†	P-value	Q-value
IV	I	protein targeting to membrane	11.16	$3.66 \cdot 10^{-25}$	$3.05 \cdot 10^{-23}$

*A selection of Gene Ontology Biological Process terms with low Q values.

†Fold enriched.

Table 2.3: RNAseq statistical contrast of treatments across genotypes.

The RNAseq data were used to extract genes differentially expressed between treatments, regardless of their expression between genotypes. This type of comparison is known as a statistical contrast. The RNAseq data was fitted to generalized linear model which takes into account genotypic and treatment gene expression changes, after which specific variables (such as genotype) can be subtracted out from the data. This leaves only the desired data for comparison: in this case, only changes between control and Spd treatments.

Gene ID	Symbol	Select GO BP*	$\log_2$FC†	P-value	Q-value
AT1G08930	ERD6	Response to water deprivation	1.5	$8.85 \cdot 10^{-5}$	0.0303
AT1G09950	RAS1	Transcription	1.83	$1.10 \cdot 10^{-3}$	0.0898
AT1G16130	WAKL2	Cell surface receptor signaling pathway	1.23	$2.56 \cdot 10^{-4}$	0.0467
AT1G35140	PHI-1	Response to hypoxia	1.49	$1.91 \cdot 10^{-4}$	0.0423
AT1G48000	MYB112	Response to salt stress	-1.28	$9.01 \cdot 10^{-7}$	0.0063
AT1G50040			1.12	$1.28 \cdot 10^{-3}$	0.0951
AT1G51800	IOS1	Defense response	1	$3.40 \cdot 10^{-4}$	0.0549
AT1G52830	IAA6	Response to auxin	1.4	$9.92 \cdot 10^{-4}$	0.0845
AT1G55450		Methylation	1.22	$1.37 \cdot 10^{-3}$	0.0975
AT1G73805	SARD1	Defense response	1.6	$6.46 \cdot 10^{-5}$	0.0261
AT1G78410		Response to oxidative stress	1.92	$1.44 \cdot 10^{-3}$	0.0991
AT2G18690			1.06	$1.25 \cdot 10^{-3}$	0.0943
AT2G20142		Signal transduction	1.63	$5.10 \cdot 10^{-4}$	0.0650
AT2G24600		Signal transduction	1.23	$9.46 \cdot 10^{-4}$	0.0825

Table 2.3 continued

Gene ID	Symbol	Select GO BP*	$\log_2$FC†	P-value	Q-value
AT2G27080			1.53	$1.27 \cdot 10^{-4}$	0.0333
AT2G32140		Defense response	1.01	$7.47 \cdot 10^{-4}$	0.0744
AT2G32210		Developmental process involved in reproduction	1.35	$3.53 \cdot 10^{-4}$	0.0564
AT2G34600	JAZ7	Response to jasmonic acid	1.02	$1.35 \cdot 10^{-4}$	0.0345
AT2G39200	MLO12	Cell death	1.58	$2.39 \cdot 10^{-5}$	0.0210
AT2G41100	TCH3	Response to temperature	1.48	$4.39 \cdot 10^{-5}$	0.0225
AT2G45220		Cell wall modification	−4.9	$1.33 \cdot 10^{-5}$	0.0151
AT2G46400	WRKY46	Response to chitin	1.03	$9.06 \cdot 10^{-5}$	0.0305
AT3G02790		Cellular response to singlet oxygen	−5.07	$8.24 \cdot 10^{-5}$	0.0301
AT3G04210		Defense response	1.12	$5.62 \cdot 10^{-5}$	0.0252
AT3G12910		Transcription	2.19	$1.94 \cdot 10^{-4}$	0.0423
AT3G16530		Response to chitin	2.34	$6.55 \cdot 10^{-4}$	0.0727
AT3G19680			1.21	$1.38 \cdot 10^{-3}$	0.0975
AT3G44300	NIT2	Indoleacetic acid biosynthetic process	−1.58	$8.73 \cdot 10^{-4}$	0.0804
AT3G50930	BCS1	Cell death	1.1	$1.22 \cdot 10^{-5}$	0.0151

Table 2.3 continued

Gene ID	Symbol	Select GO BP*	$\log_2$FC†	P-value	Q-value
AT4G01950	GPAT3	Cutin biosynthetic process	1.05	$3.15 \cdot 10^{-4}$	0.0534
AT4G02330	ATPMEPCRB	Cell wall modification	1.18	$3.51 \cdot 10^{-5}$	0.0225
AT4G13340	LRX3	Cell wall organization	1.03	$2.64 \cdot 10^{-4}$	0.0477
AT4G14365	XBAT34	Protein ubiquitination	1.3	$1.10 \cdot 10^{-4}$	0.0325
AT4G16820	PLA-Iβ2	Lipid metabolic process	1.55	$6.41 \cdot 10^{-4}$	0.0722
AT4G18253			1.72	$4.00 \cdot 10^{-5}$	0.0225
AT4G30280	XTH18	Cell wall biogenesis	1.97	$9.07 \cdot 10^{-4}$	0.0810
AT4G31540	EXO70G1	Exocytosis	-5.81	$1.49 \cdot 10^{-4}$	0.0372
AT4G31800	WRKY18	Defense response	1.32	$9.96 \cdot 10^{-7}$	0.0063
AT5G19230			1.32	$9.20 \cdot 10^{-4}$	0.0822
AT5G24110	WRKY30	Response to salicylic acid	2.33	$1.15 \cdot 10^{-3}$	0.0912
AT5G25240			1.08	$6.24 \cdot 10^{-4}$	0.0718
AT5G25930		Protein phosporylation	1.14	$2.82 \cdot 10^{-5}$	0.0210
AT5G52750		Metal ion transport	1.8	$5.47 \cdot 10^{-5}$	0.0251
AT5G52760		Metal ion transport	1.82	$2.15 \cdot 10^{-4}$	0.0442
AT5G54710		Signal transduction	1.85	$1.17 \cdot 10^{-5}$	0.0151
AT5G54720			1.64	$5.13 \cdot 10^{-4}$	0.0650

Table 2.3 continued

Gene ID	Symbol	Select GO BP*	$\log_2$FC†	P-value	Q-value
AT5G56960		Response to chitin	5.22	$4.39 \cdot 10^{-5}$	0.0225
AT5G57560	TCH4	Cell wall biogenesis	1.65	$2.55 \cdot 10^{-4}$	0.0467
AT5G64120		Response to oxidative stress	1.07	$8.82 \cdot 10^{-5}$	0.0303

*Low order Gene Ontology Biological Process term which best describes gene function.

†Log_2 Fold change. Positive values represent higher expression in Spd-treated samples

2.3.3 Combining the metabolite and transcriptomics datasets

Finding gene cluster-metabolite associations

As both metabolite measurements and transcript quantification data were available for the same tissue, genotypes and treatments, this provided an opportunity to combine these and gain new insights into the effects of MTA accumulation and fertility restoration by Spd feeding. This data combination process was done by correlating the profile of metabolite and transcript levels of WT, *mtn1-1mtn2-1*, and G3 samples, for MS and Spd treatments. The transcript profiles used were the clusters shown in Figure 2.8. The metabolites used for comparison are those from Figures 2.2, 2.3, 2.4, and 2.5. The correlation scores are shown as a heatmap in Figure 2.9, where the strength of the colour at intersection between metabolites and clusters represents how closely their profiles are matched.

Regarding the correlation scores, it is important to note that these are based on the 'shape' of the metabolite and gene expression profiles between samples – not the direction. For example, the score between cluster F and MTA is above 0.9 despite the fact that in Figure 2.8 cluster F shows a decreased expression in the *mtn1-1mtn2-1* and G3 samples, whereas in Figure 2.2 MTA levels are increased in these samples. Of course, the direction of relative gene expression change for the clusters does not necessarily have any implications regarding the overall function of the cluster genes, since they can have either activating or suppressing functions.

From Figure 2.9, two type II clusters and one type III cluster have very high correlation scores with several metabolites. The first is cluster F (type II), which has scores above 0.8 with Met, MTA, NA, Put, and SAH. This cluster, along with these metabolites, are interesting due to the fact that most of these show a large difference between WT and

mtn1-1mtn2-1, and a minor recovery in G3 towards WT. The only exceptions are NA (Figure 2.3d) and Met (Figure 2.4f), where G3 levels stay similar to *mtn1-1mtn2-1*.

Cluster H (type III) is slightly similar to F, having scores above 0.8 with Met, MTA, and NA. Looking at the gene expression profile of cluster H (Figure 2.8) reveals that unlike cluster F, G3 levels do not recover towards WT. This is also the case for Met (Figure 2.4f) and NA (Figure 2.3d), and though MTA does show some recovery it is still quite modest (Figure 2.2f).

Finally cluster G (type II) has scores above 0.8 with Cys, Put, SAH, and SAM (Figure 2.9). Looking at Figure 2.8, this cluster is particularly interesting since while *mtn1-1mtn2-1* levels are quite different from WT, G3 levels have completely recovered back to WT. Among the high scoring metabolites, SAM (Figure 2.2d) and Cys (Figure 2.4d) also follow this trend. As for the other metabolites, SAH (Figure 2.2e) and Put (Figure 2.3e) show a near complete recovery, and MTA (Figure 2.2f) shows a modest recovery in G3.

Examining sulfur usage in the combined data

To examine the effects of MTA accumulation on sulfur-related processes, and more specifically, SAM-utilizing reactions, metabolite and transcript quantification data from unopened buds for *mtn1-1mtn2-1* and G3 were combined and shown on a map of the relevant pathways (Figure 2.10). Since generally the Spd treatment did not greatly affect metabolite and transcript levels intra-genotypically, only samples untreated were considered.

When looking at changes only concerning *mtn1-1mtn2-1* in Figure 2.10, generally there appears to be a decrease in the levels of sulfur-containing metabolites. Among the quantified metabolites, Cys, Met, SAM and NA all decrease, with GSH and Spd being unchanged. This is supported by a decrease in several key transcripts such as *MS2*, *SAM1* and *SAM2*.

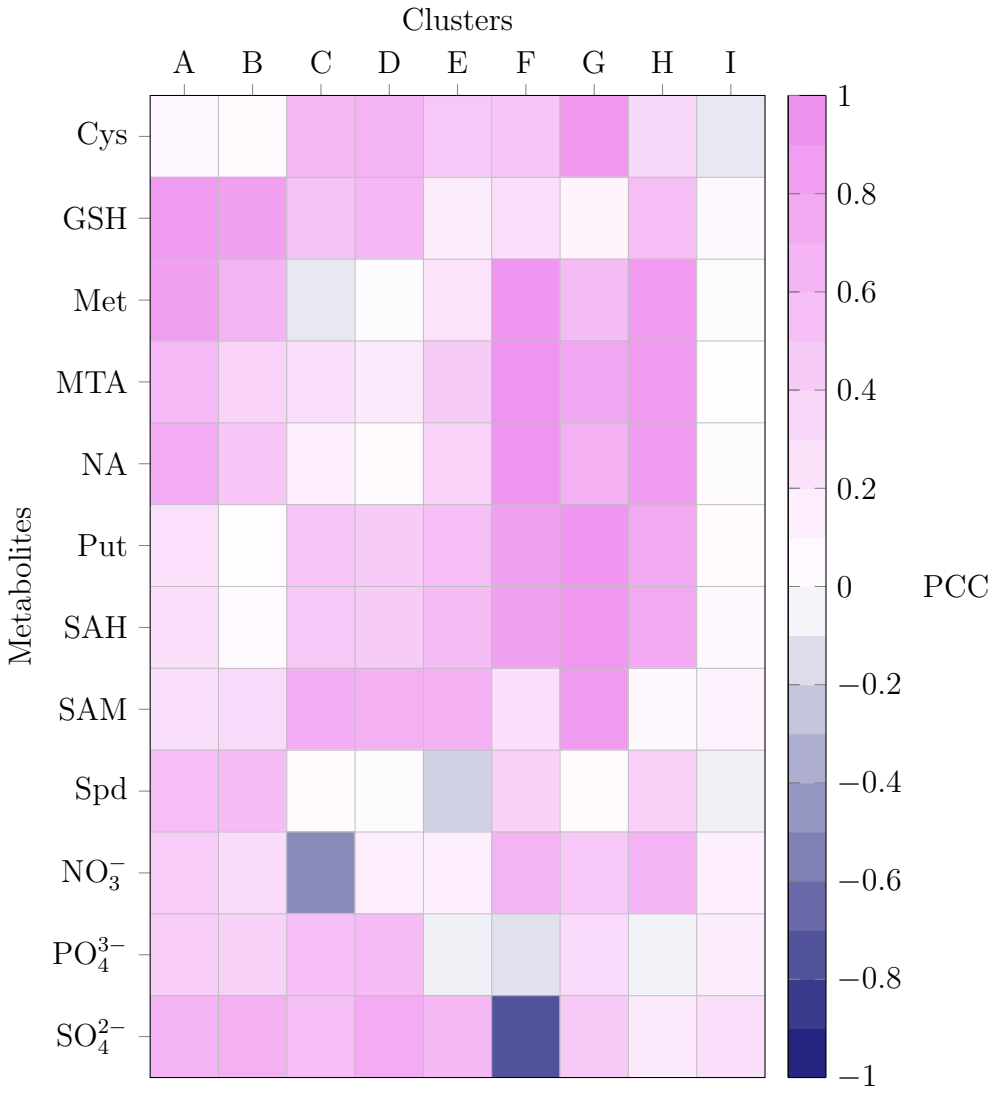

Figure 2.9: Correlating gene cluster expression and metabolite levels.

The relative gene expression profiles of the clusters were correlated with the metabolite profiles of unopened bud samples. The Pearson Correlation Coefficient (PCC) correlation score is represented in the heatmap by colour strength. This was done for the WT, *mtn1-1mtn2-1*, and G3 genotypes; and for MS and Spd treatments.

Interestingly the SAMDC transcripts *SAMDC1*, *SAMDC2* and *SAMDC4* all show increases, alongside SPDS transcripts *SPDS1* and *SPDS2*. Taken together, alongside increased Put levels, these increases suggest the plant may be attempting to offset decreased SAM to buffer Spd levels.

As for G3 levels of sulfur-containing metabolites, a partial recovery can be seen in Figure 2.10. Both Cys and SAM levels recover in G3, though interestingly this is not accompanied by increases in the transcript abundances of *MS2*, *SAM1* and *SAM2*. Furthermore while Spd levels remain unchanged, Put levels are recovered. Curiously, *SPDS1* and *SPDS2* transcript abundances increase yet again in G3.

2.3.4 Investigating DNA methylation

Changes in the methylation index

As it is hypothesized that the trans-generational fertility observed in G3 is linked to epigenetic inheritance of a certain DNA methylation profile, it was important to look for evidence of epigenome changes. This was first made possible using existing data: namely, SAM and SAH levels. These metabolites can be used to calculate the methylation index, shown in Figure 2.11. This particular index can be used as a predictor of the state of global DNA methylation (Caudill et al., 2001). Decreases in the ratio correspond with global DNA hypomethylation, though only when SAH levels are increased (Caudill et al., 2001). This means that a lower ratio from solely a reduction in SAM does not correspond with global DNA hypomethylation.

Looking at both seedlings and unopened buds in Figure 2.11, no conclusion can be drawn regarding the state of global DNA methylation of seedlings (Figure 2.11*a*). Rather,

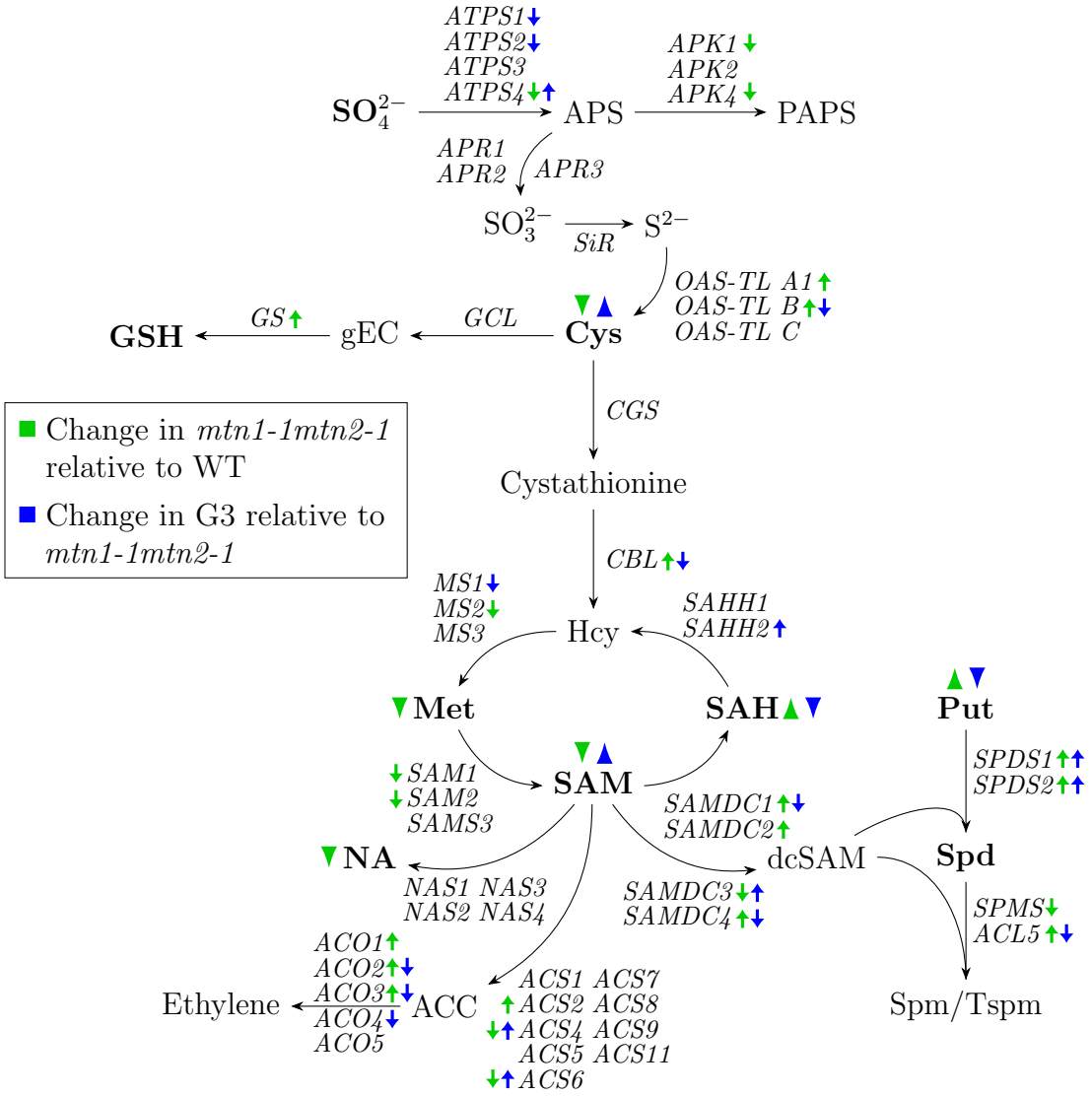

Figure 2.10: Metabolite and gene expression levels in sulfur usage.

Gene expression and metabolite data from unopened buds mapped onto sulfur usage and MTA-related pathways. Metabolites which were measured in this thesis are in bold. Gene expression data is from an RNAseq experiment. Metabolites and genes which changed significantly in *mtn1-1mtn2-1* relatively to WT have green arrows, and those which changed significantly in G3 relative to *mtn1-1mtn2-1* have blue arrows. Since generally MS and Spd samples for the metabolite and RNAseq experiments were similar, only differences between MS samples are shown. For changes to be significant, $p < 0.05$ was used as a threshold for the metabolite data (Tukey HSD post-hoc test after one-way ANOVA) and FDR < 0.1 for the RNAseq data.

it is clear that the methylation index is much more stable in buds (Figure 2.11*b*). Here it can be seen that there is a much lower ratio in *mtn1-1mtn2-1*, and a partial recovery in G3. This is accompanied by a similar pattern of increased SAH levels in *mtn1-1mtn2-1* with partial recovery for G3 (Figure 2.2*e*). Taken together, these observations suggest a state of global hypomethylation in *mtn1-1mtn2-1*, with a slight recovery in G3.

Examination of differentially expressed methylated genes

The RNAseq data from unopened buds were further investigated to explore the possibility of changes in the DNA methylation profile of *mtn1-1mtn2-1* and G3. Since transcription is heavily affected by methylation (Zhu et al., 2016), changes in the methylation of the genome may perhaps be reflected in the transcriptome. A previous study characterized the DNA methylome of unopened buds (Lister et al., 2008). This dataset was obtained for a more accurate comparison of transcription (from the RNAseq) and DNA methylation.

Using this DNA methylation data from unopened buds, genes were labelled as having high CpG, CHG, or CHH methylation. Genes were further classified based on whether these methylation marks were enriched in the promoter or within the gene body. These categories were the basis of an overrepresentation analysis of the differentially expressed genes in the RNAseq presented here, as seen in Figure 2.12. Based on this analysis, genes with gene body CpG methylation are overrepresented in the up-regulated genes of *mtn1-1mtn2-1* and G3 relative to WT. Interestingly, gene body CpG methylation is associated with constitutively transcribed genes in Arabidopsis (To et al., 2015). Based on the findigs of To et al. (2015), MTN-deficiency is correlated with the methylation state of actively transcribed genes. Furthermore it appears that there are a significant number of genes down-regulated in G3 compared to *mtn1-1mtn2-1* which have gene body CpG methylation, perhaps indicating a slight reversal of the gene body CpG methylated genes' up-regulation by MTN-deficiency.

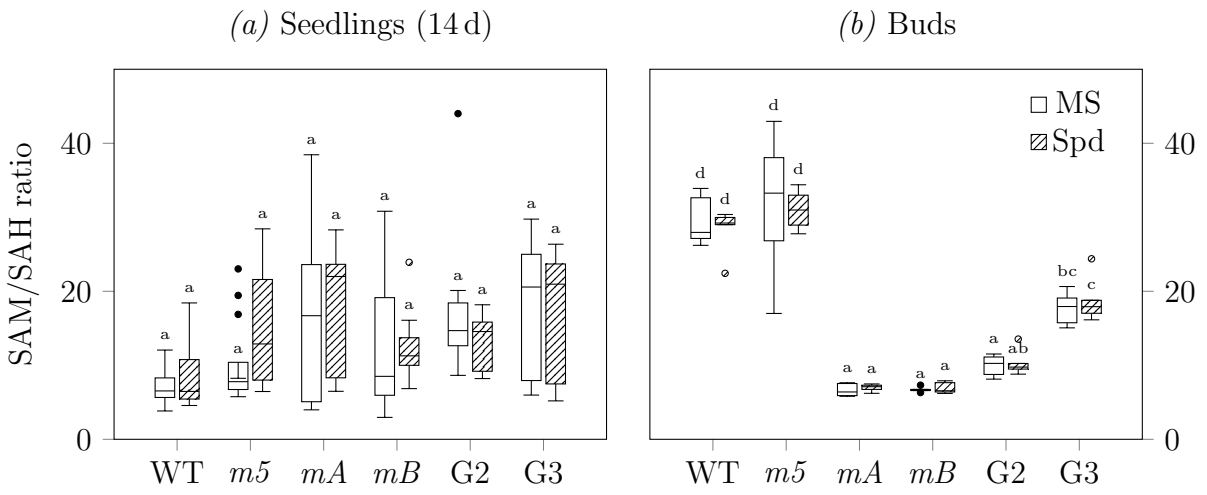

Figure 2.11: Quantifying changes in the methylation index.

HPLC measurements of *S*-adenosylmethionine (SAM) and *S*-adenosylhomocysteine for 14d seedlings *(a)* and buds *(b)* were used to calculate the methylation index. For each individual sample, the observed SAM levels were divided by the observed SAH levels. A reduction in the ratio has been shown to correlate with DNA hypomethylation (Caudill et al., 2001). Measurements were grouped based on genotype and treatment. Letters represent significant difference results from a Tukey HSD post-hoc test after a one-way ANOVA ($p < 0.05$), $n = 5$. Boxes which do no share any common letters are significantly different. *m5, mtn1-1mtn2-5. mA, mtn1-1mtn2-1* (parent with a WT copy of MTN1). *mB, mtn1-1mtn2-1* (parent with a WT copy of MTN2).

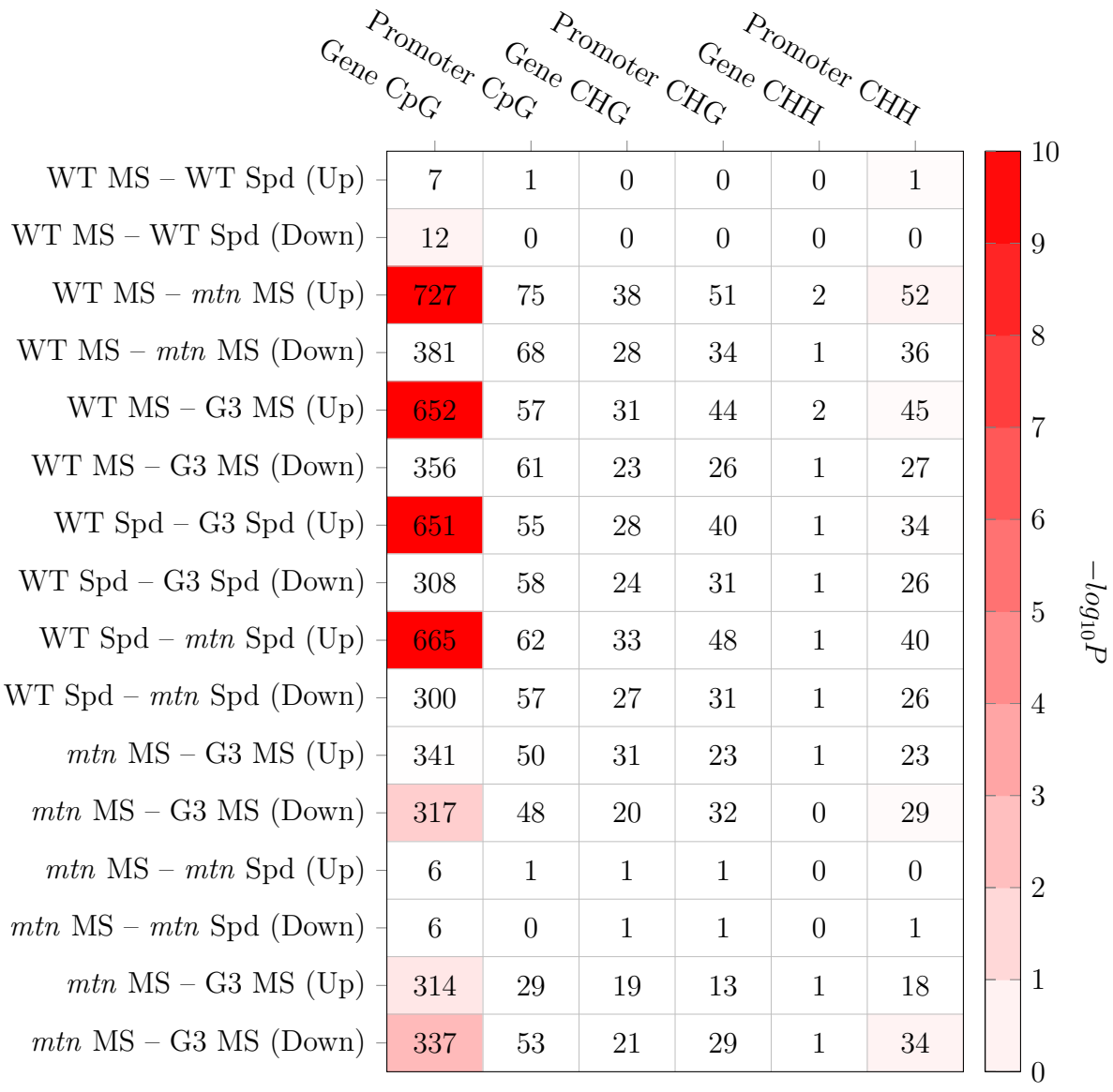

Figure 2.12: Testing for overrepresentation of methylated genes.

Bisulfite sequencing data from WT unopened buds was used to categorize genes based on their gene methylation profiles. Methylation type was divided as being gene body or promoter, and furthermore by cytosine context (CpG, CHG, and CHH). Categorized genes were used as the basis for an overrepresentation test of genes from an RNAseq experiment of unopened buds. Significance was tested for using Fisher's Exact Test. The number in each square represents the number of differentially expressed genes between the sample comparison in each particular methylation catergory.

Chop PCR analysis

siRNAs in the Arabidopsis genome can associate with chromatin and guide DNA methylation in a process called RNA-directed DNA Methylation (RdDM) in order to silence transposons and genes (Chapman and Carrington, 2007). A previous study found several loci to be under RdDM regulation, including AT3TE60430 and AT1G67105, which were hypomethylated in RdDM-deficient mutants (Kurihara et al., 2008). The general methylation status of these loci can be tested using an assay known as Chop PCR, where methylated DNA is digested using a methylation-specific enzyme before the target regions are amplified with PCR (Zhang et al., 2014). If the target regions amplify, then this suggests the region was free of methylation. This assay was done for *mtn1-1mtn2-1* and G3 plants using genomic DNA from unopened buds.

As seen in Figure 2.13, both of the tested loci appear to be mostly methylated in WT. For AT3TE60430, *mtn1-1mtn2-1* and G3 are also methylated. This is not the case for AT1G67105, where fairly strong bands from the digested samples are seen (though these are not as strong as the bands from the undigested controls). One interesting aspect is that the G3 fragments appear stronger than the *mtn1-1mtn2-1* bands. Furthermore, one of the *mtn1-1mtn2-1* fragments is quite weak.

2.3.5 Investigating PRMT5 in *mtn1-1mtn2-1*

Comparing the *mtn1-1mtn2-1* mRNA splicing profile to *prmt5*

It was recently shown that MTA accumulation has a strong inhibitory effect on human PRMT5, which is believed to lead to strong anti-proliferative effects in human cell lines (Kryukov et al., 2016; Marjon et al., 2016; Mavrakis et al., 2016). To evaluate the possibility

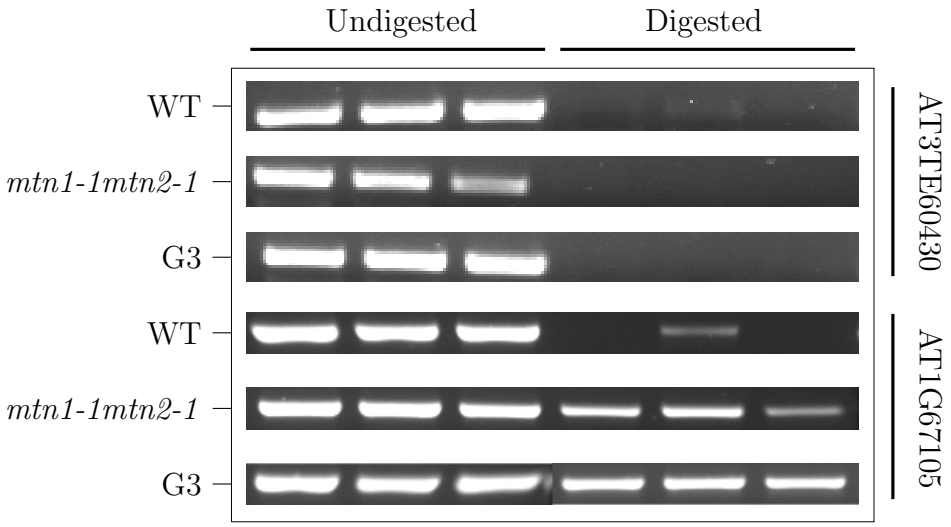

Figure 2.13: Chop PCR DNA methylation analysis.

Genomic DNA from unopened buds was digested using the methylated DNA-specific McrBc endonuclease. Primers were used to amplify regions known to be methylated by the RNA-directed DNA methylation pathway (AT3TE60430 and AT1G67105). The undigested samples serve as PCR controls. Fragments appearing in the digested samples represent successful amplification of unmethylated DNA.

of PRMT5 as a candidate target of MTA inhibition in Arabidopsis, an easy first step was to look for commonalities between the phenotypes of PRMT5 and MTN mutants. One available way to use the RNAseq data presented here is to look for the irregular alternative splicing phenotype described in *prmt5* mutant plants (Hernando et al., 2015). Arabidopsis *prmt5* mutant seedlings have alterations in alternative splicing, such as intron retention (Hernando et al., 2015). The alternative splicing profile of *prmt5* seedlings was compared to that of *mtn1-1mtn2-1* and G3 unopened buds in Figure 2.14. Here it can be confirmed that *prmt5* mutant plants have a large increase in the number of events related to intron gain and exon loss (as opposed to intron loss and exon gain) as discussed in the original study (Hernando et al., 2015). When comparing these changes to G3 and *mtn1-1mtn2-1* buds, this effect is not observed. Intron gain and exon loss events are in fact not favoured but observed at lower rates than intron loss and exon gain.

Disruption of the cell cycle by MTA

Another phenotype of *prmt5* mutant plants is cell cycle arrest at the G2 phase in root meristems (Li et al., 2016a). This can be investigated by monitoring the expression of the G2 phase cell cycle gene *CYCB1;1*. Mutants plants lacking PRMT5 accumulate pCYCB1;1-GUS and increasing CYCB1;1 transcript abundance as root meristem cells fail to move to the M phase of the cell cycle (Li et al., 2016a). The presence of G2 phase cell cycle arrest was investigated in *mtn1-1mtn2-1* plants using the pCYCB1;1-GFP reporter to record the effects of MTN-deficiency on the root meristem (Figure 2.15). Furthermore, the use of this reporter also provided the opportunity to validate the presence of the cell cycle GO term enriched from cluster H in Table 2.2.

The expression of pCYCB1;1-GFP was used for three separate calculations in roots: meristem area (Figure 2.15*b*), pCYCB1;1-GFP intensity (Figure 2.15*c*), and meristem

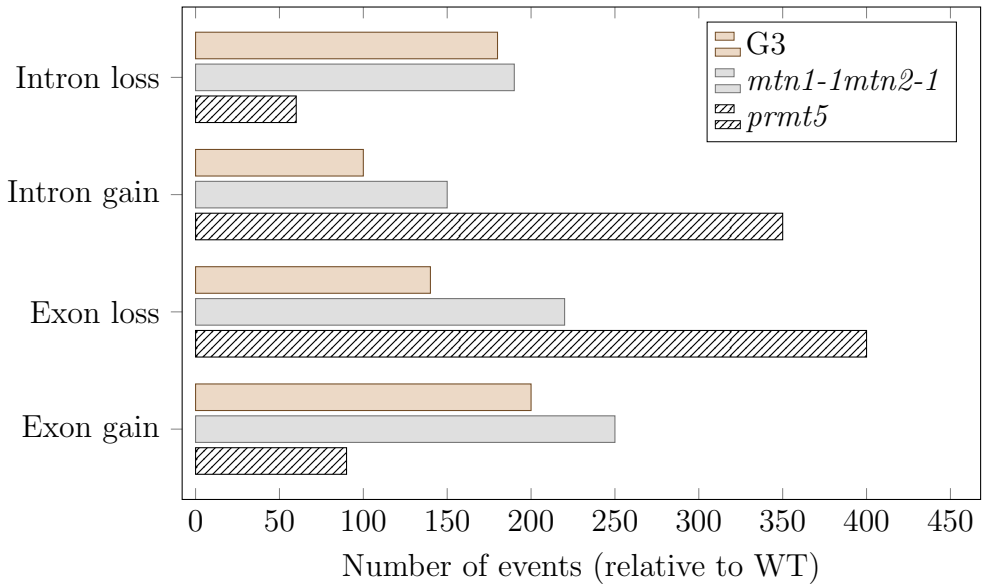

Figure 2.14: Bud RNAseq alternative splicing analysis.

Using mRNA splicing information from RNAseq data of WT as a baseline, differential splicing events for mutant samples were summarised. All genotypes, with the exception of *prmt5*, are from a single RNAseq experiment of unopened buds. The *prmt5* RNAseq experiment is of 14d old seedlings. Alternative splicing events were categorized as intron loss, intron gain, exon loss, or exon gain.

length (Figure 2.15*d*). For all three measurements *mtn1-1mtn2-1* roots had significantly lower values (Figure 2.15). The decreased pCYCB1;1-GFP signal intensity result of *mtn1-1mtn2-1* (Figure 2.15*c*) is inconsistent with the pCYCB1;1-GUS accumulation result of *prmt5* mutants (Li et al., 2016a).

2.3.6 Restoration of fertility by decapitation

The shoot apical meristem of plants plays a large role in regulating axillary branching (Leyser, 2003). Accordingly, decapitating the shoot apical meristems can have large effects on other parts of the plant both in terms of hormone and gene expression levels. In *Pisum sativum* L. seedlings, decapitation of the shoot apical meristem resulted in 2–3 fold decrease in the auxin IAA and a 5–6 fold increase in the cytokinins zeatin and zeatin riboside in the leftover stem (Kotova et al., 2004). In Arabidopsis, decapitation induces large changes in the expression of genes related to sugar usage, the cell cycle and protein synthesis in axillary shoots (Tatematsu et al., 2005).

It was accidentally observed in *mtn1-1mtn2-1* mutants that after decapitation, flowers in close proximity to the site of decapitation became fertile. This fertility recovery could be seen as early as two days post decapitation. The fertility was recorded in Figure 2.16. Decapitation would, most of the time, cause the three flowers closest to the site of decapitation to recover their fertility. Flowers in position 4–6 would also become fertile in approximately half of the decapitated branches (Figure 2.16). Beyond this, the flowers were more likely than not to remain infertile, suggesting that there may be a growth stage cutoff for fertility recovery by decapitation.

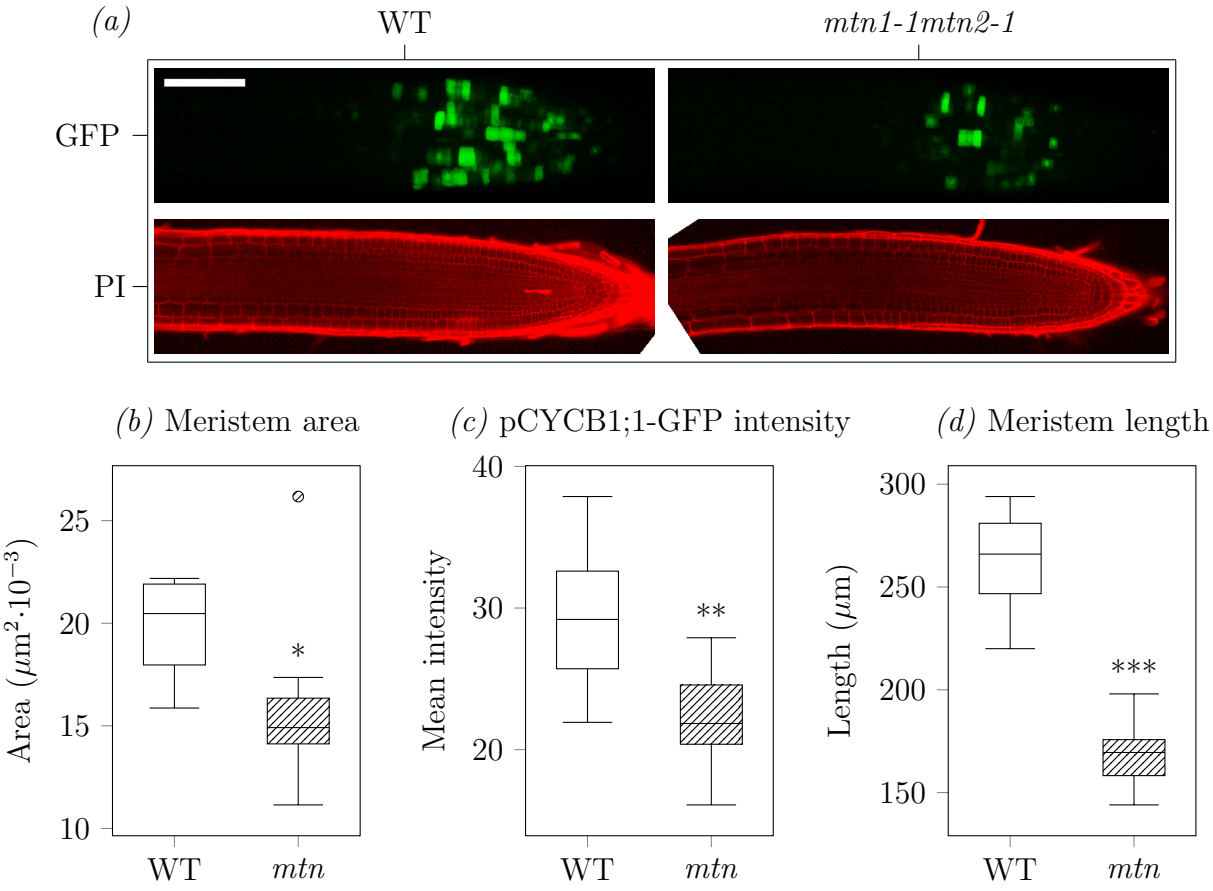

Figure 2.15: Root cell cycle analysis.

WT and *mtn1-1mtn2-1* (*mtn*) seedlings were grown vertically on MS media for 5–7 days. Roots were imaged with confocal microscopy *(a)*, with GFP signal in green and cell wall staining (propodium iodide, PI) in red. The meristem area *(b)* was determined as the region of the root tip with pCYCB1;1-GFP expression, or in other words the approximate zone of cell division. Signal intensity of pCYCB1;1-GFP *(c)* was also quantified. Finally, the length of the meristem *(d)* was quantified as the distance between the quiescent centre and the beginning of the elongation zone. Stars represent significant difference from Student's T-Tests (***$p < 0.001$, **$p < 0.01$, *$p < 0.05$), $n = 10$. Scale bar represents 300 µM. This experiment was done twice with similar results.

(a) Decapitation at 0 d

(b) Decapitation at 7 d

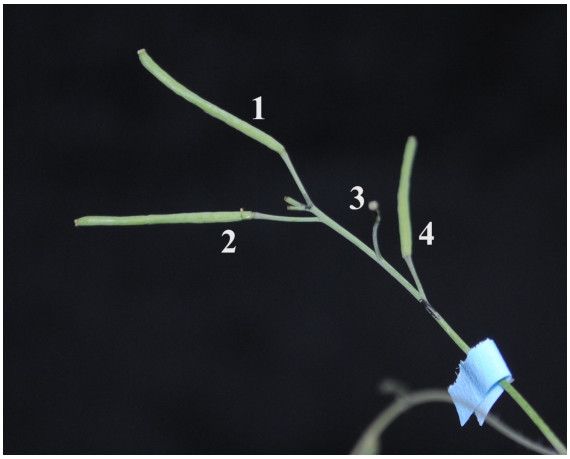

(c) Flower position and fertility ($n = 25$)

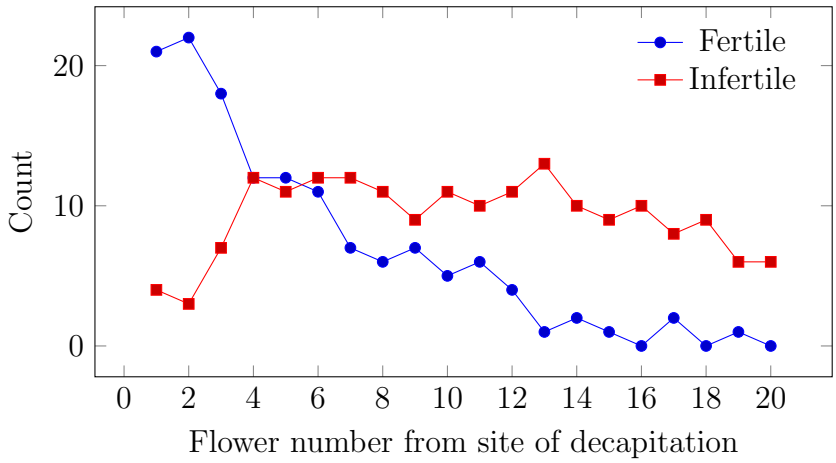

Figure 2.16: Inducing fertility in *mtn1-1mtn2-1* by decapitation.

The apical unopened bud clusters of *mtn1-1mtn2-1* were decapitated. The plants were imaged for at least a week post decapitation *(a, b)*. At this point the leftover flowers on decapitated branches were observed for fertility *(c)*. A total of 25 decapitated branches were observed, with a minimum of 3 and a maximum of 20 flowers below the site of decapitation recorded for fertility restoration.

2.3.7 Preliminary ROS quantification in *mtn1-1mtn2-1*

Several enriched GO terms from the clusters in Table 2.2 are related to ROS. ROS are especially relevant for unopened buds. For fertilization to occur, pollen are completely dependent on proper regulation of ROS (Mangano et al., 2016). ROS help mediate cell wall loosening, which is required for the polar growth of pollen tubes (Mangano et al., 2016). To determine the GO terms from the RNAseq are representative of *in vivo* alterations of ROS in *mtn1-1mtn2-1* the redox state reporter roGFP2 (Schwarzländer et al., 2008) was used to quantify the redox state of roots. Higher ROS levels correlate with increased oxidation of the roGFP2 protein. As shown in Figure 2.17, a slight but not significant increase in the ratio of oxidized to reduced roGFP2 was detected in *mtn1-1mtn2-1*.

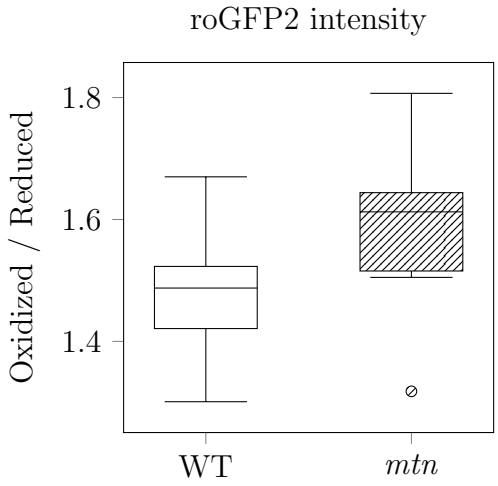

Figure 2.17: Preliminary quantification of the redox state of roots.

WT and *mtn1-1mtn2-1* (*(mtn)*) seedlings were grown vertically for 5–7 days on MS media. The roots were imaged with confocal microscopy, recording the signal intensity of the roGFP2 reporter. Both oxidized and reduced states of the reporter were quantified, and the ratio between the two calculated as a measure of the redox state of the root. No significant difference was detected using a Student's T-Test, $n = 10$. This experiment was done twice with similar results.

2.4 Discussion

2.4.1 Developmental stage-specific effects of MTN deficiency and Spd restoration

Several sulfur-related metabolites were measured from 14 d seedlings and buds of WT, *mtn1-1mtn2-5*, *mtn1-1mtn2-1*, G2, and G3 plants. When comparing the data of WT between samples it is clear they have differing metabolite profiles. It is known that the metabolite profiles of different tissues are not identical (Petersson et al., 2015). Regarding for the MTN-deficient lines, two main observations are seen: the developmental stage-specific metabolite profiles were greatly affected by differing levels of MTN-deficiency, and Spd restoration.

The MTA content of unopened buds in the MTN-deficient lines is quite different. Despite the levels of MTN activity of both *mtn1-1mtn2-1* and *mtn1-1mtn2-5* inflorescences being quite low (14.9% and 28%, respectively; Waduwara-Jayabahu, 2011), *mtn1-1mtn2-5* has similar MTA content to WT whereas *mtn1-1mtn2-1* has over ten times as much (Figure 2.2*f*). It appears that there is a tipping point (or threshold) in MTN activity that is associated with MTA accumulation; below this level of MTN activity, MTA content remains stable.

The MTA content of both *mtn1-1mtn2-1* and *mtn1-1mtn2-5* in 14 d seedlings is quite similar to WT (Figure 2.2*c*). This is likely because there is less MTA accumulation in the various seedling tissues. Not only is there less than half the amount of MTA in WT seedlings compared to unopened buds (Figure 2.2*c*, 2.2*f*), there is also less than a third the amount of SAM (the precursor of reactions which generate MTA as a byproduct) in

seedlings (Figure 2.2*a*, 2.2*d*). NA and Spd which are synthesized in reactions that produce MTA as a by-product, are similarly reduced (Figure 2.3*a*, 2.3*c*, 2.3*d*, 2.3*f*). Taken together, the tipping point of MTN activity is dependent on the amount of MTA being produced. In the case of seedlings, the reduced MTA pressure would consequently result in a lower tipping point.

Generally Spd treatment (within a generation) had very little impact on the clustering of differently treated samples within genotypes for metabolite abundance (Figure 2.1). There are two possible explanations for this. One is that the restorative effects of Spd are dependent on spatial or temporal factors. The other explanation is that there may be some relation between MTA accumulation (which could itself be dependent on spatial or temporal factors) and the effects of Spd restoration, such that the restorative effects are only revealed when a tissue or organ is experiencing a certain level of MTA pressure.

All of the above conclusions are dependent on there being a large difference in the metabolic requirements of seedlings or unopened buds (especially the relevance of pathways which generate MTA as a byproduct). Though the data presented in this chapter are insufficient to directly implicate this, one possible trigger for this change is the transition from the vegetative stage to the reproductive stage. This transition is associated with great changes in metabolism in general (Kooke and Keurentjes, 2011). Among these are those induced by increased shoot apical meristem activity, such as specification of floral identity and increased cell cycle activity (Gilbert, 2000). This increased rate of metabolism may well be contributing to the increased MTA pressure, which is also consistent with the transcript abundance of both *MTN1* and *MTN2* in the shoot apical meristem peaking at the transition stage (retrieved from the Arabidopsis eFP Browser on November 1st, 2018; Winter et al., 2007).

The association between flowering transition and changes in the shoot apical meristem

are consistent with Spd restoration having an epigenetic aspect (as suggested by Waduwara-Jayabahu et al., 2012). In fact, previous studies have noted changes in the epigenome of the shoot apical meristem during this time period (You et al., 2017). Spd-induced changes in the epigenome of MTN-deficient plants may be dependent on changes induced by the flowering transition. It is also possible that the Spd-induced changes may even be contributing to the development of the shoot apical meristem during transitioning, as seen by the partial reversal of the late-flowering phenotype of *mtn1-1mtn2-1* in Spd-restored lines: whereas no *mtn1-1mtn2-1* plants bolt at five weeks, 69% of G3 plants do (Waduwara-Jayabahu, 2011).

The lack of evidence of any MTA accumulation in seedlings suggests they are experiencing relatively little MTA pressure in all studied MTN-deficient genotypes (Figure 2.2*c*). However it is important to note that previous studies have shown that both *mtn1-1mtn2-1* and *mtn1-1mtn2-5* exhibit a number of mutant phenotypes in seedlings, such as interveinal chlorosis, cuticle defects, slower true leaf development, and altered vasculature (Waduwara-Jayabahu, 2011; Waduwara-Jayabahu et al., 2012). Though the evidence provided in this chapter shows no evidence of increased MTA accumulation in seedlings (Figure 2.2*c*), this does not mean that the plants are free of the effects of MTA. Rather it could be simply that the current experimental design for the quantification of metabolites in seedlings was not designed to capture tissue-specific data. For the seedling measurements, whole seedlings were collected which masks tissue or cell-type specific MTA accumulation. It is worth mentioning though that NA levels are lower in *mtn1-1mtn2-1* seedlings (Figure 2.3*a*), which may be an example of a particular MTA-affected process which is not masked by the collection and quantification method.

An additional possibility to consider is that the MTN protein itself may have additional functions aside from MTA hydrolysis, though currently there is no physiological evidence for this. Both MTN isoforms physically interact *in vitro* with CBL3 (Oh et al., 2008; Ok

et al., 2015). CBL3 has been implicated in the regulation of calcium responses (Batistic et al., 2010), magnesium homeostasis (Tang et al., 2015), potassium transport (Liu et al., 2013), osmotic and salt stress responses (Pandey et al., 2015), seed size and embryonic growth (Eckert et al., 2014), pollen growth (Zhou et al., 2009), and glucose response (Yan et al., 2014). Though the exact nature of this interaction has not been investigated *in vivo*, should CBL3 require MTN for some of its activities then this could potentially explain some of observed phenotypes in *mtn1-1mtn2-1* and *mtn1-1mtn2-5*.

Given the tissue-specificity of MTA producing reactions, different cell types must cope with different levels of MTA accumulation. More work is needed to carefully dissect developmental stage and tissue-specific effects of MTA accumulation, as well as the extent of MTA accumulation the specific tissues undergo. Further investigation is also needed to determine if the MTN protein itself has additional critical functions unrelated to the catalysis of MTA to MTR.

2.4.2 MTA accumulation affects several sulfur-related pathways

Combining the metabolite quantification and RNAseq transcript abundance data from unopened buds of *mtn1-1mtn2-1* reveals which sulfur-related pathways are affected by MTA accumulation. Generally in *mtn1-1mtn2-1* unopened buds there is a reduction in Met and metabolites dependent on SAM, the activated form of Met, for their synthesis (Figure 2.10). The reduction in Met-related activities may in part be originally due to reduced Cys biosynthesis (Figure 2.4*d*). This is because *de novo* Met biosynthesis requires the biosynthesis of the sulfur-containing Cys (Figure 1.2). Free sulfate levels remain unchanged in WT versus *mtn1-1mtn2-1* and there is no clear reduction in the transcript abundances of genes encoding Cys and Cys-precursor biosynthesis genes, suggesting this regulation is

post-transcriptional. Alternatively, Cys can be oxidized to form various radicalized species of Cys undetectable by the current method, which can be damaging to the plant as well as inhibiting Cys biosynthesis itself (Jacob et al., 2003; Park and Imlay, 2003).

The general reduction in the abundance of sulfur-containing metabolites is not observed for other compounds. GSH and Spd remain constant, whereas SAH even increases (Figure 2.10). The unchanging GSH and Spd levels suggests that the plant may prioritize these over other sulfur-related metabolites monitored in these analyses (Figure 2.10). For GSH, this is supported by an increase in transcript abundance of the GSH biosynthesis gene *GS*. For Spd, this prioritization can be seen in the increases in transcript abundances of *SAMDC1*, *SAMDC2*, *SAMDC4*, *SPDS1*, and *SPDS2*, as well as an increase in the precursor Put (Figure 2.10). However, it is important to note that the quantification methods used to measure Spd only took into account free, un-conjugated Spd (Heeg et al., 2008). Spd conjugates are not generally measured, but have been found to contribute significantly to the total amount of Spd in Arabidopsis seeds (Imai et al., 2004). Should this also be the case in unopened buds then the constant levels of free Spd may be a result of changes in its conjugation. A reduction in Spd conjugates could have its own consequences, as some Spd conjugates in plants have been implicated to have functions related to cell division, defence, flowering and sexual differentiation (Facchini et al., 2002).

The data do not provide a clear explanation for the increased accumulation of SAH shown in unopened buds of *mtn1-1mtn2-1* versus WT as the transcript abundance of the *SAHH1* and *SAHH2* genes remains unchanged in both genotypes (Figure 2.10). Should the regulation of SAH hydrolysis at the gene expression level be unaffected, another possibility is the accumulation of Hcy causing a change in the reaction equilibrium. Normally in Arabidopsis the hydrolysis of SAH to Hcy is heavily favoured compared to the reverse reaction (Ranocha et al., 2000). Thus the accumulation of SAH could be explained by an

accumulation in Hcy. Transcript abundance data may support this, with a decrease in abundances for the Hcy biosynthesis gene *CBL* and the Met biosynthesis gene *MS2* (Figure 2.10).

Feedback inhibition by MTA may be affecting the abundance of other metabolites monitored in this study. For NA (where a feedback inhibition mechanism has been described; Herbik, 1997) this is clearly supported, with a severe decrease in NA (Figure 2.3*d*) despite steady transcript abundances of NAS-encoding genes relative to WT (Figure 2.10). Though feedback inhibition of ACS has been described previously (Hyodo and Tanaka, 1986), it was not measured in this study. The transcript data could be suggestive of this occurring though, with increases for *ACO1*, *ACO2*, and *ACO3* (Figure 2.10). If this is the case, the plant might increase the expression of ACO to make up for a decrease in ACC. Spd is in a similar yet different situation. Transcript abundances of genes allowing for Spd biosynthesis are increased in unopened buds as mentioned earlier. However as opposed to NA which shows a clear decrease, Spd remains constant. Furthermore, there is only *in silico* evidence of an interaction between SPDS and MTA (Waduwara-Jayabahu et al., 2012). Unless Spd levels are being maintained by changes in Spd conjugates as discussed previously, then SPDS could simply be less sensitive to feedback inhibition to MTA.

While there is clear evidence of the wide-ranging impacts of MTA accumulation on sulfur-related metabolites, more work is needed to elucidate the particular regulatory mechanisms underlying these changes, and how MTA is interfering with these. Furthermore, it remains to be seen to what extent the activity of SPDS is affected by MTA accumulation.

2.4.3 Some pathways affected by MTA accumulation are restored in G3

Some metabolites which have decreased abundances in *mtn1-1mtn2-1* show a recovery in the transgenerationally Spd-restored G3. This recovery is quite obviously very specific, with only Cys, SAM, SAH, and Put showing recovery towards WT levels (Figure 2.10). For Cys this change may still be due to the influence of Spd on a post-transcriptional regulatory mechanism, as there are no clear increases in the transcript abundances of Cys and Cys-precursor biosynthesis genes. Alternatively should Cys in *mtn1-1mtn2-1* be oxidized to radicalized species as discussed earlier (Jacob et al., 2003; Park and Imlay, 2003), then there may be some mechanisms involving a suppression of the generation of these radicalized Cys species. The increase in Cys could also be used to justify the increase in SAM, though this is a bit more difficult with the current evidence. Not only do the transcript abundances of *SAM1* and *SAM2* remain lower than WT, additionally *CBL* and *MS1* decrease as well (Figure 2.10).

On the other hand if the decrease in *CBL* transcript abundance is representative of a decrease in Hcy, then this could explain the decrease in SAH due to a relief in the feedback inhibition of Hcy on SAH hydrolysis. Additionally the transcript abundance of *SAHH2* is increased (Figure 2.10); and while it is the less expressed of the two SAHH-encoding genes (Li et al., 2008), its expression is comparable to *SAHH1* in stage 12 petals and anthers (retrieved from the Arabidopsis eFP Browser on November 1st, 2018; Winter et al., 2007). Regardless, a decrease in SAH back to WT levels would likely be a benefit to the health of *mtn1-1mtn2-1* unopened buds, with SAH accumulation being associated with negative impacts on methyl homeostasis and the stability of the epigenome (Ouyang et al., 2012).

Considering the WT-levels of Spd in *mtn1-1mtn2-1* and G3, the decrease in Put levels

back to WT and the further increase in transcript abundances of *SPDS1* and *SPDS2* is somewhat mysterious (Figure 2.10). One possibility invokes changes to the pool of conjugated Spd mentioned previously. In this scenario, the increase in Spd (as perhaps suggested by the decrease in Put and increase in *SPDS1* and *SPDS2*) would not be captured using the current quantification method as it would instead be diverted to replenish the pool of conjugated Spd. Another possibility can also be envisaged: the reduction of Put along with decreases in *SAMDC1* and *SAMDC4* transcripts would be due to a reduction in the feedback inhibition of SPDS by MTA. This can be considered since MTA levels actually show a modest decrease in G3 (Figure 2.2*f*). Regardless there is no strong evidence for either scenario: evidence of MTA-driven feedback inhibition of SPDS as well as measurements of conjugated Spd are needed to address this.

The restoration of Cys, Put, SAH and SAM correlates well with the gene expression profile of cluster G (Figure 2.9). One of the GO terms enriched within this cluster included the cell cycle (Table 2.2). The importance of SAM and SAH in proper regulation of the cell cycle has been clearly demonstrated in yeast (Hayashi et al., 2018; Park et al., 2015). Should this also be the case in Arabidopsis and considering the importance of cell division in a rapidly developing organ such as unopened buds, then this could implicate irregularities in the progression of the cell cycle as one of the key factors resulting in infertility in *mtn1-1mtn2-1*. This is also seen in the decrease in cell division activity in *mtn1-1mtn2-1* roots (Figure 2.15).

Now that some headway has been made into investigating which specific pathways are required for the transgenerational restoration of fertility, research is needed to investigate how and why these particular pathways can reverse male and female *mtn1-1mtn2-1* sterility (Waduwara-Jayabahu et al., 2012).

2.4.4 Spd treatment has different short and long term effects

Though metabolites were measured from all genotypes and developmental stages with and without Spd treatment, only the 14 d seedling tissue samples were directly exposed to Spd when sampling was performed. By the time the unopened buds were collected, the parent plant had not been directly exposed to Spd for 3-4 weeks. This distinction between the sampling time and Spd exposure leads to a consideration of the dissection of both short-term and long-term effects of Spd treatment. This analysis is only rudimentary however, as different developmental stages will have different metabolisms. From the metabolite measurements in Figures 2.2–2.5, clearly the Spd treatment was nearly completely ineffective in all developmental stages, with only subsequent G2 and G3 generations showing changes relative to the previous generation.

However despite Spd treatment having little impact on the metabolite profiles of either developmental stages, this is not quite the case for the transcriptomes. An RNAseq experiment has been done previously for WT, *mtn1-1mtn2-1* and *mtn1-1mtn2-5* 14 d seedlings grown with and without Spd (M. Saechao and B. Moffatt, personal communication, 2018). Though this data will not be discussed, one aspect of the effect of Spd treatment was clear: the impact of Spd treatment on WT and *mtn1-1mtn2-1* seedlings was large, and furthermore, both genotypes responded differently. This is in opposition with the impact of Spd treatment on WT and *mtn1-1mtn2-1* unopened buds: not only was the impact quite subtle, as seen in Figure 2.6, the impact on the overall transcriptomes appeared to affect the genotypes somewhat similarly.

The RNAseq evidence suggests that Spd has different short-term and long-term effects, each of which may be mechanistically different. Short term effects in this case may reflect Spd playing a role in affecting transcriptional regulation, whereas the long-term effects

could be from changes induced by Spd in the epigenome. This idea is somewhat comparable to the concept of stress memory: plants have an immediate response to an environmental stress, and later in the plant's lifetime (or even in the next generation) the same stress will induce a different response (Lämke and Bäurle, 2017). This different response is thought to be caused by the plant changing its epigenome after the first exposure to the stress in order to create a stress memory, allowing the plant to improve its response to the stress and better adapt to its environmental conditions (Lämke and Bäurle, 2017). However for either short-term and long-term responses to Spd treatment, their ultimate impacts on the plant physiology of WT and *mtn1-1mtn2-1* plants (within a single generation) are not yet known as the transcriptional changes are not reflected in the limited metabolite data presented here.

2.4.5 Evidence of an altered epigenome in *mtn1-1mtn2-1*

The transgenerational restoration of fertility by Spd has been suggested to involve an epigenetic mechanism (Waduwara-Jayabahu et al., 2012). Assuming this to be correct, two (not mutually exclusive) possibilities exist for the effects of Spd on the epigenome: *(i)* Spd induces new changes in parts of the epigenome of *mtn1-1mtn2-1* which is unaffected by MTA accumulation, and *(ii)* Spd is restoring parts of the epigenome of *mtn1-1mtn2-1* which have been altered by MTA accumulation. Since the restoration is transgenerational, it is more likely to involve changes in DNA methylation (Budhavarapu et al., 2013). This research was used to investigate these options. Three pieces of evidence were considered: metabolite quantification data of SAM and SAH, transcript abundance data of genes with specific methylation patterns, and Chop PCR results of two previously studied loci under the control of RdDM.

A reduction in the methylation index which is at least partially caused by an increase in SAH has long been used in mammalian systems as a marker of global DNA hypomethylation (Caudill et al., 2001). Though this concept has not been widely applied to Arabidopsis, previous work has linked increased SAH with DNA hypomethylation and increased expression of transposable elements (Ouyang et al., 2012). Since there is both a reduction in the methylation index (Figure 2.11) and an increase in SAH (Figure 2.2*e*) in *mtn1-1mtn2-1*, it is logical to consider that the epigenome may be affected. It becomes interesting then to consider how those epigenetic marks are affected by transgenerational Spd-driven restoration. In G2 the methylation index and SAH content are slightly restored towards WT levels; in G3 plants these are nearly completely restored. Should these methylation-related changes also be reflective of the state of the epigenome, this suggests that Spd restoration increasingly normalizes the *mtn1-1mtn2-1* epigenome towards WT over subsequent generations. This is actually consistent with previous phenotypic observations of these plants where such phenotypes as seed yield and flowering time recovered increasingly over subsequent generations (Waduwara-Jayabahu, 2011).

Changes in the epigenome are usually reflected in the transcriptome (Zhu et al., 2016). With this in mind transcript abundance of methylated and unmethylated genes in unopened buds was analyzed (Figure 2.12). The Arabidopsis epigenome changes in response to environmental stresses (Lämke and Bäurle, 2017). MTA may be acting as a stress and inducing changes in the epigenome. Furthermore, different environmental conditions can affect specific types of DNA methylation (i.e. location: gene body methylation, promoter methylation; cytosine context: CpG, CHG, CHH; Dubin et al., 2015). There was a clear enrichment in the increased transcript abundance of genes with CpG gene body methylation in *mtn1-1mtn2-1*, which has been linked with the expression of highly transcribed genes (To et al., 2015). The enrichment for differentially expressed genes with a specific methylation

type suggests that MTA stress may not be inducing DNA methylation changes in a totally untargeted manner. Abnormal CpG gene body methylation in *mtn1-1mtn2-1* is actually consistent with previous work showing that reduced CpG gene body methylation in the *met1* mutant is accompanied with an overall increase in expression of those genes which are normally under the influence of this type of DNA methylation (Zilberman and Henikoff, 2007). Transgenerational Spd restoration may be implicated: there is a slight enrichment in CpG gene body methylated genes down-regulated in G3 compared to *mtn1-1mtn2-1* (Figure 2.12). These findings connect MTA accumulation to specific changes in DNA methylation, and a targeting of these same DNA methylation changes by Spd.

Finally the Chop PCR data (Figure 2.13) supports that *mtn1-1mtn2-1* and G3 plants have changes in the RdDM pathway. Targets of the RdDM pathway usually do not include genes under the influence of CpG gene body methylation, rather it tends to target transposons and transposable elements (He et al., 2014). The methylation at these sites is usually non-CpG (Dubin et al., 2015). Since there was no significant enrichment of differentially expressed genes in *mtn1-1mtn2-1* with non-CpG methylation, it could be that a possible disturbance in the RdDM pathway does not contribute substantially to the MTA accumulation phenotype. This is further supported by the fact that the G3 samples show no recovery compared to *mtn1-1mtn2-1* in the Chop PCR result (Figure 2.13), suggesting it is not necessary for fertility.

It remains to be seen what the changes in the epigenome are specifically and how these are related to the mutant phenotype.

2.4.6 Mixed evidence for reduced PRMT5 in *mtn1-1mtn2-1*

Since inhibition of PRMT5 is now believed to be a major contributor to the negative impact of MTA accumulation in mammalian systems (Kryukov et al., 2016; Marjon et al., 2016; Mavrakis et al., 2016), it was of interest to investigate whether the Arabidopsis PRMT5 is similarly affected by MTA accumulation in MTN-deficient mutants. PRMT5-deficient Arabidopsis have a number of mutant phenotypes, including growth retardation, late flowering, improper pre-mRNA splicing, salt intolerance, calcium insensitivity, iron accumulation, cell cycle arrest, and disruption of root and shoot meristem maintenance (Deng et al., 2010; Fan et al., 2014; Fu et al., 2013; Hernando et al., 2015; Li et al., 2016a; Wang et al., 2007; Yue et al., 2013; Zhang et al., 2011). Similarly *mtn1-1mtn2-1* plants have been shown to undergo growth retardation and late flowering, though instead of accumulating iron they instead suffer from iron deficiency (Waduwara-Jayabahu, 2011; Waduwara-Jayabahu et al., 2012). An investigation to look for mutant phenotypes indicative of PRMT5 deficiency in *mtn1-1mtn2-1* was performed.

The evidence in Figure 2.14 suggests that even if *mtn1-1mtn2-1* unopened buds undergo differential alternative splicing compared to WT, it does not follow the pattern of intron retention seen in *prmt5* mutant seedlings (Hernando et al., 2015). This is not definitive however as evidence of tissue-specific alternative splicing patterns has been presented previously (Estrada et al., 2015; Li et al., 2016b). Since RNAseq data of *mtn1-1mtn2-1* seedlings is available (Saechao et al.), then analyzing this data for this intron retention pattern is needed.

Finally, *mtn1-1mtn2-1* were tested for the G2 phase cell cycle arrest phenotype of *prmt5* mutant seedling roots (Li et al., 2016a). Looking at Figure 2.15, no accumulation of the G2 phase reporter pCYCB1;1-GFP was detected. While this could be indicative of a lack

of altered PRMT5 function, another possibility is an overall suppression of root meristem activity (Figure 2.15). In this case, even should G2 phase cell cycle arrest be occurring (proportionally) at rates higher than WT, due to the overall decrease in meristem activity it would not be detected with mere reporter signal intensity.

Overall the evidence for altered PRMT5 function in *mtn1-1mtn2-1* remains mixed. Due to the possible significance of PRMT5 involvement in MTA accumulation-driven phenotypes, this issue requires further investigation.

2.4.7 A possible link between decapitation, MTA content, and ROS in the pollen defects of *mtn1-1mtn2-1*

The restoration of fertility of *mtn1-1mtn2-1* flowers on decapitated stems was quite surprising. Despite this, there may exist a simple explanation. In mammalian tissues, MTA generation and MTAP activity are positively correlated with actively dividing cells (Sunkara et al., 1985). The high levels of MTA accumulation in *mtn1-1mtn2-1* unopened buds (where there is a high rate of cell division) relative to other developmental stages (Figures 2.2*c*, 2.2*f*; Waduwara-Jayabahu, 2011) may support this. MTA moves between human cells via a facilitated diffusion mechanism (Cartenì-Farina et al., 1983) and may be similarly transported in Arabidopsis. Assuming this to be the case, a working model that fits these observation can be proposed as follows: flowers on *mtn1-1mtn2-1* stems become infertile as a result of large amounts of MTA diffusing from the apical unopened bud cluster. Decapitation, then, would allow for a relief from this MTA pressure and thus fertility could occur.

From this model, a couple considerations arise. The first consideration is that MTA-driven infertility can be reverted only in flowers which have detached from the apical

unopened bud cluster. Stage 9 flowers would be the earliest that could be restored because this is when the unopened bud separates from the apical unopened bud cluster (Smyth et al., 1990). However, *mtn1-1mtn2-1* plants are both male and female sterile (Waduwara-Jayabahu et al., 2012), so considering pollen and ovule development near this stage is crucial in determining the exact stages of gametogenesis susceptible to recovery.

For pollen, the major event at this stage is the beginning of tapetum degeneration (Sanders et al., 1999) induced by an accumulation of ROS (Yi et al., 2016). Part of the tapetum which must be degraded includes a special callose wall (Bedinger, 1992). From the GO terms enriched from the RNAseq gene expression clusters (Table 2.2), there is a possible involvement of ROS mis-regulation in *mtn1-1mtn2-1* unopened buds. While this is currently not supported by ROS measurements in seedling roots (Figure 2.17), this result could still be attributed to the comparably low amount of MTA present in this developmental stage (Figure 2.2*c*). Furthermore, from previous work there is some evidence of improper callose degradation in pollen (Perera, 2018; Waduwara-Jayabahu et al., 2012).

In terms of ovule development, stage 9 roughly corresponds with ovule initiation (Cucinotta et al., 2014). At this point, an important factor in maintaining cell identity during ovule initiation is the proper regulation of the movement of transcription factors between cells via plasmodesmata (Cucinotta et al., 2014). One of the main components which controls plasmodesmatal conductivity is callose (De Storme and Geelen, 2014). Considering improper callose degradation is a possible factor in the male sterility of *mtn1-1mtn2-1*, then this could also be a contributing element to female sterility.

The second consideration for this model is the speed at which this fertility reversal occurs (detectable as early as within two days after decapitation). This suggests that while a rapid change in the transcriptional program of the plant is possible, it is more likely a post-translational or biochemical mechanism. Such mechanisms could include ROS

homeostasis and callose degradation. With this in mind, the model proposed above can be extended in that MTA accumuation interferes with callose and ROS regulation, which would be quickly returned to normal once MTA levels drop post decapitation. Of course, the evidence for this model is still rather circumstantial and requires a further exploration of the pollen and ovule developmental defects in *mtn1-1mtn2-1* as well as how MTA would directly be interfering with callose and ROS regulation.

Chapter 3

Identification and early characterization of *METHYLTHIOADENOSINE RESISTANT* mutants

3.1 Introduction

In Arabidopsis, MTN catalyzes the formation of MTR from MTA. MTN is encoded for by two genes, MTN1 (AT4G38800) and MTN2 (AT4G34840). MTA is formed as a byproduct of several reactions which use SAM, the active form of Met as a substrate. These are NA biosynthesis by NAS, ACC (the precursor the ethylene) biosynthesis by ACS, and the biosynthesis of the PAs Spd, Spm and Tspm by SPDS, SPMS and ACL5, respectively. MTA is recycled back to Met via Met salvage cycle.

NA is secreted by the root system to chelate and dissolve soil bound iron, making it available for transport into the roots (Higuchi et al., 1999). The plant hormone ethylene has many roles in plant development and stress response (Dubois et al., 2018). The PAs Spm and Tspm are involved in stress response and vascular development, respectively (Clay and Nelson, 2005; Tiburcio et al., 2014; Yamaguchi et al., 2006). The PA Spd is involved in numerous processes including gene regulation, ROS scavenging and stress responses (Tiburcio et al., 2014).

Met biosynthesis occurs *de novo* with the assimilation of sulfur. During sulfur-sufficient conditions, the Met salvage cycle is unnecessary. In fact several Met salvage cycle knockout mutants have WT phenotypes under sulfur-sufficient conditions (Bürstenbinder et al., 2007; Zierer et al., 2016). Despite this, blocking the progression from MTA to MTR has great consequences on plant health. The *mtn1-1mtn2-1* double mutant, which has 14.9% residual MTN activity, has a severe pleiotropic mutant phenotype including delayed bolting, fasciation, and male and female sterility (Waduwara-Jayabahu et al., 2012). *mtn1-1* single mutant seedlings grown on media supplemented with 500 µM MTA are severely growth-inhibited, represented by a distinctive short-root phenotype (Bürstenbinder et al., 2010).

Current understanding of the mechanisms of MTA toxicity is lacking. Part of the toxicity is believed to originate from MTA-feedback inhibition of reactions which generate it as a byproduct. Previous studies have used *in vitro* inhibitor studies to described the inhibitory activities of MTA on NAS and ACS (Herbik, 1997; Hyodo and Tanaka, 1986). NA levels are decreased in adult *mtn1-1mtn2-1* plants and *mtn1-1* seedlings grown on MTA (Bürstenbinder et al., 2010; Waduwara-Jayabahu et al., 2012), though ethylene measurements from these plants show no change (Bürstenbinder et al., 2010; Washington et al., 2016). An *in silico* analysis suggests MTA can interact with SPDS and ACL5

(Waduwara-Jayabahu et al., 2012), but no evidence of this interaction being inhibitory exists in Arabidopsis. Spd and Spm measurements in adult *mnt1-1mtn2-1* plants and *mtn1-1* seedlings grown on MTA suggest they are unaffected (Bürstenbinder et al., 2010; Waduwara-Jayabahu et al., 2012).

With all of the mixed evidence concerning which processes are affected by MTA accumulation, the goal of this study was to increase our understanding of MTA toxicity using a forward genetics approach. This was done via a suppressor screen experiment to identify which MTA-affected pathways contribute significantly to the mutant phenotypes of MTN-deficient plants which accumulate MTA. This study yielded several unique suppressor mutants, one of which implicates glucosinolates (GLS) and auxin biosynthesis with MTA accumulation in MTN-deficient plants.

3.2 Materials and methods

3.2.1 Plant growth

The growth of *Arabidopsis thaliana* (Col-0 ecotype) seedlings and adult plants was done as described in Chapter 2. Preparation of MTA media was as described by Bürstenbinder et al. (2007). PCR genotyping was performed as described by Bürstenbinder et al. (2010).

3.2.2 Mutant generation and screening

Approximately 5,000 *mtn1-1* seeds were mixed with 25 mL 0.2% ethyl-methanesulfonate (EMS). This was left to gently shake for 15 h. The M1 seed were washed with water eight times and split into ten pools. After keeping the seeds at 4 °C for 2 d, the M1 pools were sown in soil and grown to maturity. M2 seeds were collected and surface sterilized. A thousand M2 seeds from individual pools were grown vertically on media containing 500 µM MTA. Putative suppressor mutants were screened for increased root length and transferred to empty plates to recover, before transplanting into soil.

3.2.3 Metabolite measurements

Sample collection and extraction

Seedlings were collected and frozen with liquid nitrogen, then weighed to ∼25 mg in 1.5 mL microcentrifuge tubes. The plant material was ground to a fine powder with a homogenizer and stored at −80 °C. For extraction of metabolites, 1 mL of 0.1 M HCl was added to the tubes, and vortexed every ∼30 s for 15 min. The tubes were subsequently centrifuged at

Table 3.1: Primers used for genotyping and Sanger sequencing.

Primer name	Sequence (5′ to 3′)
SNP1F	CTCCAACGCTTGTTGAAGAG
SNP1R	TGTGAGCAGCCATGAGAAAC
SNP3F	TGATGCCACTTCCACAGGTA
SNP3R	AGCATTTCGAAGGCACTGAT
SNP4F	AGCCGTGAGAGACAAGGAAG
SNP4R	CATGGAAGACAACGCTCAGA
SNP5Fv2	TCCCAAAATGGGCACACGAA
SNP5Rv2	TACAGGTTCAGGCTTAGCGG
NSP1F	ATTAGGCCAAAATGCGAGAG
NSP1R	CGTTTTCAACACATCCATCG
072600LP	TATGACAAGAAATTCGTCCCG
072600RP	ACCTTCTCCTTTTTGCTCCAC
IONTORR-F	CCATCTCATCCCTGCGTGTC
IONTORR-R	GGTGATGCGGAGGCGAAAGG
IONT-R95	CCACTACGCCTCCGCTTTCCTCTCTATGGGC
	AGTCGGTGATTTGTTGCTTCCTTCCAGACCA
IONT-R96	CCATCTCATCCCTGCGTGTCTCCGACTCAGTT
	AGCGGTCGATAGTGGAAACATTCGGTGTGAG
*mtn1-1*F	TGACGGAGACCAACTCCATAC
*mtn1-1*R	GAGGCTCTTCCTTTGGTCAAC
LBb1.3	ATTTTGCCGATTTCGGAAC

16 000 RCF, 4 °C, for 5 min. The supernatants were transferred to new tubes and stored at −80 °C.

Derivatisation and quantification of thiols, adenosines, and nicotianamine

The thiols Cys and GSH, the adenosines SAM, SAH and MTA, and NA were derivatised and quantified exactly as described in Chapter 2.

3.2.4 Whole genome sequencing

Approximately 1 g of vegetative tissue was frozen with liquid nitrogen and ground with a mortar and pestle. The ground tissue was added to 10 mL CTAB extraction buffer (100 mM Tris-HCl pH 8, 20 mM EDTA pH 8, 1.4 M NaCl, 2% CTAB, 1% PVP 40, 000). This extract was incubated at 65 °C for 10 min, and gently inverted every 2 min. After incubation 10 mL chloroform:isoamyl alcohol (24:1) was added and mixed by inversion for 5 min. The solution was centrifuged for 10 min at max speed in a bench-top centrifuge (model 5415R; Eppendorf, Hamburg, Germany). The aqueous phase was separated and mixed with 0.7 volumes of isopropanol. After incubating for 5 min, it was centrifuged for 5 min at max speed in a bench-top centrifuge. The liquid was discarded and the DNA pellet was washed with 80% ethanol and then centrifuged for 5 min at max speed in a bench-top centrifuge. The DNA was resuspended in 50 µL TE buffer (pH 8). RNase A was added to the solution to a final concentration of 10 µg mL^{-1} and incubated for 1 h at 37 °C. Afterward the DNA was stored at 4 °C. The DNA was cleaned using a DNeasy Plant Mini Kit (Qiagen Inc., Toronto, ON, Canada). For Whole Genome Sequencing (WGS), preparation of 350 bp insert DNA libraries was performed by Novogene Corporation (Sacramento, CA, USA) and sequenced

with a HiSeq X Ten platform (Illumina Inc., San Diego, CA, USA) with a paired-end 150 bp sequencing strategy.

3.2.5 Sanger and ION Torrent sequencing

Target regions were amplified with PCR. Sanger sequencing of amplicons was performed with a ABI 3730XL (ThermoFisher Scientific, Mississauga, ON, Canada) sequencer at The Centre for Applied Genomics (Toronto, ON, Canada). Ion Torrent sequencing of amplicons was performed with an Ion Torrent Personal Genome Machine (ThermoFisher Scientific, Mississauga, ON, Canada) at the Genomics Core Facility (Sunnybrook Research Institute, Toronto, ON, Canada).

3.2.6 Bioinformatics analysis

Raw reads were quality trimmed with Trim Galore! v0.4.5 (Krueger, 2012). These were mapped onto the TAIR10 Arabidopsis reference genome (Lamesch et al., 2012) with bwa v0.7.17 (Li and Durbin, 2009). Duplicated reads were removed with Picard v2.15.0 (McKenna et al., 2010). Read recalibration and Single Nucleotide Polymorphism (SNP) calling was done with GenomeAnalysisTK v3.8 (McKenna et al., 2010). The tool SnpSift v4.3 (Cingolani et al., 2012) was used to annotate SNPs. SNP Chromosome (Chr) density analysis and identification of Heterozygous (Het) and Homozygous (Homo) SNPs were performed with the R language (R Core Team, 2018). Candidate suppressor gene orthologs were retrieved from OrthoDB (Kriventseva et al., 2018), and Amino Acid (AA) sequences aligned with Clustal Omega v1.2.3 (Sievers and Higgins, 2018). All statistical tests including one-way ANOVA and Tukey HSD tests were done with the R language (R Core Team, 2018).

3.3 Results

3.3.1 Detailed analysis of the impact of MTA feeding on seedling growth for use in a suppressor screen

The effects of MTA accumulation in MTN-deficient Arabidopsis plants are still not well understood, despite previous work involving metabolite analyses and careful physiological observations (Bürstenbinder et al., 2010; Waduwara-Jayabahu et al., 2012). In an attempt to understand the specific mechanisms behind the negative effects of MTA accumulation, a suppressor screen approach was developed to identify genes that affect the phenotype of MTN-deficient mutants. Suppressor screens are known to be useful for revealing protein interactors or relevant functions for the phenotype under study (Li and Zhang, 2016). First however, it was necessary define conditions under which a suppressor mutation would be revealed (i.e., mutations that allow the mutant to have a more WT phenotype).

The single mutants *mtn1-1* and *mtn2-1* show no phenotype under control conditions (Bürstenbinder et al., 2010), and the double mutant *mtn1-1mtn2-5* exhibits a clear but moderate mutant phenotype (Waduwara-Jayabahu, 2011; Waduwara-Jayabahu et al., 2012). The *mtn1-1mtn2-1* double mutant instead has a highly variable and very severe mutant phenotype including male and female infertility under control conditions (Waduwara-Jayabahu et al., 2012). Since working with an infertile plant would make the suppressor screen not possible, it was not considered. Since a suppressor screen based purely on the external phenotypes of MTN-deficient mutants would likely be inefficient a simple assay was needed. Previously it has been observed that single mutant *mtn1-1* seedlings grow short roots when fed MTA as a sole sulfur source (Bürstenbinder et al., 2010). Considering how quickly this assay can be performed, a careful analysis of this assay was first decided

upon for use in a suppressor screen. The effects of different concentrations of MTA on the root growth of various MTN-deficient mutants were studied.

Seedlings were grown vertically on media supplemented with various concentrations of MTA; root growth was measured at 7 d. The results of this analysis are shown in Figure 3.1. The *mtn1-1mtn2-1* mutant, as well as the Spd-restored G2 and G3, grew shorter roots at even the lowest tested concentration (10 µM MTA). Due to seed stock limitations, as well as the need to genotype *mtn1-1mtn2-1* seedlings to confirm their identity, not all concentrations were tested on all genotypes.

The *mtn1-1* and *mtn1-1mtn2-5* mutants required higher concentrations of MTA (100 µM MTA) to begin exhibiting a short root phenotype (Figure 3.1). The difference in root length between WT and these two mutants increased further at higher concentrations. Fortunately, both *mtn1-1* and *mtn1-1mtn2-5* are completely fertile opening up the opportunity of mutagenizing homozygous seed to identify mutations that restore normal root growth. This allowed for a quick and high through-put screening method. Since both *mtn1-1* and *mtn1-1mtn2-5* reacted similarly to high concentrations of MTA, *mtn1-1* was ultimately chosen for use in the suppressor screen in order to avoid any unknown effects from the *m*tn2-5 mutation unrelated to root length.

3.3.2 Recovery of M2 generation *mtn1-1mtar* mutants and re-screening

To allow for the recovery of homozygous recessive mutations, EMS-mutagenized *mtn1-1* were advanced to the M2 generation. The M2 seed was pooled from groups of M1 plants, creating 10 distinct M2 seed populations. Approximately a thousand M2 seeds from each pool were grown vertically on media containing 500 µM MTA. Seedlings which had

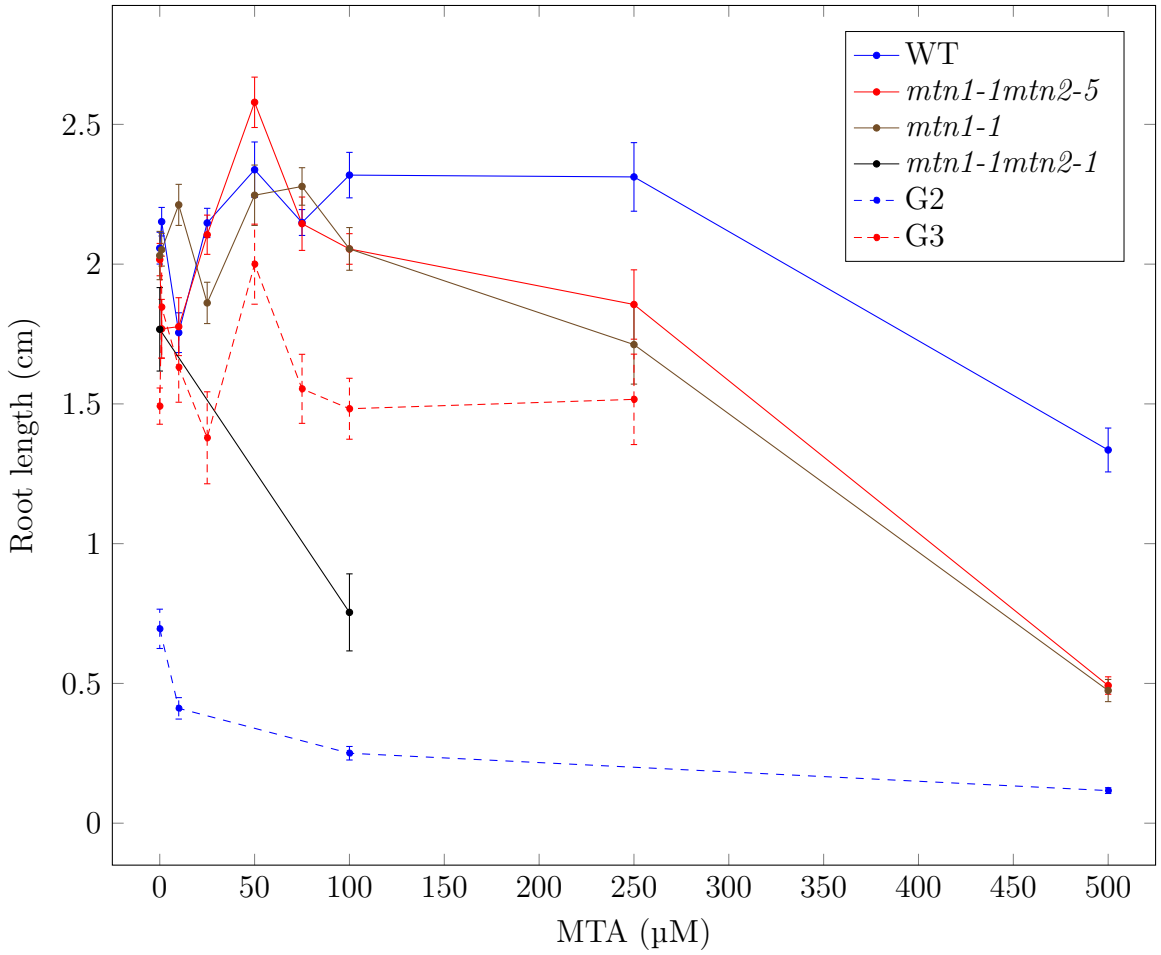

Figure 3.1: Root length analysis of MTN-deficient mutants grown on MTA.

Seeds were sown on media containing either 500 µM $MgSO_4$ (shown as 0 µM MTA) or various concentrations of MTA and grown vertically for 7 d. Seedlings were imaged at the end of the experiment for root length measurements ($n = 20$).

longer roots by 4 d were separated out, up about until 10 d at which point the inhibitory effects of MTA weakened. Three rounds of screening were performed, and 11 putative mutants were selected (Figure 3.2, Table 3.2). The suppressor mutations were named METHYLTHIOADENOSINE RESISTANT (MTAR). In order to avoid false positives, they were genotyped to ensure they carried the *mtn1-1* mutation and re-screened individually (Table 3.2). Several putative mutants were removed from consideration; for example, the putative *mtn1-1mtar1* seedling was WT. Putative mutants were backcrossed with *mtn1-1*. By screening the F1 and F2 progeny, it was revealed that all mutants were recessive, with the exception of one dominant mutant. The first *mtar* considered for sequencing was *mtar2*, being the first succesful putative mutant. The next putative mutant considered for study was *mtar8* for having a stronger suppressor phenotype than other putative suppressors. Finally, *mtar11-d* is also being investigated for being the only dominant putative suppressor.

In order to determine whether the *mtar* mutations could restore fertility in infertile *mtn1-1mtn2-1* mutants (Waduwara-Jayabahu et al., 2012), *mtn1-1mtar* plants were crossed with $\frac{mtn1\text{-}1}{mtn1\text{-}1} \cdot \frac{\text{MTN2}}{mtn2\text{-}1}$ plants. F2 seed were sown on $MgSO_4$ or MTA-containing media before genotyping. Only those exhibiting signs of having the long-root *mtar* phenotype were genotyped from the MTA-treated plates, meaning that from the $MgSO_4$-genotyped F2 some likely did not containing two copies of the *mtar* mutations. The resulting genotypes compared (Table 3.3). Unexpectedly, the F2 seedlings did not follow typical Mendelian inheritance, rather favouring the genotyping without any copy of *mtn2-1*. This seemed to be more pronounced for the MTA-treated seedlings for the *mtar2* and *mtar8* lines. Furthermore complete MTA-treated double mutants could only be recovered for the *mtar2* mutants. These results suggest either the *mtar* phenotype is suppressed by the addition of one or two copies of *mtn2-1*, or that a full *mtn1-1mtn2-1mtar* triple mutant is embryo lethal. More work is needed to confirm the number sin Table 3.3, and currently these

seedlings have yet to be grown until adulthood to check for fertility.

3.3.3 Metabolite analysis of M2 generation *mtn1-1mtar* mutants

The opportunity arose to quantify several key MTA-related metabolites in some of the putative *mtn1-1mtar* mutants. The measurements were performed in two individual experiments. The *mtn1-1mtar2* and *mtn1-1mtar5* were measured together in the first experiment; *mtn1-1mtar8*, *mtn1-1mtar10* and *mtn1-1mtar11-d* were evaluated in the second. Each experiment has its own WT and *mtn1-1* controls. In an effort to recreate the conditions from the suppressor screen, vertically grown 7 d seedlings were collected with and without 500 µM MTA supplementation. Most of the metabolites (i.e., SAM, MTA, Cys, GSH and NA) have been previously quantified in 4 d *mtn1-1* mutant seedlings (Bürstenbinder et al., 2010).

The data from WT and *mtn1-1* measurements were mostly consistent between experiments, and with previous results (Bürstenbinder et al., 2010). SAM, SAH and MTA all increased for both genotypes on MTA, with a slightly larger increase for *mtn1-1*, in experiments 1 and 2 (Figure 3.3). Cys increased in *mtn1-1* on MTA for both experiments as well (Figures 3.3*a*, 3.3*d*). All of these changes (except SAH which has not been quantified previously) are in agreement with previous measurements (Bürstenbinder et al., 2010). GSH increased on in *mtn1-1* MTA for experiment 1 (Figure 3.4*b*), but stayed stable in experiment 2 (Figure 3.4*e*). Both of these are actually not in agreement with a previous result where instead an increase in GSH was seen (Bürstenbinder et al., 2010). Finally, NA was lower in *mtn1-1* compared to WT for all conditions, and MTA treatment reduced this further in *mtn1-1* on MTA in the second experiment (Figures 3.4*c*, 3.4*f*). Previous NA measurements in *mtn1-1* seedlings had high variation (Bürstenbinder et al., 2010), so

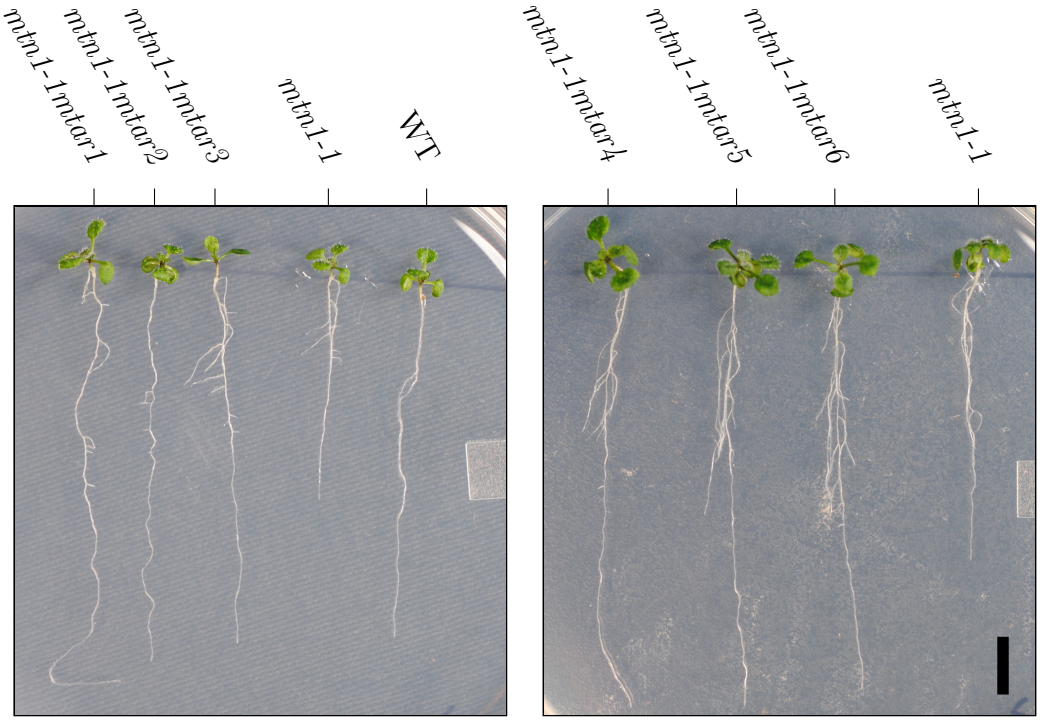

(a) Round 1 (10 d)

(b) Round 2 (14 d)

Figure 3.2: First two rounds of *mtar* screening.

Putative *mtn1-1mtar2* seedlings were moved from plates with no MTA once they were identified during the suppressor screen. Once they had recovered they were photographed alongside control genotypes which had also been grown on plates containing 500 µM MTA as used for the screen. Putative mutants recovered during round 1 of screening were imaged several days after having been moved to plates without any MTA for recovery. Round 1 putative mutants were imaged at 10 d *(a)*, and round 2 putative mutants at 14 d *(b)*. Scale bar represents 0.7 cm.

Table 3.2: Recovering M2 generation *mtar* mutants and rescreening.

Putative *mtn1-1mtar* mutants were found in three rounds of screening involving various pools of M2 seed. The putative suppressors were genotyped for *mtn1-1* to confirm their identity as M2 plants. Finally individual putative suppressors were re-screened to confirm the phenotype.

mtar	Screening round	M2 pool	Correct genotype*	Passed rescreen
1	1	6	no	-
2	**1**	**6**	**yes**	**yes**
3	1	5	yes	no
4	2	4	yes	no
5	**2**	**9**	**yes**	**yes**
6	2	10	yes	no
7	3	-	yes	no
8	**3**	**-**	**yes**	**yes**
9	3	-	yes	no
10	**3**	**-**	**yes**	**yes**
11-d‡	**3**	**-**	**yes**	**yes**

*Putative *mtn1-1mtar* mutants were genotyped for *mtn1-1*.

‡The *mtar11-d* mutation was found to be dominant.

Table 3.3: F2 segregation results after crossing *mtn1-1mtar* mutants with *mtn1-1mtn2-1*.

mtn1-1mtar mutants were crossed with *mtn1-1mtn2-1* plants. F2 seed were grown on $MgSO_4$ (only *mtar2* and *mtar8*) or MTA-containing media, and genotyped for *mtn2-1* after one week of seedling growth. For the MTA-treated seedlings, only those which grew long roots were genotyped. aaBB = $\frac{mtn1\text{-}1}{mtn1\text{-}1} \cdot \frac{\text{MTN2}}{\text{MTN2}}$, aaBb = $\frac{mtn1\text{-}1}{mtn1\text{-}1} \cdot \frac{\text{MTN2}}{mtn2\text{-}1}$, aabb = $\frac{mtn1\text{-}1}{mtn1\text{-}1} \cdot \frac{mtn2\text{-}1}{mtn2\text{-}1}$

Mutant	Treatment	aaBB	aaBb	aabb	*n*
mtar2	MTA	90.2%	7.3%	2.4%	41
	$MgSO_4$	43.3%	50%	6.6%	30
mtar8	MTA	100%	0%	0%	26
	$MgSO_4$	54.2%	37.5%	8.3%	24
mtar10	MTA	100%	0%	0%	19
	$MgSO_4$	-	-	-	-
mtar11	MTA	75%	25%	0%	24
	$MgSO_4$	-	-	-	-
Expected percentage		25%	50%	25%	

it cannot be determined whether this result is in agreement with the significant decrease detected in *mtn1-1* in this study.

The impact of the MTAR mutations on the seedling metabolomes were quite evident. The MTA-driven increase in SAM was completely suppressed (Figures 3.3*a*), 3.3*d*), and MTA accumulation itself only rose to WT levels (Figures 3.3*c*), 3.3*f*). SAH was increased in a manner similar to WT (though not as highly as in *mtn1-1*) by MTA treatment (Figures 3.3*b*, 3.3*e*). Cys remained unchanged by MTA treatment in all *mtar* mutants except *mtn1-1mtar10* (Figures 3.4*a*, 3.4*d*). The *mtn1-1mtar2* samples showed a clear decrease in GSH and *mtn1-1mtar5* no change in GSH versus the increase in *mtn1-1* when treated with MTA (Figure 3.4*b*). GSH measurements were quite variable in experiment 2 and showed no clear pattern (Figure 3.4*e*).

3.3.4 Whole genome sequencing of the *mtn1-1mtar2* mutant

Due to the large number of mutations induced by the original EMS treatment, it was necessary to remove as many of these as possible before sequencing. The removal of extraneous SNPs was done by backcrossing the *mtn1-1mtar* mutants with fresh *mtn1-1* plants, then screening F2 to select for the SNP. A pool of 40 *mtn1-1mtar2* F2 plants were used for WGS with 40× coverage in a mapping-by-sequencing approach to SNP mapping (James et al., 2013). The reads were mapped to the TAIR10 reference genome (Lamesch et al., 2012). In order to account for differences between the reference genome and the *mtn1-1* parent, WGS of *mtn1-1* was also performed. Only those SNPs possibly caused by EMS (C→T and G→A) were extracted and assigned as Het ($< 75\%$) or Homo ($\geq 75\%$) with the R language. To find the causal SNP, the density of mapped Het and Homo SNPs were first examined (Figure 3.5). Since the backcross and subsequent F2 selection would

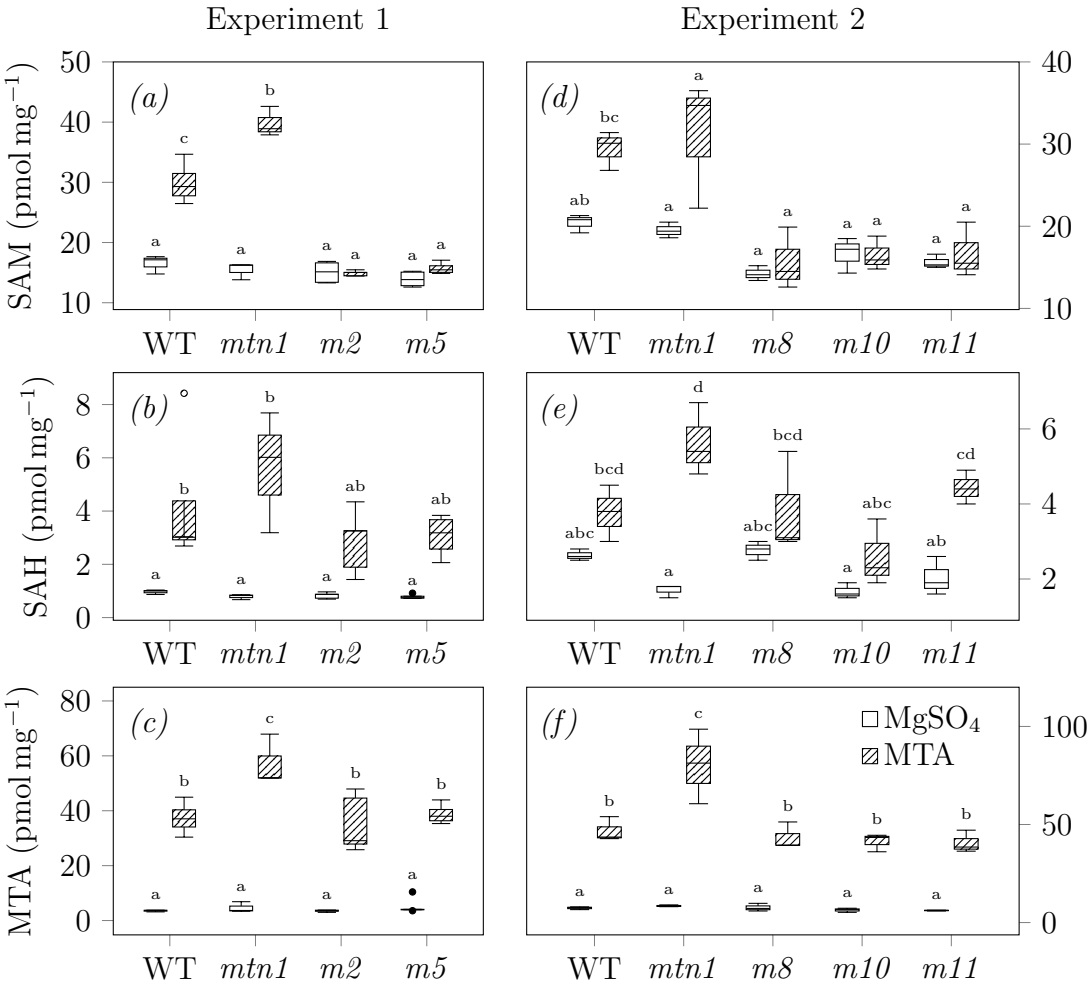

Figure 3.3: SAM, SAH and MTA measurements of *mtn1-1mtar* seedlings.

Seedlings were grown vertically for 7 d on media containing either 500 µM $MgSO_4$ or 500 µM MTA as a sulfur source. The mutants were grown and collected in two separate experiments, with *mtn1-1mtar2* (*m2*) and *mtn1-1mtar5* (*m5*) in experiment 1 *(a)-(c)*, then *mtn1-1mtar8* (*m8*), *mtn1-1mtar10* (*m10*) and *mtn1-1mtar11* (*m11*) in experiment 2 *(d)-(f)*. SAM (*a*, *d*), SAH (*b*, *e*) and MTA (*c*, *f*) were measured simultaneously with HPLC. Significant difference was tested for using a one-way ANOVA ($p < 0.05$), followed up with a Tukey's HSD post-hoc test ($n = 5$). Significant differences are represented as unique letters above the individual boxes.

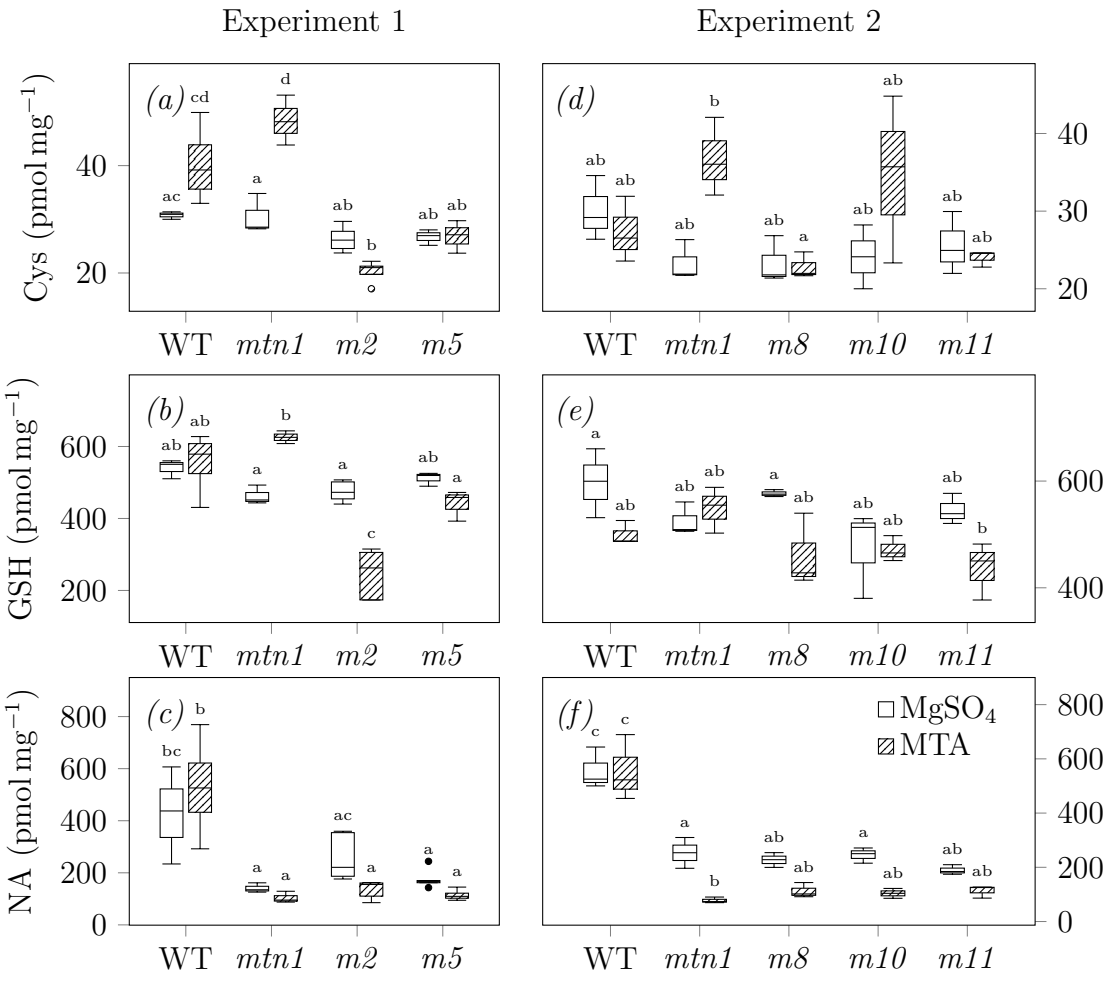

Figure 3.4: Cys, GSH and NA measurements of *mtn1-1mtar* seedlings.

Seedlings were grown vertically for 7 d on media containing either 500 µM $MgSO_4$ or 500 µM MTA as a sulfur source. The mutants were grown and collected in two separate experiments, with *mtn1-1mtar2* (*m2*) and *mtn1-1mtar5* (*m5*) in experiment 1 *(a)-(c)*, then *mtn1-1mtar8* (*m8*), *mtn1-1mtar10* (*m10*) and *mtn1-1mtar11* (*m11*) in experiment 2 *(d)-(f)*. Cys (*a*, *d*) and GSH (*b*, *e*) were measured simultaneously, followed by NA (*c*, *f*), with HPLC. Significant difference was tested for using a one-way ANOVA ($p < 0.05$), followed up with a Tukey's HSD post-hoc test ($n = 5$). Significant differences are represented as unique letters above the individual boxes.

decrease the frequency of the non-causal SNPs, the causal SNP would likely be found within a region of linked Homo SNPs (James et al., 2013). Two regions with high Homo and low Het SNP density were found: on Chr 3 and 5, though intragenic SNPs were only found in the former (Figure 3.5).

3.3.5 Identification and analysis of candidate *mtar2* SNPs

The WGS of backcrossed *mtn1-1mtar2* revealed the causal SNP was likely within a cluster of intragenic SNPs on Chr 3 (Figure 3.5), listed in Table 3.4. Only SNPs which resulted in a non-synonymous AA change were considered. A total of five of these SNPs were identified across a 7.6 Mbp region. Each was confirmed to be present in *mtn1-1mtar2* by Sanger sequencing of PCR amplified segments of Chr 3. To identify the causal SNP, the AA sequences of protein orthologs were examined for conservation at the site changed by the SNP (Table 3.5). Plant orthologs were identified using OrthoDB (Kriventseva et al., 2018) and aligned with Clustal Omega (Sievers and Higgins, 2018), at which point the number of orthologs with the original AA, the new SNP-caused AA and gaps at the AA position were counted and listed in Table 3.5 and also shown in Figure 3.6 as sequence logos. No ortholog group for SNP5 could be found, so only SNPs 1, 3, 4 and 6 AA conservation were investigated. Among these SNPs 1 and 3 had a number of orthologs with the SNP-caused AA, suggesting any impacts from such SNPs would not greatly affect protein function.

While both SNPs 4 and 6 had nearly no orthologs with the alternative AA, the majority of orthologs for the SNP4 protein had gaps at the SNP AA site. This left the consideration of causal SNPs down to SNPs 5 and 6. The SNP6 gene, NSP1 (AT3G16400), was previously demonstrated to function in nitrile formation (Burow et al., 2009). No function has been currently attributed to the SNP5 gene, but it has been characterized as a small open reading

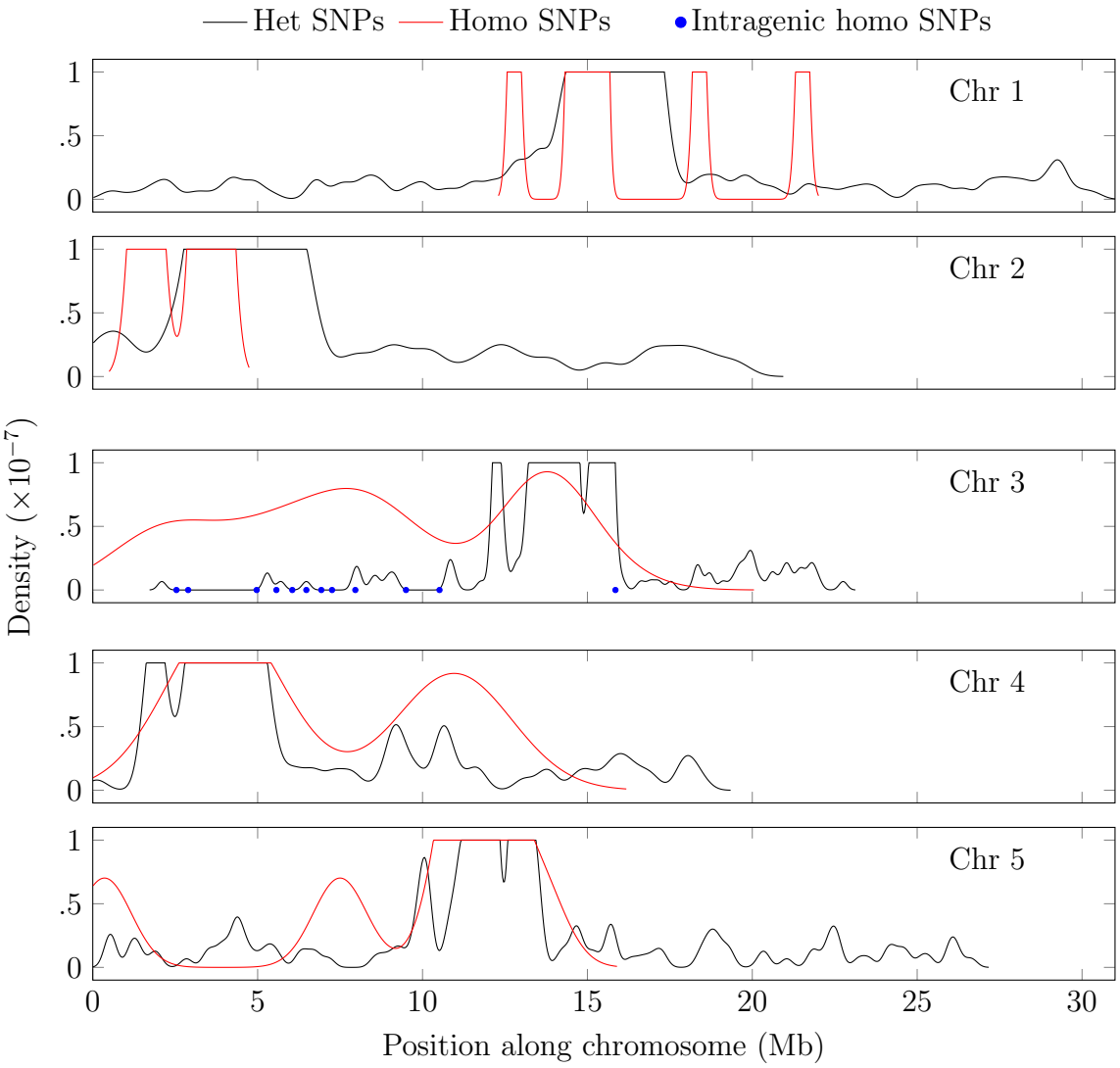

Figure 3.5: SNP density in along genome of *mtn1-1mtar2*.

SNPs from WGS of *mtn1-1mtar2* were categorized as Het ($< 75\%$) or Homo ($\geq 75\%$) and separated by chromosome. The densities of Het and Homo SNPs were calculated using the kernel density estimation function of R and a ceiling of 10^{-7} was applied to the density values. Homo intragenic SNPs were highlighted using blue dots.

frame (sORF; Hanada et al., 2007). While it is generally unknown whether most of these sORFs are functional, some have been shown to affect plant morphogenesis (Hanada et al., 2013). Since both SNP5 and SNP6 genes could have important functional impacts and the AA conservation analysis did not discount either, they required further validation to determine which was the final causal SNP.

Between the SNP5 and SNP6 proteins, a protein structure is only available for the latter, NSP1 (Zhang et al., 2017). Shown in Figure 3.7*a*, SNP6 causes a substitution at position 372 from alanine to valine deep within the protein core. The valine adds two additional sidechains which could potentially destabilizing effects on the protein structure (A. Doxey, personal communication, 2018).

3.3.6 ION Torrent analysis of candidate *mtar2* SNPs

To find which of SNP5 and SNP6 was the causal SNP, a different sequencing approach was used. A previous study argued that the causal SNP can be differentiated from closely linked SNPs by sequencing a large number of genomes with high read counts (Hartwig et al., 2012). This particular method uses ION Torrent technology (Rothberg et al., 2011) to sequence a small region around the candidate SNPs resulting in thousands of reads. To investigate both SNPs, approximately 200 backcrossed *mtn1-1mtar2* F2 plants were pooled for ION Torrent sequencing. Both SNPs were sequenced with over $10,000$ reads each (Table 3.6). Based on this analysis SNP6 had more reads with the SNP, at 80% of reads versus 50% of SNP5 reads with the SNP (Table 3.6). While this suggested SNP6 to be the causal SNP, in the original method the SNPs were found in over 90% of reads (Hartwig et al., 2012). As a result this experiment would need to be repeated to properly replicate the method. Alternatively, it could also suggest that neither SNP is the causal SNP.

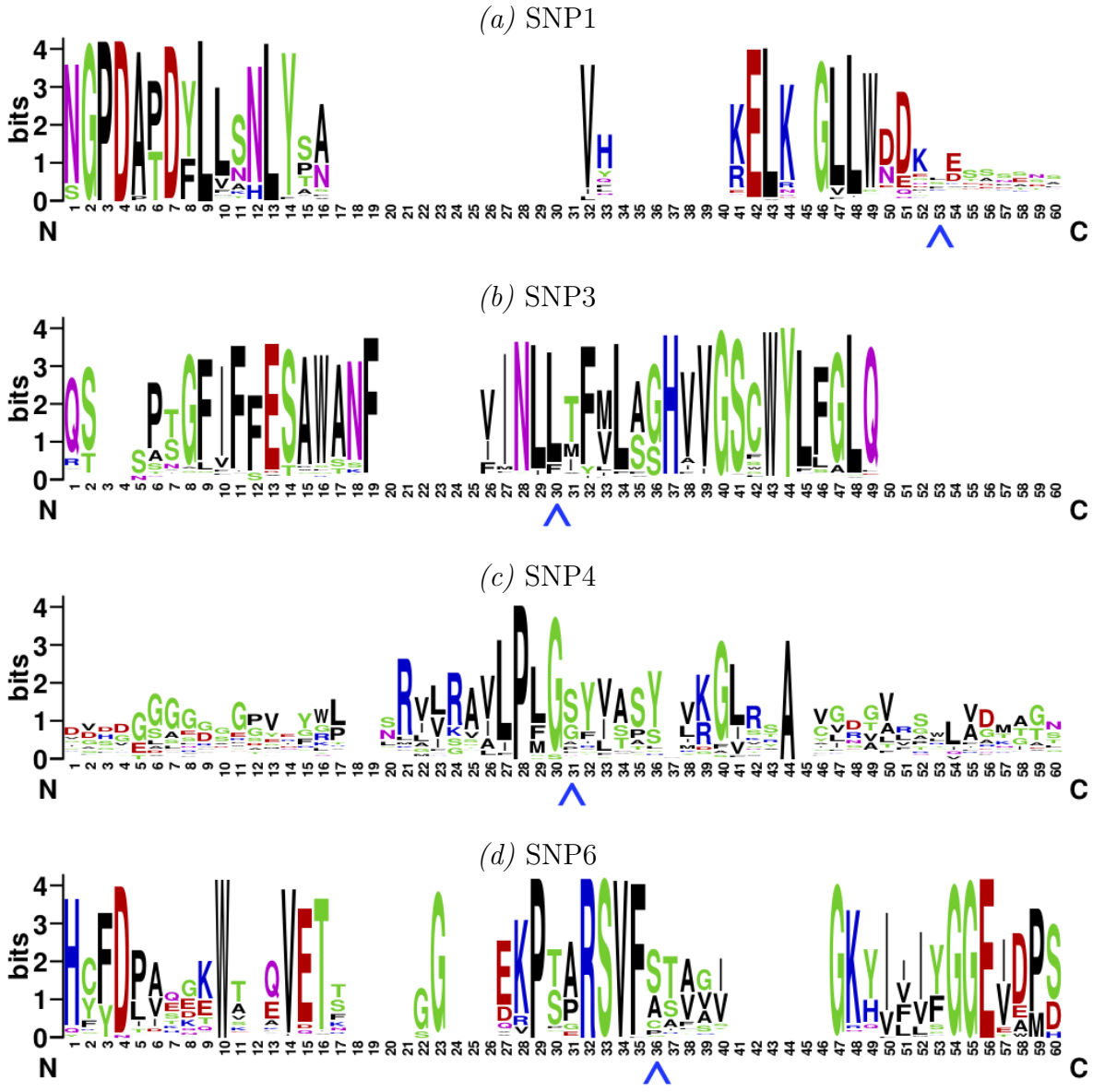

Figure 3.6: Amino acid conservation of putative *mtar2* protein orthologs.

Plant OrthoDB clusters from Table 3.4 were aligned, and the resulting multiple sequence alignment converted to sequence logos using WebLogo (Crooks et al., 2004). Only the row containing the putative *mtar2* SNP from the multiple sequence alignments were used to generate the sequence logos. The location of the putative *mtar2* SNP for each protein is pointed to with a blue arrow. The amino acid substitutions in each putative *mtar2* protein are: G to S for SNP1 *(a)*, L to F for SNP3 *(b)*, G to S for SNP4 *(c)*, and A to V for SNP6 *(d)*.

(a) *(b)*

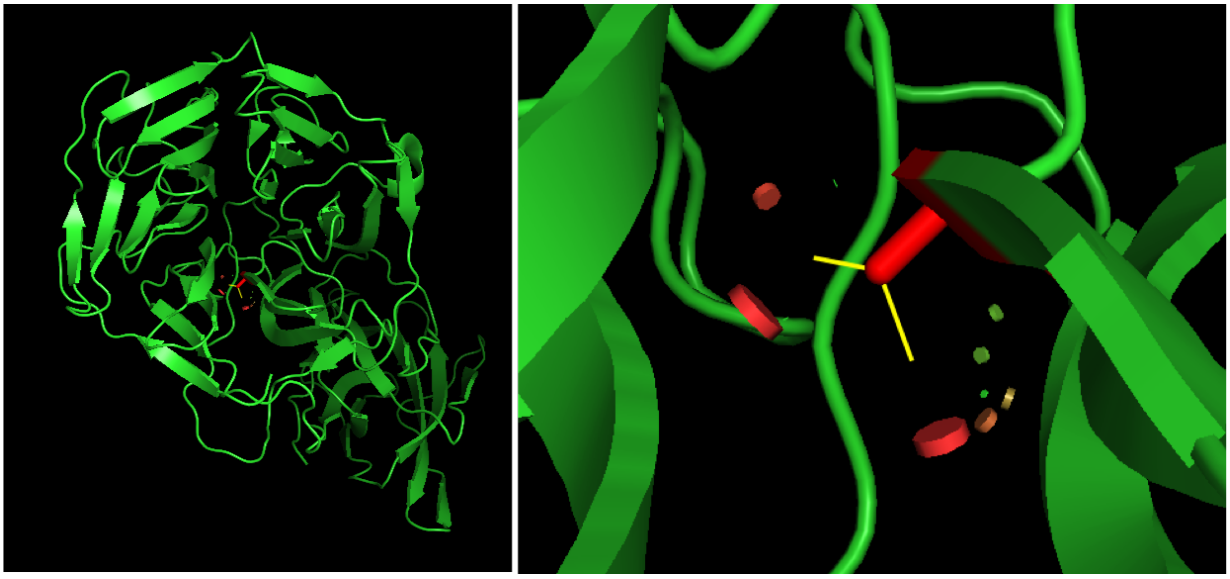

Figure 3.7: Modelling *mtar2* amino acid substitution.

The alanine at position 372 in the protein NSP1 was substituted with valine, the putative *mtar2* mutation. The image in *(b)* is a closeup of the core from the protein in *(a)*. Position 372 is buried deep within the protein. Alanine side chains are shown in red, and additional sidechains introduced by a valine substitution shown in yellow. The valine sidechains would extend the original alanine sidechains and potential destabilize the protein structure. Analysis and illustration curtesy of A. Doxey (personal communication, 2018).

Table 3.4: List of candidate *mtar2* mutations.

Homozygous mutations in WGS data of *mtn1-1mtar2* were extracted. Those which introduced AA substitution are listed.

SNP*	Position on Chr3	Resident gene	Gene symbol	DNA change	AA change
1	2892611	AT3G09400	PLL3	C→T	G→S
3	6050541	AT3G17700	CNBT1	C→T	L→F
4	6930590	AT3G19920	-	C→T	G→S
5	10514696	AT3G28193	-	G→A	L→F
6	5568032	AT3G16400	NSP1	C→T	A→V

*SNP2 was originally mistakenly thought to be within a coding region. It was removed from consideration once the mistake was discovered.

Table 3.5: Analysis of AA conservation in candidate *mtar2* genes.

Plant OrthoDB clusters which included the candidate genes were found. The AA sequences of all cluster members were aligned and the AA conservation of the SNP site was investigated.

SNP	AA change	OrthoDB cluster*	Ortholog count	Original AA†	New AA‡	Gap§
1	G→S	61898at33090	283 in 98 species	7	42	27
3	L→F	35874at33090	250 in 102 species	190	20	27
4	G→S	1012685at2759	184 in 87 species	38	1	124
5	L→F	none	-	-	-	-
6	A→V	123585at3193	164 in 93 species	42	0	6

*The biggest exclusively plant OrthoDB cluster containing the gene of interested was selected, and the protein sequences of all the cluster orthologs were aligned.

†After alignment, the number of orthologs which shared the same AA as the gene of interest at the SNP position were counted.

‡Number of orthologs which have the same AA as that caused by the SNP in the gene of interest at the SNP position.

§Number of orthologs which have a gap in their alignment at the position of SNP in the gene of interest.

Table 3.6: Comparing SNP5 and SNP6 homozygosity with ION Torrent.

Genomic DNA from nearly 200 *mtn1-1mtar2* were extracted. Fragments surrounded the two candidate SNPs were amplified and sent for ION Torrent sequencing. The number of reads with the candidate SNPs were investigated.

SNP	Total reads	Reads with SNP	SNP percent
5	18947	9397	50
6	12548	10036	80

3.3.7 T-DNA analysis of NSP1 as the candidate causal *mtar2* SNP

As an alternative approach to finding the causal SNP, T-DNA insertion mutants in the SNP genes were introduced into a *mtn1-1* background in the hope of finding one which could replicate the original *mtar* phenotype. Between the SNP5 and SNP6 genes, T-DNA mutants could only be found for the SNP6 gene (NSP1). The SALK_072600C line (Alonso et al., 2003) which has a T-DNA insertion in the second exon of NSP1, previously renamed *nsp1-1* (Wittstock et al., 2016), was crossed into a *mtn1-1* background. Homo *mtn1-1nsp1* seedlings were grown on MTA to recreate the conditions of the suppressor screen (Figure 3.8). In this experiment, *mtn1-1nsp1-1* roots did not grow as long as *mtn1-1mtar2* roots on MTA, however were still longer than *mtn1-1* and closer to *mtn1-1mtar8 mtn1-1mtar11* in length (Figure 3.8).

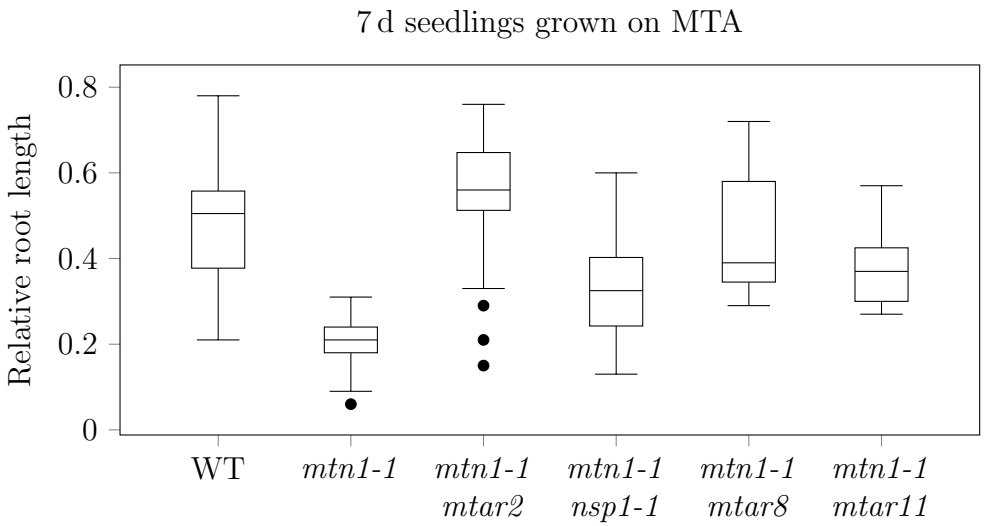

Figure 3.8: Preliminary root length analysis of *mtar* mutants.

Seedlings were grown vertically on media with either 500 µM MTA or 500 µM $MgSO_4$ for 7 d before imaging and root measurements were performed. For each genotype, the relative root length was calculated as the root lengths from growth on MTA divided by the root lengths from growth on $MgSO_4$. The *mtn1-1mtar2* and *mtn1-1mtar11* lines were back-crossed once. (n = 14–30)

3.4 Discussion

3.4.1 Seedling root growth did not respond linearly to increasing MTA concentration

Previous work has shown that *mtn1-1*, but not *mtn2-1*, seedling shoot fresh weight decreased when grown on media containing 500 µM MTA (Bürstenbinder et al., 2010). No negative effects occurred when *mtn1-1* seedlings were grown on media containing 100 µM MTA (Bürstenbinder et al., 2010). This is generally in agreement with the root length measurements of *mtn1-1* seedlings grown on MTA-containing media in this work (Figure 3.1). Additional concentrations were tested, allowing for a more detailed analysis of the impact of MTA on seedling growth of MTN-deficient mutants.

Going from 100 µM MTA to 250 µM MTA, and finally 500 µM MTA, there was a near linear relation ship between decreasing root length and increasing MTA concentration in *mtn1-1* and *mtn1-1mtn2-5* seedlings. This successful result allowed for its use as a suppressor screen assay. However, during this experiment inadvertently another interesting result was noted at lower concentrations. For the most part, low MTA had little effect on the growth of these two genotypes. However, 50 µM MTA (and to a lesser extent 75 µM MTA) the seedlings grew longer roots. This was most pronounced for the G3 seedlings. G3 seedling roots, which were overall sensitive to much lower concentrations of MTA, also showed remarkable root length recovery at 50 µM MTA (*mtn1-1mtn2-1* and G2 genotypes were not tested at this concentration).

Seeing positive root growth responses to MTA is surprising in MTN-deficient plants, as it was never believed MTA accumulation could have beneficial effects on plant health

(Bürstenbinder et al., 2010; Waduwara-Jayabahu et al., 2012). Despite this, the concept of differential responses to changing treatment concentration has been reported for other compounds. In fact, a similar effect can be seen in the root growth of seedlings grown on media containing IAA (Evans et al., 1994; Li et al., 2015). Different concentrations of exogenous IAA will induce auxin signalling via different pathways. For example, low IAA will induce IAA7 signalling, whereas high IAA will induce IAA12 signalling (Calderón Villalobos et al., 2012). For MTA, it could be that there is some positive signalling response to mild amounts of exogenous MTA, and after a certain threshold high exogenous MTA will instead trigger a negative response.

Studying the effects of high MTA accumulation is important to understanding the short root phenotypes of MTN-deficient seedlings grown on MTA-supplemented media as well as the severe mutant phenotype of adult *mtn1-1mtn2-1* plants. However studying the effects of lower MTA accumulation could still be beneficial. For example, the *mtn1-1mtn2-5* mutant does not accumulate MTA any more so than WT (to any detectable degree) in adult plants yet still displays mutant phenotypes, such as delayed bolting and increased vasculature (Waduwara-Jayabahu et al., 2012). The same can be said of *mtn1-1mtn2-1* seedlings, which while exhibiting abnormal phenotypes such as delayed development, interveinal chlorosis and altered cuticle development do not accumulate MTA more than WT to any detectable degree (see chapter 2). Determining the underlying basis for the response to low MTA supplementation could well be informative but would be technically difficult.

3.4.2 Control of SAM accumulation is likely a significant contributor to suppression of the short root phenotype

Perhaps the most surprising result from the metabolite measurements of *mtn1-1mtar* seedlings after MTA treatment was the complete lack of increase in SAM levels (Figure 3.3*a*, 3.3*d*). When grown on MTA-supplemented media, the SAM content of WT and *mtn1-1* seedlings increases (2-fold and 3-fold, respectively) relative to control conditions. Surprisingly this same increase in SAM content did not occur in *mtn1-1mtar* seedlings (Figure 3.3*a* and 3.3*d*). This response (or lack thereof) in MTA-treated *mtn1-1mtar* seedlings is likely a significant contributor in the suppressive effects of the *mtar* mutation.

The mechanism behind the increase in SAM in WT seedlings grown on MTA is unknown. One simplistic explanation for this response is an increased rate of Met regeneration and subsequent SAM formation via the Met salvage cycle. This explanation however does not properly explain the reason for MTA not accumulating past WT amounts in *mtn1-1mtar* seedlings. If MTA was being used for increased SAM biosynthesis in *mtn1-1mtar* mutants then this could make sense. However, SAM levels show absolutely no increase in *mtn1-1mtar* seedlings grown on MTA (Figure 3.3*c*, 3.3*f*).

There are two possible explanations for the mysterious lack of SAM and MTA accumulation in *mtn1-1mtar* seedlings. The easiest is a simple restriction to the movement of exogenous MTA into the plant. The evidence for this is lacking though, as MTA transport studies in human cell lines have revealed there are no specific MTA transporters and rather it moves via a facilitated diffusion mechanism (Cartenì-Farina et al., 1983). The other explanation is that Met regeneration is indeed occurring at a higher rate, but it is not being converted to SAM or SAM is being used at a rate equal to its production. Both these explanations also require that Cys levels not increase, as Cys stays stable in MTA-treated

mtn1-1mtar seedlings (whereas it increases in MTA-treated *mtn1-1*; Figures 3.4*a*, 3.4*d*).

The former explanation involving the restriction of MTA transport into the plant would be harder to validate. The latter explanation concerning a distribution of regenerated Met away from SAM could be validated by further measurements of MTA-related metabolites and a flux analysis of Met. Both possibilities heavily implicate the control of SAM levels in the suppression of the short root phenotype of MTA-treated *mtn1-1* seedlings.

3.4.3 NSP1 and suppression of the short root phenotype

While the evidence is not conclusive, among all of the candidate *mtar2* SNPs the NSP1 SNP, lying in a GLS-related gene, seems most likely to be the causal SNP. GLS are precursor plant defence compounds which are degraded by myrosinases to an unstable intermediate upon herbivory attack (Bones and Rossiter, 1996). The intermediate is spontaneously converted to the defence compound isothiocyanate (ITC); alternatively, specifier proteins can associate with enzymes which use this intermediate to form of nitriles, epithionitriles and thiocyanates (Bones and Rossiter, 2006). NSP1 (one of five copies of NSP) is a specifier protein which induces the formation of simple nitriles (Bones and Rossiter, 2006). The majority of GLS in seedlings generally are converted to simple nitriles, with the majority of the formation of these simple nitriles being attributed to the activity of NSP1 specifically (Wittstock et al., 2016).

Assuming that the activity of NSP1 is affected in *mtn1-1mtar2* allows for an extension of one of the models proposed earlier to explain the effects of MTA feeding. This model proposed Met was being regenerated at a higher rate, but equally being used in other processes indicative of a higher flux through this route of metabolism. By reducing NSP1 activity, the plant could be attempting to maintain normal levels of simple nitriles

by diverting excess Met towards aliphatic GLS production. This would prevent the accumulation of SAM.

An alternative model for the suppressive effects of a mutated NSP1 invokes the relationship of this pathway to auxin synthesis. Aliphatic GLS can be converted to simple nitriles which can form the auxin precursor indole-3-acetonitrile (IAN) (Malka and Cheng, 2017). In this model, sulfur in MTA-treated *mtn1-1* is used for GLS biosynthesis instead of Met, and the excess GLS becomes excess auxin. This elevated auxin biosynthesis would then result in the short root phenotype seen in seedlings grown on higher concentrations of auxin (Evans et al., 1994; Li et al., 2015). By reducing the activity of NSP1 in *mtn1-1mtar2* seedlings, the increased auxin biosynthesis phenotype is suppressed. Of course, as opposed to the previous model, the lack of SAM accumulation is not explained.

More work is needed to validate the NSP1 SNP as being the causal *mtar2* mutation. Furthermore, measurements of ITC, simple nitriles, and auxin would be required to explore the proposed models.

Chapter 4

Conclusion

4.1 Spd transgenerational restoration likely is epigenetic and begins in some cells in the shoot apical meristem

One of the most interesting aspects of Spd transgenerational fertility-restored *mtn1-1mtn2-1* plants is the initial difficulty in generating these lines. After the application of Spd treatment to seedlings only a small fraction of *mtn1-1mtn2-1* plants will be successfully restored, and even so at this point only one or two branches will be fertile (Waduwara-Jayabahu, 2011). This first generation Spd-restored plant (G1) will also otherwise be phenotypically identical to *mtn1-1mtn2-1* plants which have not been Spd-treated, such as exhibiting interveinal chlorosis, thick vasculature, stem fasciation, reduced cuticle, and delayed bolting (Waduwara-Jayabahu, 2011). Amazingly, these phenotypes become increasingly less apparent in subsequent generations (G2, G3), alongside an increase in

fertility; and by the G3 generation, the plants are completely fertile (Waduwara-Jayabahu, 2011). Based on the fertility changing from generation to generation, I propose two hypotheses. First, Spd restoration initially occurs in some cells in the shoot apical meristem of treated seedlings. Second, Spd restoration is epigenetic (specifically at the level of DNA methylation, which is heritable; Budhavarapu et al., 2013). This epigenetic restoration increases over subsequent generations through a positive feedback loop which induces changes in the epigenome.

Considering that the Spd treatment occurs at the seedling stage, it is curious that not only are the metabolite profiles of *mtn1-1mtn2-1* seedlings generally not significantly different from WT, those of the G2 and G3 Spd-restored generations are also unchanged (Chapter 2). In this case, whatever the Spd treatment is doing is only active or triggered past a certain developmental stage or in specific tissues. One such tissue present in seedlings which undergoes huge developmental changes is the shoot apical meristem. The shoot apical meristem is a population of pluripotent cells which generate new leaves and floral organs (Murray et al., 2012). As these cells are individual progenitors of entire organs, random mutations in these cells can result in chimeric plants where different organs have non-identical genomes (Burian et al., 2016). This effectively means that after flowering occurs, these chimeric plants can produce genetically distinct progeny. Borrowing this concept, I propose that during the initial treatment, Spd will randomly affect the pluripotent cells within the shoot apical meristem. This will sometimes result in Spd affecting some cells, which results in the corresponding branches becoming fertile.

The progeny from the few fertile branches in the first generation of Spd restored *mtn1-1mtn2-1* will now be made up of cells which all originated from single Spd-affected shoot apical meristem cells. This explains why these progeny will have the Spd-induced fertility spread across nearly all branches (Waduwara-Jayabahu, 2011). Since the progeny

seedlings share the same metabolite profiles as naive *mtn1-1mtn2-1*, this likely means the changes induced by Spd only become active after a certain developmental trigger. With the current evidence, I suggest this trigger is flowering. Past this point huge changes in the metabolite profiles of the unopened buds of Spd-restored progeny can be detected (Chapter 2). Of course, this does not explain how Spd is affecting these shoot apical meristem cells, nor why the restoration phenotype continues to become stronger over subsequent generations (Waduwara-Jayabahu, 2011).

The second hypothesis takes into consideration the specific mechanism of Spd restoration: that Spd induces epigenetic changes in some kind of positive feedback loop. Though there is yet to be any evidence showing that Spd can induces changes in the epigenome of Arabidopsis, it has been shown to interact with DNA and histones in mammalian cells (Childs et al., 2003) and recent studies indicate Spd can positively benefit human health epigenetically (Madeo et al., 2018). Additionally, epigenetic positive feedback loops are known to occur, for example during accelerated evolution (Furasawa and Kaneko, 2013). Using this information, I propose that Spd induces changes in the epigenome of *mtn1-1mtn2-1*, and additionally there is a positive feedback loop which increases the level of restoration between generations. Of course, with the current evidence there is no way to know which epigenetic changes are involved.

4.2 A unifying model for MTA accumulation, glucosinolates, auxin and callose

While previous studies have carefully described the various mutant phenotypes of the severe *mtn1-1mtn2-1* mutant (Bürstenbinder et al., 2010; Waduwara-Jayabahu et al., 2012), our understanding of the mechanisms causing these phenotypes is still unclear. In this work metabolite measurements and an RNAseq experiment of the *mtn1-1mtn2-1* mutant have allowed for additional insights into the effects of MTA accumulation on the underlying physiology of these plants, at two separate developmental stages. Additionally, metabolite measurements of seedlings treated with exogenous MTA and suppressor mutant experiments were used for an analysis of the impact of artificially high MTA on the main MTA-related pathways. With this information, I propose an overarching model (Figure 4.1) which attempts to explain how MTA accumulation could negatively impact plant physiology throughout a plant's lifespan.

Beforehand, a clarification of the most direct physical effects of MTA accumulation is required. It was previously suggested the most significant direct effects were the feedback inhibition of ethylene, NA, Spd, Spm and Tspm biosynthesis enzymes (Bürstenbinder et al., 2010; Waduwara-Jayabahu et al., 2012). Of these, there is the most evidence supporting the inhibition of NA biosynthesis. Not only have reduced NA levels been detected in both seedling and unopened bud samples tested in this study (Chapter 2), previous studies also corroborate this (Bürstenbinder et al., 2010; Waduwara-Jayabahu et al., 2012). Furthermore the inhibitory activity of MTA on NAS has been previously described (Herbik, 1997). While it is almost certain NA biosynthesis is affected by MTA accumulation, its overall impact on the mutant phenotype is less certain. While this can probably be used to explain

the interveinal chlorosis phenotype of *mtn1-1mtn2-1* mutants (Waduwara-Jayabahu et al., 2012), this could very well be the extent of the effects of reduced NA. At the very least, it is not a major contributing factor in the male and female infertility of *mtn1-1mtn2-1* plants, as transgenerationally Spd-restored G3 plants continue to have severely reduced NA (Chapter 2).

The evidence for an effect on ethylene is unfortunately lacking. It has been shown that MTA inhibits ethylene biosynthesis enzymes *in vitro* (Hyodo and Tanaka, 1986). The *in vivo* evidence of reduced ethylene biosynthesis in MTA-accumulating conditions is sparse. Bürstenbinder et al. (2010) measured ethylene in etiolated single mutant seedlings at 4 d exposed to 500 µM MTA and found no change compared to WT. Washington et al. (2016) measured ethylene from leaves of adult *mtn1-2mtn2-2* mutants under control conditions and also found no change compared to WT. While these two measurements would suggest ethylene biosynthesis is unaffected, it is important to understand the limitations of the measurement method: only ethylene which escapes the plant is measured, and thus internal ethylene levels remain unknown. In this study, RNAseq data of *mtn1-1mtn2-1* unopened buds shows that transcript abundances of ethylene biosynthesis genes *ACO1*, *ACO2* and *ACO3* are increased, perhaps as a response of reduced ethylene (Chapter 2). Waduwara-Jayabahu et al. (2012) also noted a delayed senescence phenotype in *mtn1-1mtn2-1* plants, similar to ethylene-deficient mutants. With all of this mixed evidence, it remains to be seen whether altered ethylene metabolism contributes to the MTN-deficient phenotype.

As for the PAs Spd, Spm and Tspm, the current evidence would suggest the biosynthesis of PAs is not affected by MTA-driven feedback inhibition. In this study and previous studies, Spd levels are never decreased regardless of tissue or level of MTN-deficiency (Chapter 2; Bürstenbinder et al., 2010; Waduwara-Jayabahu et al., 2012). Spm has also been measured previously with the same result, showing no decrease (Bürstenbinder et al.,

2010; Waduwara-Jayabahu et al., 2012). As for Tspm, the low abundance of this metabolite has made it difficult to measure. Despite this, there is some phenotypic evidence of Tspm levels being unaffected by MTA accumulation: Tspm-deficient adult plants have a severe dwarf phenotype unseen even in the severe *mtn1-1mtn2-1* mutant (Clay and Nelson, 2005). Waduwara-Jayabahu et al. (2012) provided *in silico* evidence of the existence of an interaction between SPDS and ACL5 with MTA. Even so, this is not evidence of an inhibitory relationship. In fact, it has been shown that while SPDS in *Plasmodium falciparum* also interacts with MTA *in vitro*, there is no inhibitory relationship (Sprenger et al., 2016). With all of this information, I suggest that the PA biosynthesis enzymes in Arabidopsis are simply not feedback inhibited by MTA under MTA-accumulating conditions. At this point an *in vitro* inhibitor study would be needed to show otherwise.

I also propose two additional direct effects of MTA accumulation. The first is a feedback inhibition of MTA onto sulfur assimilation via Cys. As shown in Figure 4.1*a*, sulfur is incorporated and stored in the form of APS. At this point APS can be used to form PAPS for sulfonation reactions, or Cys. I propose that MTA inhibits the flow of sulfur towards Cys. The sulfur metabolites H_2S, Cys and GSH (Figure 1.2) have been shown to feedback inhibit sulfur assimilation through some unknown sulfur sensing mechanism (Kopriva, 2006). It would not be unreasonable to extend this to include the sulfur-containing MTA among these. This suppression of sulfur assimilation via Cys is supported by the metabolite data of unopened buds from *mtn1-1mtn2-1* mutants in Chapter 2. This mutant accumulates over ten times as much MTA in unopened buds, making this tissue ideal to study the effects of MTA accumulation. In the metabolite data of unopened buds, the key sulfur metabolites Cys, Met and SAM are all decreased. Some of these data are actually consistent with a previous metabolome study of sulfur-starved Arabidopsis. Nikiforova et al. (2005) showed that both Cys and SAM decreased. Interestingly, under sulfur-limiting conditions

Nikiforova et al. (2005) an increase in Put was also noted, which is consistent with the increase in Put detected in *mtn1-1mtn2-1* unopened buds. While I cannot suggest the exact MTA interaction which would induce this inhibition of sulfur assimilation into Cys as the sulfur sensing mechanism in Arabidopsis is unknown, amongst the data provided in Chapter 2 are clear signs that a reduction in sulfur assimilation via Cys is occurring. With MTA being the only measured sulfur metabolite accumulating to a large degree, it is a likely candidate for this inhibition.

The second direct effect of MTA accumulation I propose involves the formation of ROS. This would occur either via the direct formation of radical MTA species, or by another directly MTA-induced ROS-forming mechanism. Unfortunately there are currently no previous studies which could support this, but assuming that high MTA can lead to a direct increase in ROS allows for a simple explanation of some of the phenotypes seen in *mtn1-1mtn2-1* mutants. Among some of the enriched GO terms from differentially expressed gene clusters in the RNAseq of *mtn1-1mtn2-1* unopened buds are those related to various stress responses, including ROS (Chapter 2). While this by itself is not strong evidence, I would suggest the fertility restoration on *mtn1-1mtn2-1* stems which have had the apical bud cluster decapitated supports this conclusion. In Chapter 2 I argued that fertility was being restored due to a quick and dramatic decrease in MTA levels in the remaining flowers on decapitated stems, which were originally rendered infertile by high ROS. In order for the rapid decrease in MTA levels to correlate closely with ROS levels, some closely linked interaction would be necessary. MTA being a direct, or at least near-direct, source of ROS would allow for a simple explanation of this phenomenon.

With a clarification of specific MTA-affected processes, a more in-depth discussion of how these processes subsequently affect plant physiology can begin. I propose that the sulfur not being used for sulfur assimilation via Cys is instead being used for the production of GLS

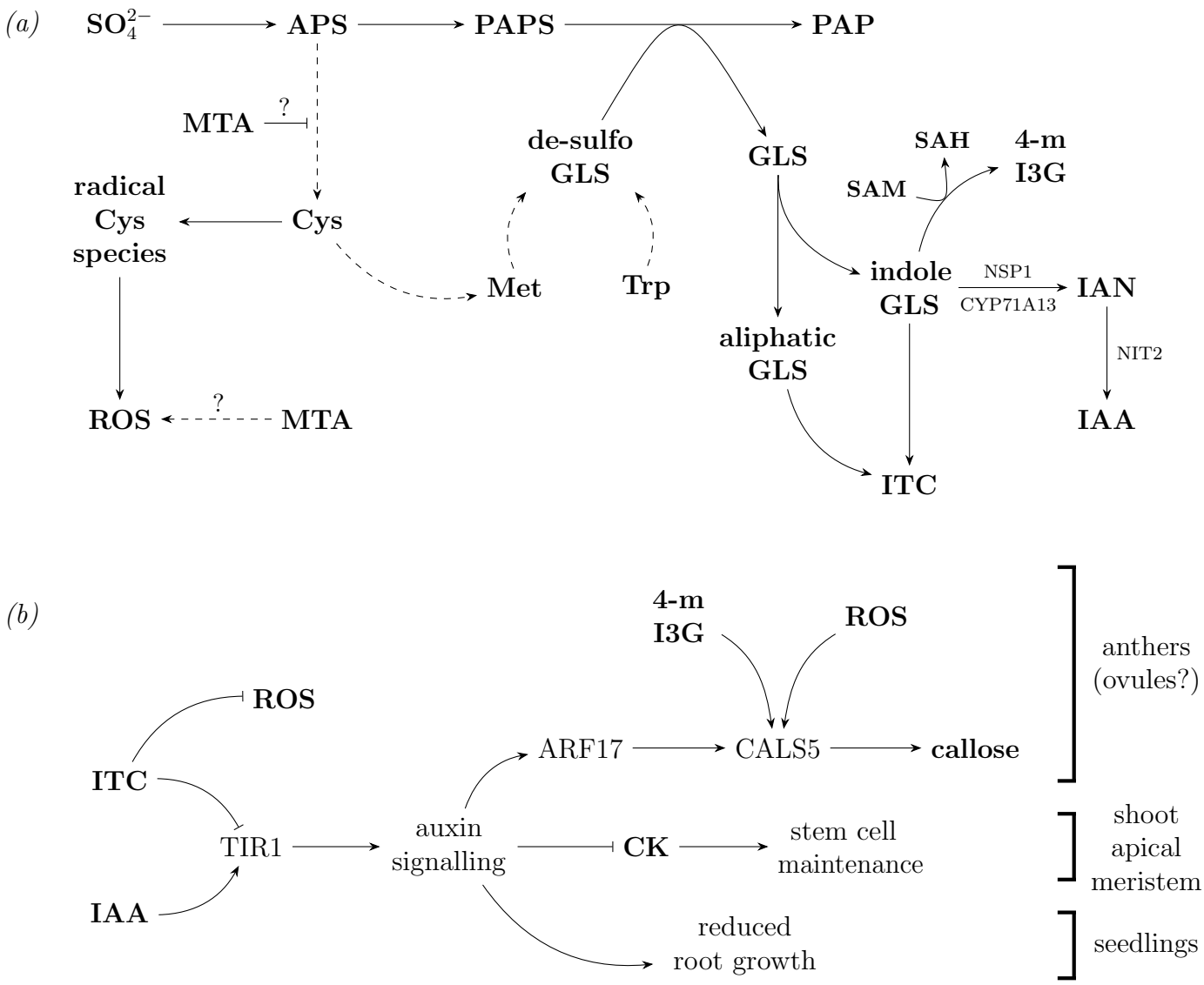

Figure 4.1: A combined model for the involvement of MTA in auxin, callose, glucosinolates and sulfur assimilation.

In *(a)*, MTA suppresses sulfur assimilation through cysteine and also contributes to increased ROS. Sulfur is driven towards GLS, which drives auxin biosynthesis through the formation of IAN. In *(b)*, increased auxin signalling and ROS levels negatively affect various tissues under MTA-accumulating conditions. *4-m I3G, 4-methoxy-indol-3-ylmethylglucosinolate. APS, adenylylsulfate. Cys, cysteine. GLS, glucosinolates. GSH, glutathione. IAA, auxin. IAN,* *(continued on next page)*

Figure 4.1: PA combined model for the involvement of MTA in auxin, callose, glucosinolates and sulfur assimilation. (Cont)

indole-3-acetonitrile. ITC, isothyocyanate. Met, methionine. MTA, methylthioadenosine. PAP, 3′-phosphoadenosine 5′-phosphate. PAPS, 3′-phosphoadenylyl sulfate. ROS, reactive oxygen species. SAH, S-adenosylhomocysteine. SAM, S-adenosylmethionine. Trp, tryptophan.

(Figure 4.1*a*). There are three classes of GLS, derived from different amino acids: aliphatic (alanine, isoleucine, leucine, methionine, valine), aromatic (phenylalanine, tyrosine), and indole (tryptophan; Ishida et al., 2014). GLS upon being hydrolyzed by myrosinases, GLS will spontaneously form ITC, but the alternative products nitriles, epithionitriles and thiocyanates can also be formed by the association of specifier proteins with the respective enzymes (Ishida et al., 2014). ITC are bitter defence compounds produced by plants to discourage herbivory predation, but have also been shown to have anti-oxidant properties (Ishida et al., 2014). Interestingly, nitriles formed from indole GLS can be further processed to form the auxin precursor IAN, which is believed to contribute significantly to the total auxin pool in Arabidopsis (Malka and Cheng, 2017).

From the RNAseq experiment of unopened buds from *mtn1-1mtn2-1*, transcript abundance of the IAN biosynthesis genes *CYP71A13* was increased twenty-fold, and transcript abundance of the auxin biosynthesis gene *NIT2* (which uses IAN as a substrate) was increased sixty-four-fold (Chapter 2). Combined with a suppression of sulfur assimilation towards Cys, this would suggest an increase in auxin biosynthesis from GLS (Figure 4.1*a*). This is also supported by the discovery of the NSP1 mutant *mtar2* as a potential suppressor of the short root phenotype of MTA-fed *mtn1-1* seedlings (Chapter 3). NSP1 is a specifier protein which is required for the formation of IAN from indole GLS (Malka and Cheng, 2017). The suppressor mutant experiment suggests that the MTA-induced short root phenotype could perhaps be suppressed by preventing auxin biosynthesis from indole GLS.

These GLS could instead form ITC, which could help reduce ROS levels (Ishida et al., 2014). Additionally, ITC is further broken down to indole-3-carbinol (I3C), which has been shown to act as auxin antagonist by binding the auxin-binding pocket of auxin signaling protein TIR1 (Katz et al., 2015).

Taken together, these results support a model wherein MTA accumulation leads to increased ROS and auxin biosynthesis. These metabolites could act together to lead to some of the phenotypes seen in MTN-deficient mutants (Figure 4.1*b*). In seedlings, high auxin leads to the short root phenotype (Evans et al., 1994; Li et al., 2015). In anthers, (where increased callose deposition has been observed for *mtn1-1mtn2-1* mutants; N. Perera, E. Yeung and B. Moffatt, personal communication, 2018; Waduwara-Jayabahu et al., 2012), increased auxin signalling (via ARF17) and ROS leads to a CALS5-dependent increase in callose (Shi et al., 2015). It could also be possible for the indole GLS product 4-methoxy-indol-3-ylmethylglucosinolate (4-m I3G), which induces CALS5 activity (Clay et al., 2009), to contribute to this. Finally, high auxin biosynthesis negatively affects stem cell maintenance in the shoot apical meristem. This is usually performed by cytokinin, however cytokinin biosynthesis in the shoot apical meristem is suppressed by auxin (Su et al., 2011). By disturbing the careful balance between auxin and cytokinin in the shoot apical meristem, this results in a larger meristem and altered phyllotaxy (Su et al., 2011). Though the size of the shoot apical meristem of MTN-deficient mutants is unknown, signs of a disturbed shoot apical meristem are present: for example, delayed bolting and increased number of shoots in *mtn1-1mtn2-1* mutants (Waduwara-Jayabahu, 2011).

One weakness of this proposed model is that it does not explain the transgenerational Spd restoration, though at the very least there are hints that it is related. For example, there are signs that the inhibition of sulfur assimilation is reduced in unopened buds of G3 plants: Cys and SAM levels increase, and even Put decreases (Chapter 2). Furthermore, transcript

abundance of the auxin biosynthesis gene *NIT2* decreases eleven-fold in G3 unopened buds relative to *mtn1-1mtn2-1* (Chapter 2). Further work is required to investigate the exact mechanism behind transgenerational Spd restoration.

4.3 Future work

There are four main directions which require further investigation. The first is to determine the involvement of PRMT5 in MTN-deficient plants. While the evidence provided in Chapter 2 would suggest PRMT5 is unrelated, this evidence is incomplete. Two possible experiments would include *in vitro* inhibitor assays of MTA and PRMT5, and observing the phenotype of triple mutant *prmt5mtn1-1mtn2-1* plants. If this triple mutant is phenotypically identical to *mtn1-1mtn2-1*, then it could suggest PRMT5 is already affected.

The second is a continued exploration of the *mtar* suppressor mutants. Further validation of NSP1 as *mtar2* is required, which in the simplest case involves repeating the root length analysis of NSP1 T-DNA insertion mutants. By confirming that different mutant alleles can be used to replicate the suppression mutant, this could help validate NSP1 as the *mtar2* gene. WGS of *mtar8* is also underway, with plans for WGS of *mtar11* as well. Identification of additional MTAR genes will help decipher the effects MTA accumulation, and could contribute the model proposed in Figure 4.1.

More evidence in general is needed to support the model proposed in Figure 4.1. This would include measurements of key metabolites in unopened buds of *mtn1-1mtn2-1* plants. For example: auxin, cytokinin, IAN, ITC and 4-m I3G. Evidence of increased ROS and callose in anthers is required. Experiments are also underway to observe stem cell maintenance in the shoot apical meristem of *mtn1-1mtn2-1* plants using the double reporter *pCLV3:mCherry-NLS pWUS:3xVENUS-NLS* (Pfeiffer et al., 2016).

Finally, further experiments are needed to deepen on understanding of transgenerational Spd restoration. One such planned experiment is bisulfite sequencing of unopened buds from WT, *mtn1-1mtn2-1*, and G3 plants. This would allow for a comparison of the DNA

methylation profiles of these plants. By doing this, the epigenetic changes induced by Spd in G3 could be known and increase our understanding of restoration.

References

Adams, D. and Yang, S. (1977). Methionine metabolism in apple tissue: implication of *s*-adenosylmethionine as an intermediate in the conversion of methionine to ethylene. *Plant Physiology*, 60:892–896.

Albers, E. (2009). Metabolic characteristics and importance of the universal methionine salvage pathway recycling methionine from 5′-methylthioadenosine. *IUBMB Life*, 61(12):1132–1142.

Alonso, J. M., Stepanova, A. N., Leisse, T. J., Kim, C. J., Chen, H., Shinn, P., Stevenson, D. K., Zimmerman, J., Barajas, P., Cheuk, R., Gadrinab, C., Heller, C., Jeske, A., Koesema, E., Meyers, C. C., Parker, H., Prednis, L., Ansari, Y., Choy, N., Deen, H., Geralt, M., Hazari, N., Hom, E., Karnes, M., Mulholland, C., Ndubaku, R., Schmidt, I., Guzman, P., Aguilar-Henonin, L., Schmid, M., Weigel, D., Carter, D. E., Marchand, T., Risseeuw, E., Brogden, D., Zeko, A., Crosby, W. L., Berry, C. C., and Ecker, J. R. (2003). Genome-wide insertional mutagenesis of *Arabidopsis thaliana*. *Science*, 301(5633):653–657.

Andreu-Pérez, P., Esteve-Puig, R., de Torre-Minguela, C., López-Fauqued, M., Bech-Serra, J. J., Tenbaum, S., Garcia-Trevijano, E. R., Canals, F., Merlino, G., Avila, M. A.,

and Recio, J. A. (2011). Protein arginine methyltransferase 5 regulates ERK1/2 signal transduction amplitude and cell fate through CAF. *Science Signaling*, 4:ra58.

Avila, M., García-Trevijano, E., Lu, S., Corrales, F., and Mato, J. (2004). Methylthioadenosine. *The International Journal of Biochemistry & Cell Biology*, 36(11):2125–2130.

Batistic, O., Waadt, R., Steinhorst, L., Held, K., and Kudla, J. (2010). CBL-mediated targeting of CIPKs facilitates the decoding of calcium signals emanating from distinct cellular stores. *The Plant Journal*, 61(2):211–222.

Bedinger, P. (1992). The remarkable biology of pollen. *Plant Cell*, 4:879–887.

Belda-Palazón, B., Almendáriz, C., Martí, E., Carbonell, J., and Ferrando, A. (2016). Relevance of the axis spermidine/eIF5A for plant growth and development. *Frontiers in Plant Science*, 7:245.

Belda-Palazón, B., Ruiz, L., Martí, E., Tárraga, S., Tiburcio, A., Culiánez, F., Farras, R., Carrasco, P., and Ferrando, A. (2012). Aminopropyltransferases involved in polyamine biosynthesis localize preferentially in the nucleus of plant cells. *PLoS One*, 7(10):e46907.

Benne, R. and Hershey, J. (1978). The mechanism of action of protein synthesis initiation factors from rabbit reticulocytes. *The Journal of Biological*, 253:3078–3087.

Beroukhim, R., Mermel, C. H., Porter, D., Wei, G., Raychaudhuri, S., Donovan, J., Barretina, J., Boehm, J. S., Dobson, J., Urashima, M., Henry, K. T. M., Pinchback, R. M., Ligon, A. H., Cho, Y.-J., Haery, L., Greulich, H., Reich, M., Winckler, W., Lawrence, M. S., Weir, B. A., Tanaka, K. E., Chiang, D. Y., Bass, A. J., Loo, A., Hoffman, C., Prensner, J., Liefeld, T., Gao, Q., Yecies, D., Signoretti, S., Maher, E., Kaye, F. J., Sasaki, H., Tepper, J. E., Fletcher, J. A., Tabernero, J., Baselga, J., Tsao,

M.-S., Demichelis, F., Rubin, M. A., Janne, P. A., Daly, M. J., Nucera, C., Levine, R. L., Ebert, B. L., Gabriel, S., Rustgi, A. K., Antonescu, C. R., Ladanyi, M., Letai, A., Garraway, L. A., Loda, M., Beer, D. G., True, L. D., Okamoto, A., Pomeroy, S. L., Singer, S., Golub, T. R., Lander, E. S., Getz, G., Sellers, W. R., and Meyerson, M. (2010). The landscape of somatic copy-number alteration across human cancers. *Nature*, 463:899–905.

Bhagavan, N. and Ha, C.-E. (2015). *Essentials of Medical Biochemistry*, chapter 15: Protein and Amino Acid Metabolism, pages 227–268. Academic Press, Cambridge, Massachusettes, USA, 2nd edition.

Bistulfi, G., Affronti, H. C., Foster, B. A., Karasik, E., Gillard, B., Morrison, C., Mohler, J., Phillips, J. G., and Smiraglia, D. J. (2016). The essential role of methylthioadenosine phosphorylase in prostate cancer. *Oncotarget*, 7(12).

Blanchet, F., Cardona, A., Letimier, F., Hershfield, M., and Acuto, O. (2005). CD28 costimulatory signal induces protein arginine methylation in T cells. *Journal of Experimental Medicine*, 202(3):371–377.

Bones, A. and Rossiter, J. (1996). The myrosinase-glucosinolate system, its organisation and biochemistry. *Physiologia Plantarum*, 97(1):194–208.

Bones, A. and Rossiter, J. (2006). The enzymatic and chemically induced decomposition of glucosinolates. *Phytochemistry*, 67(11):1053–1067.

Budhavarapu, V., Chavez, M., and Tyler, J. (2013). How is epigenetic information maintained through DNA replication? *Epigenetics & Chromatin*, 6:32.

Burian, A., Barbier de Reuille, P., and Kuhlemeier, C. (2016). Patterns of stem cell divisions contribute to plant longevity. *Current Biology*, 26(11):1385–1394.

Burow, M., Losansky, A., Müller, R., Plock, A., Kliebenstein, D., and Wittstock, U. (2009). The genetic basis of constitutive and herbivore-induced ESP-independent nitrile formation in Arabidopsis. *Plant Physiology*, 149(1):561–574.

Bürstenbinder, K., Rzewuski, G., Wirtz, M., Hell, R., and Sauter, M. (2007). The role of methionine recycling for ethylene synthesis in Arabidopsis. *The Plant Journal*, 49(2):238–249.

Bürstenbinder, K., Waduwara, I., Schoor, S., Moffatt, B. A., Wirtz, M., Minocha, S. C., Oppermann, Y., Bouchereau, A., Hell, R., and Sauter, M. (2010). Inhibition of 5′-methylthioadenosine metabolism in the yang cycle alters polyamine levels, and impairs seedling growth and reproduction in Arabidopsis. *The Plant Journal*, 62(6):977–988.

Calderón Villalobos, L., Lee, S., De Oliveira, C., Ivetac, A., Brandt, W., Armitage, L., Sheard, L., Tan, X., Parry, G., Mao, H., Zheng, N., Napier, R., Kepinski, S., and Estelle, M. (2012). A combinatorial TIR1/AFB-Aux/IAA co-receptor system for differential sensing of auxin. *Nature Chemical Biology*, 8(5):477–485.

Carpenter, A. and Sabatini, D. (2004). Systematic genome-wide screens of gene function. *Nature Reviews Genetics*, 5(1):11–22.

Cartenì-Farina, M., della Ragione, F., Cacciapuoti, G., Porcelli, M., and Zappia, V. (1983). Transport and metabolism of 5′-methylthioadenosine in human erythrocytes. *Biochimica et Biophysica Acta – Biomembranes*, 727(2):221–229.

Caudill, M., Wang, J., Melnyk, S., Pogribny, I., Jernigan, S., Collins, M., Santos-Guzman, J., Swendseid, M., Cogger, E., and James, S. (2001). Intracellular *s*-adenosylhomocysteine concentrations predict global DNA hypomethylation in tissues of methyl-deficient cystathionine β-synthase heterozygous mice. *The Journal of Nutrition*, 131(11):2811–2818.

Chapman, E. and Carrington, J. (2007). Specialization and evolution of endogenous small RNA pathways. *Nature Reviews Genetics*, 8:884–896.

Chattopadhyay, M., Tabor, C., and Tabor, H. (2005). Studies on the regulation of ornithine decarboxylase in yeast: effect of deletion in the *MEU1* gene. *Proceedings of the National Academy of Sciences of the United States of America*, 102:16158–16163.

Cheng, C.-Y., Krishnakumar, V., Chan, A. P., Thibaud-Nissen, F., Schobel, S., and Town, C. D. (2017). Araport11: a complete reannotation of the *Arabidopsis thaliana* reference genome. *The Plant Journal: For Cell and Molecular Biology*, 89(4):789–804.

Childs, A., Mehta, D., and Gerner, E. (2003). Polyamine-dependent gene expression. *Cellular and Molecular Life Sciences*, 60(7):1394–1406.

Chung, J., Karkhanis, V., Tae, S., Yan, F., Smith, P., Ayers, L. W., Agostinelli, C., Pileri, S., Denis, G. V., Baiocchi, R. A., and Sif, S. (2013). Protein arginine methyltransferase 5 (PRMT5) inhibition induces lymphoma cell death through reactivation of the retinoblastoma tumor suppressor pathway and polycomb repressor complex 2 (PRC2) silencing. *The Journal of Biological*, 288:35534–35547.

Cingolani, P., Patel, V., Coon, M., Nguyen, T., Land, S., Ruden, D., and Lu, X. (2012). Using *Drosophila melanogaster* as a model for genotoxic chemical mutational studies with a new program, SnpSift. *Frontiers in Genetics*, 3.

Clay, N., Adio, A., Denoux, C., Jander, G., and Ausubel, F. (2009). Glucosinolate metabolites required for an Arabidopsis innate immune response. *Science*, 323(5910):95–101.

Clay, N. and Nelson, T. (2005). Arabidopsis *thickvein* mutation affects vein thickness and

organ vascularization, and resides in a provascular cell-specific spermine synthase involved in vein definition and in polar auxin transport. *Plant Physiology*, 138(2):767–777.

Crooks, G., Hon, G., Chandonia, J., and Brenner, S. (2004). WebLogo: a sequence logo generator. *Genome Research*, 14:1188–1190.

Cucinotta, M., Colombo, L., and Roig-Villanova, I. (2014). Ovule development, a new model for lateral organ formation. *Frontiers in Plant Science*, 5:117.

Cunningham-Rundles, S. and Maas, W. (1975). Isolation, characterization, and mapping of *Escherichia coli* mutants blocked in the synthesis of ornithine decarboxylase. *Journal of Bacteriology*, 124:791–799.

Das, K. and Misra, H. (2004). Hydroxyl radical scavenging and singlet oxygen quenching properties of polyamines. *Molecular and Cellular Biochemistry*, 262:127–133.

de Poel, B. V. and Straeten, D. V. D. (2014). 1-aminocyclopropane-1-carboxylic acid (ACC) in plants: more than just the precursor of ethylene! *Frontiers in Plant Science*, 5:640.

De Storme, N. and Geelen, D. (2014). Callose homeostasis at plasmodesmata: molecular regulators and developmental relevance. *Frontiers in Plant Science*, 5:138.

Deng, X., Gu, L., Liu, C., Lu, T., Lu, F., Lu, Z., Cui, P., Pei, Y., Wang, B., Hu, S., and Cao, X. (2010). Arginine methylation by the *Arabidopsis* homolog of PRMT5 is essential for proper pre-mRNA splicing. *Proceedings of the National Academy of Sciences of the United States of America*, 107(44):19114–19119.

Desai, M., Rangarajan, P., Donahue, J., Williams, S., Land, E., Mandal, M., Phillippy, B., Perera, I., Raboy, V., and Gillaspy, G. (2014). Two inositol hexakisphosphate kinases drive inositol pyrophosphate synthesis in plants. *The Plant Journal*, 80(4):642–653.

Dobin, A., Davis, C. A., Schlesinger, F., Drenkow, J., Zaleski, C., Jha, S., Batut, P., Chaisson, M., and Gingeras, T. R. (2013). Star: ultrafast universal RNA-seq aligner. *Bioinformatics*, 29(1):15–21.

Dubin, M., Zhang, P., Meng, D., Remigereau, M., Osborne, E., Paolo Casale, F., Drewe, P., Kahles, A., Jean, G., Vilhjálmsson, B., Jagoda, J., Irez, S., Voronin, V., Song, Q., Long, Q., Rätsch, G., Stegle, O., Clark, R., and Nordborg, M. (2015). DNA methylation in Arabidopsis has a genetic basis and shows evidence of local adaption. *eLife*, 4:e05255.

Dubois, M., den Broeck, L. V., and Inzé, D. (2018). The pivotal role of ethylene in plant growth. *Trends in Plant Science*, 23(4):311–323.

Eckardt, N. (2010). Myo-inositol biosynthesis genes in Arabidopsis: differential patterns of gene expression and role in cell death. *The Plant Cell*, 22(3):537.

Eckert, C., Offenborn, J., Heinz, T., Armarego-Marriott, T., Schültke, S., Zhang, C., Hillmer, S., Heilmann, M., Schumacher, K., Bock, R., Heilmann, I., and Kudla, J. (2014). The vacuolar calcium sensors CBL2 and CBL3 affect seed size and embryonic development in *Arabidopsis thaliana*. *The Plant Journal*, 78(1):146–156.

Estrada, A., Freese, N., Blakley, I., and Loraine, A. (2015). Analysis of pollen-specific alternative splicing in *Arabidopsis thaliana* via semi-quantitative PCR. *PeerJ*, 3:e919.

Evans, M., Ishikawa, H., and Estelle, M. (1994). Responses of *Arabidopsis* roots to auxin studied with high temporal resolution: comparison of wild type and auxin-response mutants. *Planta*, 194(2):215–222.

Facchini, P., Hagel, J., and Zulak, K. (2002). Hydroxycinnamic acid amide metabolism: physiology and biochemistry. *Canadian Journal of Botany*, 80:577–589.

Fan, H., Zhang, Z., Wang, N., Cui, Y., Sun, H., Liu, Y., Wu, H., Zheng, S., Bao, S., and Ling, H. (2014). SKB1/PRMT5-mediated histone H4R3 dimethylation of Ib subgroup bHLH genes negatively regulates iron homeostasis in *Arabidopsis thaliana*. *The Plant Journal*, 77(2):209–221.

Feng, H., Chen, Q., Feng, J., Zhang, J., Yang, X., and Zuo, J. (2007). Functional characterization of the Arabidopsis eukaryotic translation initiation factor 5A-2 that plays a crucial role in plant growth and development by regulating cell division, cell growth, and cell death. *Plant Physiology*, 144(3):1531–1545.

Ferla, M. and Patrick, W. (2014). Bacterial methionine biosynthesis. *Microbiology*, 160:1571–1584.

Finkelstein, J. D. and Martin, J. J. (2000). Homocysteine. *The International Journal of Biochemistry & Cell Biology*, 32(4):385–389.

Friesen, W. J., Paushkin, S., Wyce, A., Massanet, S., Pesiridis, G. S., Van Duyne, G., Rappsilber, J., Mann, M., and Dreyfuss, G. (2001). The methylosome, a 20S complex containing JBP1 and pICIn, produces dimethylarginine-modified Sm proteins. *Molecular Cell Biology*, 21:8289–8300.

Fu, Y., Zhang, G., Lv, X., Guan, Y., Yi, H., and Gong, J. (2013). Arabidopsis histone methylase CAU1/PRMT5/SKB1 acts as an epigenetic suppressor of the calcium signaling gene CAS to mediate stomatal closure in response to extracellular calcium. *Plant Cell*, 25(8):2878–2891.

Fujisawa, S. and Kadoma, Y. (2005). Kinetic evaluation of polyamines as radical scavengers. *Anticancer Research*, 25:965–969.

Furasawa, C. and Kaneko, K. (2013). Epigenetic feedback regulation accelerate adaptation and evolution. *PLoS ONE*, 8(5):e61251.

Gianotti, A., Tower, P., Sheley, J., Conte, P., Spiro, C., Ferro, A., Fitchen, J., and Riscoe, M. (1990). Selective killing of *Klebsiella pneumoniae* by 5′-trifluoromethylthioribose. chemotherapeutic exploitation of the enzyme 5′-methylthioribose kinase. *The Journal of Biological*, 265:831–837.

Gigolashvili, T. and Kopriva, S. (2014). Transporters in plant sulfur metabolism. *Frontiers in Plant Science*, 5:442.

Gil-Amado, J. and Gomez-Jimenez, M. (2012). Regulation of polyamine metabolism and biosynthetic gene expression during olive mature-fruit abscission. *Planta*, 235:1221–1237.

Gilbert, S. (2000). *Developmental Biology*, chapter 20: An overview of plant development. Sinauer Associates, Sunderland, Massachusettes, USA, 6th edition.

Gotoh, I., Uekita, T., and Seiki, M. (2007). Regulated nucleo-cytoplasmic shuttling of human aci-reductone dioxygenase (hADI1) and its potential role in mRNA processing. *Genes Cells*, 12:105–117.

Gregio, A., Cano, V., Avaca, J., Valentini, S., and Zanelli, C. (2009). eIF5A has a function in the elongation step of translation in yeast. *Biochemical and Biophysical Research Communications*, 380:785–790.

Groppa, M. (2008). Polyamines and abiotic stress: recent advances. *Amino Acids*, 34:35–45.

Guranowski, A., Chiang, P., and Cantoni, G. (1981). 5′-methylthioadenosine nucleosidase: Purification and characterization of the enzyme from *Lupinus luteus* seeds. *European Journal of Biochemistry*, 114:293–299.

Ha, H., Sirisoma, N., Kuppusamy, P., Zweier, J., Woster, P., and Casero, R. (1998). The natural polyamine spermine functions directly as a free radical scavenger. *Proceedings of the National Academy of Sciences of the United States of America*, 95:11140–11145.

Hanada, K., Higuchi-Takeuchi, M., Okamoto, M., Yoshizumi, T., Shimizu, M., Nakaminami, K., Nishi, R., Ohashi, C., Iida, K., Tanaka, M., Horii, Y., Kawashima, M., Matsui, K., Toyoda, T., Shinozaki, K., Seki, M., and Matsui, M. (2013). Small open reading frames associated with morphogenesis are hidden in plant genomes. *Proceedings of the National Academy of Sciences of the United States of America*, 110(6):2395–2400.

Hanada, K., Zhang, X., Borevitz, J., Li, W., and Shiu, S. (2007). A large number of novel coding small open reading frames in the intergenic regions of the *Arabidopsis thaliana* genome are transcribed and/or under purifying selection. *Genome Research*, 17(5):632–640.

Hartwig, B., James, G., Konrad, K., Schneeberger, K., and Turck, F. (2012). Fast isogenic mapping-by-sequencing ethyl methanesulfonate-induced mutant bulks. *Plant Physiology*, 160:591–600.

Hayashi, T., Teruya, T., Chaleckis, R., Morigasaki, S., and Yanagida, M. (2018). *s*-adenosylmethionine synthetase is required for cell growth, maintenance of G0 phase, and termination of quiescence in fission yeast. *iScience*, 5:38–51.

He, X.-J., Ma, Z.-Y., and Liu, Z.-W. (2014). Non-coding RNA transcription and RNA-directed DNA methylation in *Arabidopsis*. *Molecular Plant*, 7(9):1406–1414.

Heeg, C., Kruse, C., Jost, R., Gutensohn, M., Ruppert, T., Wirtz, M., and Hell, R. (2008). Analysis of the Arabidopsis o-acetylserine(thiol)lyase gene family demonstrates

compartment-specific differences in the regulation of cysteine synthesis. *The Plant Cell Online*, 20(1):168–185.

Henderson, A. and Hershey, J. (2011). Eukaryotic translation initiation factor (eIF) 5A stimulates protein synthesis in *Saccharomyces cerevisiae*. *Proceedings of the National Academy of Sciences of the United States of America*, 108:6415–6419.

Henrich, F., Singer, K., Poller, K., Bernhardt, L., Strobl, C., Limm, K., Ritter, A., Gottfried, E., Völkl, S., Jacobs, B., Peter, K., Mougiakakos, D., Dettmer, K., Oefner, P., Bosserhoff, A., Kreutz, M., Aigner, M., and Mackensen, A. (2016). Suppressive effects of tumor cell-derived 5′-deoxy-5′-methylthioadenosine on human T cells. *Oncoimmunology*, 5(8):e1184802.

Herbik, A. (1997). *Proteinchemische und molecular biologische charakterisierung der Tomaten mutante chloronerva*. PhD thesis, Humboldt Unversity, Berlin, Germany.

Hernando, C. E., Sanchez, S. E., Mancini, E., and Yanovsky, M. J. (2015). Genome wide comparative analysis of the effects of prmt5 and prmt4/carm1 arginine methyltransferases on the *Arabidopsis thaliana* transcriptome. *BMC Genomics*, 16(1).

Hibasami, H., Borchardt, R., Chen, S., Coward, J., and Pegg, A. (1980). Studies of inhibition of rat spermidine synthase and spermine synthase. *Biochemical Journal*, 187:419–428.

Higuchi, K., Suzuki, K., Nakanishi, H., Yamaguchi, H., Nishizawa, N.-K., and Mori, S. (1999). Cloning of nicotianamine synthase genes, novel genes involved in the biosynthesis of phytosiderophores. *Plant Physiology*, 119(2):471–480.

Hildebrandt, T., Nesi, A., Araújo, W., and Braun, H.-P. (2015). Amino acid catabolism in plants. *Molecular Plant*, 8(11):1563–1579.

Hsu, J. M., Chen, C. T., Chou, C. K., Kuo, H. P., Li, L. Y., Lin, C. Y., Lee, H. J., Wang, Y. N., Liu, M., Liao, H. W., Shi, B., Lai, C. C., Bedford, M. T., Tsai, C. H., and Hung, M. C. (2011). Crosstalk between Arg 1175 methylation and Tyr 1173 phosphorylation negatively modulates EGFR-mediated ERK activation. *Nature Cell Biology*, 13:174–181.

Hura, T., Dziurka, M., Hura, K., Ostrowska, A., and Dziurka, K. (2015). Free and cell wall-bound polyamines under long-term water stress applied at different growth stages of $\times$*Triticosecale Wittm*. *PLOS ONE*, 10(8):e0135002.

Hyodo, H. and Tanaka, K. (1986). Inhibition of 1-aminocyclopropane-1-carboxylic acid synthase activity by polyamines, their related compounds and metabolites of *s*-adenosylmethionine. *Plant and Cell Physiology*, 27:391–398.

Icekson, I., Bakhanashvili, M., and Apelbaum, A. (1986). Inhibition by ethylene of polyamine biosynthetic enzymes enhanced lysine decarboxylase activity and cadaverine accumulation in pea seedlings. *Plant Physiology*, 82:607–609.

Igarashi, K. and Kashiwagi, K. (2006). Polyamine modulon in *Escherichia coli*: genes involved in the stimulation of cell growth by polyamines. *Journal of Biochemistry*, 139:11–16.

Igarashi, K. and Kashiwagi, K. (2010). Modulation of cellular function by polyamines. *The International Journal of Biochemistry & Cell Biology*, 42:39–51.

Imai, A., Hanzawa, Y., Komura, M., Yamamoto, K., Komeda, Y., and Takahashi, T. (2006). The dwarf phenotype of the Arabidopsis *acl5* mutant is suppressed by a mutation in an upstream ORF of a bHLH gene. *Development*, 133(18):3575–3595.

Imai, A., Matsuyama, T., Hanzawa, Y., Akiyama, T., Tamaoki, M., Saji, H., Shirano, Y., Kato, T., Hayashi, H., Shibata, D., Tabata, S., Komeda, Y., and Takahashi, T. (2004).

Spermidine synthase genes are essential for survival of Arabidopsis. *Plant Physiology*, 135(3):1565–1573.

Ishida, M., Hara, M., Fukino, N., Kakizaki, T., and Morimitsu, Y. (2014). Glucosinolate metabolism, functionality and breeding for the improvement of Brassicaceae vegetables. *Breeding Science*, 64(1):48–59.

Jacob, C., Giles, G., Giles, N., and Sies, H. (2003). Sulfur and selenium: the role of oxidation state in protein structure and function. *Angewandte Chemie International Edition*, 42(39):4742–4758.

James, G., Patel, V., Nordström, K., Klasen, J., Salomé, R., Weigel, D., and Schneeberger, K. (2013). User guide for mapping-by-sequencing in *Arabidopsis*. *Genome Biology*, 14:R61.

Katz, E., Nisani, S., Yadav, B., Woldemariam, M., Shai, B., Obolski, U., Ehrlich, M., Shani, E., Jander, G., and Chamovitz, D. (2015). The glucosinolate breakdown product indole-3-carbinol acts as auxin antagonist in roots of *Arabidopsis thaliana*. *The Plant Journal*, 82(4):547–555.

Kemper, W., Berry, K., and Merrick, W. (1976). Purification and properties of rabbit reticulocyte protein synthesis initiation factors M2Balpha and M2Bbeta. *The Journal of Biological*, 251:5551–5557.

Klatte, M., Schuler, M., Wirtz, M., Fink-Straube, C., Hell, R., and Bauer, P. (2009). The analysis of Arabidopsis nicotianamine synthase mutants reveals functions for nicotianamine in seed iron loading and iron deficiency responses. *Plant Physiology*, 150(1):257–271.

Kooke, R. and Keurentjes, J. (2011). Multi-dimensional regulation of metabolic networks sharing plant development and performance. *Journal of Experimental Botany*, 63(9):3353–3365.

Koornneef, M. and Meinke, D. (2010). The development of Arabidopsis as a model plant. *The Plant Journal*, 61:909–921.

Kopriva, S. (2006). Regulation of sulfate assimilation in *Arabidopsis* and beyond. *Annals of Botany*, 97(4):479–495.

Kotova, L., Kotov, A., and Kara, A. (2004). Changes in phytohormone status in stems and roots after decapitation of pea seedlings. *Russian Journal of Plant Physiology*, 51(1):107–111.

Kriventseva, E., Kuznetsov, D., Tegenfeldt, F., Manni, M., Dias, R., ao, F. S., and Zdobnov, E. (2018). OrthoDB v10: sampling the diversity of animal, plant, fungal, protist, bacterial and viral genomes for evolutionary and functional annotations of orthologs. *Nucleic Acids Research*, page gky1053.

Krueger, F. (2012). *Trim Galore! Software, Version 0.4.5*. Babraham Institute.

Kryukov, G. V., Wilson, F. H., Ruth, J. R., Paulk, J., Tsherniak, A., Marlow, S. E., Vazquez, F., Weir, B. A., Fitzgerald, M. E., Tanaka, M., Bielski, C., Scott, J., Dennis, C., Cowley, G., Boehm, J., Root, D., Golub, T., Clish, C., Bradner, J., Hahn, W., and Garraway, L. (2016). Mtap deletion confers enhanced dependency on the PRMT5 arginine methyltransferase in cancer cells. *Science*, 351(6278):1214–1218.

Kubota, M., Kajander, E., and Carson, D. (1985). Independent regulation of ornithine decarboxylase and *s*-adenosylmethionine decarboxylase in methylthioadenosine phosphorylase-deficient malignant murine lymphoblasts. *Cancer Research*, 45:3567–3572.

Kurihara, Y., Matsui, A., Kawashima, M., Kaminuma, E., Ishida, J., Morosawa, T., Mochizuki, Y., Kobayashi, N., Toyoda, T., Shinozaki, K., and Seki, M. (2008). Identification of candidate genes regulated by RNA-directed DNA methylation in *Arabidopsis*. *Biochemical and Biophysical Research Communications*, 376(3):553–557.

Lamesch, P., Berardini, T. Z., Li, D., Swarbreck, D., Wilks, C., Sasidharan, R., Muller, R., Dreher, K., Alexander, D. L., Garcia-Hernandez, M., Karthikeyan, A., Lee, C., Nelson, W., Ploetz, L., Singh, S., Wensel, A., and Huala, E. (2012). The Arabidopsis Information Resource (TAIR): improved gene annotation and new tools. *Nucleic Acids Research*, 40(D1):D1202–D1210.

Lämke, J. and Bäurle, I. (2017). Epigenetic and chromatin-based mechanisms in environmental stress adaption and stress memory in plants. *Genome Biology*, 18:124.

Langfelder, P. and Horvath, S. (2008). Wgcna: an R package for weighted correlation network analysis. *BMC Bioinformatics*, 9(1):559.

Langfelder, P. and Horvath, S. (2012). Fast R functions for robust correlations and hierarchical clustering. *Journal of Statistical Software*, 46(11).

Leyser, O. (2003). Regulation of shoot branching by auxin. *Trends in Plant Science*, 8:541–545.

Li, C., Yu, N., Jiang, S., Shangguan, X., Wang, L., and Chen, X. (2008). Down-regulation of *S*-adenosyl-*l*-homocysteine hydrolase reveals a role of cytokinin in promoting transmethylation reactions. *Planta*, 228(1):125–136.

Li, G., Zhu, C., Gan, L., Ng, D., and Xia, K. (2015). GA_3 enhances root responsiveness to exogenous IAA by modulating auxin transport and signalling in Arabidopsis. *Plant Cell Reports*, 34(3):483–494.

Li, H. and Durbin, R. (2009). Fast and accurate short read alignment with Burrows-Wheeler transform. *Bioinformatics*, 25(14):1754–1760.

Li, H., Handsaker, B., Wysoker, A., Fennell, T., Ruan, J., Homer, N., Marth, G., Abecasis, G., Durbin, R., and Subgroup, . G. P. D. P. (2009). The sequence alignment/map format and samtools. *Bioinformatics (Oxford, England)*, 25(16):2078–2079.

Li, Q., Zhao, Y., Yue, M., Xue, Y., and Bao, S. (2016a). The protein arginine methylase 5 (PRMT5/SKB1) gene is required for the maintenance of root stem cells in response to DNA damage. *Journal of Genetics and Genomics*, 43(4):187–197.

Li, S., Yamada, M., Han, X., Ohler, U., and Benfey, P. (2016b). High-resolution expression map of *Arabidopsis* root reveals alternative splicing and lincRNA regulation. *Developmental Cell*, 39:508–522.

Li, X. and Zhang, Y. (2016). Suppressor screens in Arabidopsis. *Methods in Molecular Biology*, 1363:1–8.

Lindsey, B., Rivero, L., Calhoun, C., Grotewold, E., and Brkljacic, J. (2017). Standardized method for high-throughput sterilization of Arabidopsis seeds. *Journal of Visualized Experiments*, 128:e56587.

Lister, R., O'Malley, R. C., Tonti-Filippini, J., Gregory, B. D., Berry, C. C., Millar, A. H., and Ecker, J. R. (2008). Highly integrated single-base resolution maps of the epigenome in Arabidopsis. *Cell*, 133(3):523–536.

Liu, H., Ma, X., Han, H., Hao, Y., and Zhang, X. (2016). AtPRMT5 regulates shoot regeneration through mediating histone H4R3 dimethylation on KRPs and pre-mRNA splicing of RKP in Arabidopsis. *Molecular Plant*, 9(12):1634–1646.

Liu, L., Ren, H., Chen, L., Wang, Y., and Wu, W. (2013). A protein kinase, calcineurin B-like protein-interacting protein Kinase9, interacts with calcium sensor calcineurin B-like Protein3 and regulates potassium homeostasis under low-potassium stress in Arabidopsis. *Plant Physiology*, 161(1):266–277.

Lun, A. T. L., Chen, Y., and Smyth, G. K. (2016). *It's DE-licious: A Recipe for Differential Expression Analyses of RNA-seq Experiments Using Quasi-Likelihood Methods in edgeR*, volume 1418, page 391–416. Springer New York.

Madeo, F., Eisenberg, T., Pietrocola, F., and Kroemer, G. (2018). Spermidine in health and disease. *Science*, 359(6374):eaan2788.

Malka, S. and Cheng, Y. (2017). Possible interaction between the biosynthetic pathways of indole glucosinolate and auxin. *Frontiers in Plant Science*, 8:2131.

Mangano, S., Juárez, S., and Estevez, J. (2016). ROS regulation of polar growth in plant cells. *Plant Physiology*, 171(3):1593–1605.

Marjon, K., Cameron, M. J., Quang, P., Clasquin, M. F., Mandley, E., Kunii, K., McVay, M., Choe, S., Kernytsky, A., Gross, S., Konteatis, Z., Murtie, J., Blake, M., Travins, J., Dorsch, M., Biller, S., and Marks, K. (2016). MTAP deletions in cancer create vulnerability to targeting of the MAT2A/PRMT5/RIOK1 axis. *Cell Reports*, 15(3):574–587.

Mavrakis, K. J., McDonald, E. R., Schlabach, M. R., Billy, E., Hoffman, G. R., deWeck, A., Ruddy, D. A., Venkatesan, K., Yu, J., McAllister, G., Stump, M., deBeaumont, R., Ho, S., Yue, Y., Liu, Y., Yan-Neale, Y., Yang, G., Lin, F., Yin, H., Gao, H., Kipp, D., Zhao, S., McNamara, J., Sprague, E., Zheng, B., Lin, Y., Cho, Y., Gu, J., Crawford, K., Ciccone, D., Vitari, A., Lai, A., Capka, V., Hurov, K., Porter, J., Tallarico, J., Lees, C. M. E., Pagliarini, R., Keen, N., Schmelzle, T., Hofmann, F., Stegmeier, F., and Sellers,

W. (2016). Disordered methionine metabolism in MTAP/CDKN2A-deleted cancers leads to dependence on PRMT5. *Science*, 351(6278):1208–1213.

McKenna, A., Hanna, M., Banks, E., Sivachenko, A., Cibulskis, K., Kernytsky, A., Garimella, K., Altshuler, D., Gabriel, S., Daly, M., and DePristo, M. (2010). The Genome Analysis Toolkit: a MapReduce framework for analyzing next-generation dna sequencing data. *Genome Research*, 20(9):1297–1303.

Meinke, D., Cherry, J., Dean, C., Rounsley, S., and Koornneef, M. (1998). *Arabidopsis thaliana*: a model plant for genome analysis. *Science*, 282(5389):662–682.

Miller-Fleming, L., Olin-Sandoval, V., Campbell, K., and Ralser, M. (2015). Remaining mysteries of molecular biology: the role of polyamines in the cell. *Journal of Molecular Biology*, 427(21):3389–3406.

Miyazaki, J. and Yang, S. (1987). The methionine salvage pathway in relation to ethylene and polyamine biosynthesis. *Physiologia Plantarum*, 69:366–370.

Mizuno, D., Higuchi, K., Sakamoto, T., Nakanishi, H., Mori, S., and Nishizawa, N. (2003). Three nicotianamine synthase genes isolated from maize are differentially regulated by iron nutritional status. *Plant Physiology*, 132(4):1989–1997.

Moschou, P. and Roubelakis-Angelakis, K. (2013). Polyamines and programmed cell death. *Journal of Experimental Botany*, 65(5):1285–1296.

Murashige, T. and Skoog, F. (1962). A revised medium for rapid growth and bio assays with tobacco tissue cultures. *Physiologia Plantarum*, 15(3):473–497.

Murray, J., Jones, A., Godin, C., and Traas, J. (2012). Systems analysis of shoot apical

meristem growth and development: integrating hormonal and mechanical signaling. *The Plant Cell*, 24(10):3907–3919.

Nikiforova, V., Kopka, J., Tolstikov, V., Fiehn, O., Hopkins, L., Hawkesford, M., Hesse, H., and Hoefgen, R. (2005). Systems rebalancing of metabolism in response to sulfur deprivation, as revealed by metabolome analysis of Arabidopsis plants. *Plant Physiology*, 138(1):304–318.

Norman, J. V. and Benfey, P. (2009). *Arabidopsis thaliana* as a model organism in systems biology. *Wiley Interdisciplinary Reviews: Systems Biology and Medicine*, 1(3):372–379.

Odenlund, M., Holmqvist, B., Baldetorp, B., Hellstrand, P., and Nilsson, B.-O. (2009). Polyamine synthesis inhibition induces S phase cell cycle arrest in vascular smooth muscle cells. *Amino Acids*, 36:273–282.

Oh, S.-I., Park, J., Yoon, S., Kim, Y., Park, S., Ryu, M., Nam, M. J., Ok, S. H., Kim, J.-K., Shin, J.-S., and et al. (2008). The Arabidopsis calcium sensor calcineurin B-like 3 inhibits the 5′-methylthioadenosine nucleosidase in a calcium-dependent manner. *Plant Physiology*, 148(4):1883–1896.

Ok, S. H., Cho, J. H., Oh, S.-I., Choi, M. N., Ma, J.-Y., Shin, J.-S., and Kim, K.-N. (2015). Calcineurin B-like 3 calcium sensor associates with and inhibits 5′-methylthioadenosine nucleosidase 2 in Arabidopsis. *Plant Science*, 238:228–240.

Oram, S., Ai, J., Pagani, G., Hitchens, M., Stern, J., Eggener, S., Pins, M., Xiao, W., Cai, X., Haleem, R., Jiang, F., Pochapsky, T., Hedstrom, L., and Wang, Z. (2007). Expression and function of the human androgen-responsive *ADI1* in prostate cancer. *Neoplasia*, 9:643–651.

Ouyang, B., Fei, Z., Joung, J., Kolenovsky, A., Koh, C., Nowak, J., Caplan, A., Keller, W., Cui, Y., Cutler, A., and Tsang, E. (2012). Transcriptome profiling and methyl homeostasis of an Arabidopsis mutant deficient in *s*-adenosylhomocysteine hydrolase1 (SAHH1). *Plant Molecular Biology*, 79(4–5):315–331.

Pandey, G., Kanwar, P., Singh, A., Steinhorst, L., Pandey, A., Yadav, A., Tokas, I., Sanyal, S., Kim, B., Lee, S., Cheong, Y., Kudla, J., and Luan, S. (2015). Calcineurin B-like protein-interacting kinase CIPK21 regulates osmotic and salt stress responses in Arabidopsis. *Plant Physiology*, 169(1):780–792.

Pandey, S., Ranade, S., Nagar, P., and Kumar, N. (2000). Role of polyamines and ethylene as modulators of plant senescence. *Journal of Biosciences*, 25:291–299.

Parikshak, N., Gandal, M., and Geschwind, D. (2015). Systems biology and gene networks in neurodevelopmental and neurodegenerative disorders. *Nature Reviews Genetics*, 16(8):441–458.

Park, M., Lee, Y., and Joe, Y. (1997). Hypusine is essential for eukaryotic cell proliferation. *Neurosignals*, 6:115–123.

Park, S. and Imlay, J. (2003). High levels of intracellular cysteine promote oxidative DNA damage by driving the Fenton reaction. *Journal of Bacteriology*, 185(6):1942–1950.

Park, S., Kong, H., Kim, Y., Lee, Y., and Park, J. (2015). Inhibition of *s*-adenosylhomocysteine hydrolase decreases cell mobility and cell proliferation through cell cycle arrest. *American Journal of Cancer Research*, 5(7):2127–2138.

Pegg, A. (2009). Mammalian polyamine metabolism and function. *IUBMB Life*, 61(9):880–894.

Pegg, A., Borchardt, R., and Coward, J. (1981). Effects of inhibitors of spermidine and spermine synthesis on polyamine concentrations and growth of transformed mouse fibroblasts. *Biochemical Journal*, 194(1):79–89.

Pegg, A. and McCann, P. (1982). Polyamine metabolism and function. *American Journal of Physiology – Cell Physiology*, 243(5):C212–C221.

Pegg, A., Xiong, H., Feith, D., and Shantz, L. (1998). *s*-Adenosylemethionine decarboxylase: structure, function and regulation by polyamines. *Biochemical Society Transactions*, 26(4):580–586.

Perera, A. (2018). Exploring the effect of spermidine on early vascular and reproductive development in methylthioadenosine nucleosidase deficient plant embryos. Master's thesis, University of Waterloo, Waterloo, Canada.

Perera, N., Yeung, E., and Moffatt, B. Cross sections of arabidopsis *mtn1-1mtn2-1* developing pollen. Unpublished.

Pertea, M., Pertea, G. M., Antonescu, C. M., Chang, T.-C., Mendell, J. T., and Salzberg, S. L. (2015). Stringtie enables improved reconstruction of a transcriptome from RNA-seq reads. *Nature Biotechnology*, 33(3):290–295.

Petersson, S., Lindén, P., Moritz, T., and Ljung, K. (2015). Cell-type specific metabolic profiling of *Arabidopsis thaliana* protoplasts as a tool for plant systems biology. *Metabolomics*, 11(6):1679–1689.

Pfeiffer, A., Janocha, D., Dong, Y., Medzihradszky, A., Schöne, S., Daum, G., Suzaki, T., Forner, J., Langenecker, T., Rempel, E., Schmid, M., Wirtz, M., Hell, R., and Lohmann, J. (2016). Integration of light and metabolic signals for stem cell activation at the shoot apical meristem. *eLife*, 5:e17023.

Pommerrenig, B., Feussner, K., Zierer, W., Rabinovych, V., Klebl, F., Feussner, I., and Sauer, N. (2011). Phloem-specific expression of Yang cycle gene and identification of novel Yang cycle enzymes in *Plantago* and *Arabidopsis*. *The Plant Cell*, 23(5):1904–1919.

Quan, J., Zhang, C., Zhang, S., Meng, S., Zhao, Z., and Xu, X. (2014). Molecular cloning and expression analysis of the MTN gene during adventitious root development in IBA-induced tetraploid black locust. *Gene*, 553(2):140–150.

R Core Team (2018). *R: A Language and Environment for Statistical Computing*. R Foundation for Statistical Computing, Vienna, Austria.

Raina, A., Hyvönen, T., Eloranta, T., Voutilainen, M., Samejima, K., and Yamanoha, B. (1984). Polyamine synthesis in mammalian tissues. isolation and characterization of spermidine synthase from bovine brain. *Biochemical Journal*, 219:991–1000.

Ranocha, P., McNeil, S., Ziemak, M., Li, C., Tarczynski, M., and Hanson, A. (2000). The *s*-methylmethionine cycle in angiosperms: ubiquity, antiquity and activity. *The Plant Journal*, 25(5):575–584.

Ravanel, S., Gakiére, B., Job, D., and Douce, R. (1998). The specific features of methionine biosynthesis and metabolism in plants. *Proceedings of the National Academy of Sciences of the United States of America*, 95:7805–7812.

Ray, R., Zimmerman, B., McCormack, S., Patel, T., and Johnson, L. (1999). Polyamine deletion arrests cell cycle and induces inhibitors p21 (Waf/Cip1), p27 (Kip1), and p53 in IEC-6 cells. *American Journal of Physiology*, 276:C684–C691.

Ren, B., Chen, Q., Hong, S., Zhao, W., Feng, J., Feng, H., and Zuo, J. (2013). The Arabidopsis eukaryotic translation initiation factor eIF5A-2 regulates root protoxylem development by modulating cytokinin signaling. *Plant Cell*, 25(10):3841–3857.

Ren, J., Wang, Y., Liang, Y., Zhang, Y., Bao, S., and Xu, Z. (2010). Methylation of ribosomal protein S10 by protein-arginine methyltransferase 5 regulates ribosomal biogenesis. *The Journal of Biological*, 285:12695–12705.

Rider, J., Hacker, A., Mackintosh, C., Pegg, A., Woster, P., and Casero, R. (2007). Spermine and spermidine mediate protection against oxidative damage caused by hydrogen peroxide. *Amino Acids*, 33:231–240.

Robinson, M. D., McCarthy, D. J., and Smyth, G. K. (2010). edgeR: a Bioconductor package for differential expression analysis of digital gene expression data. *Bioinformatics*, 26(1):139–140.

Rothberg, J., Hinz, W., Rearick, T., Schultz, J., Mileski, W., Davey, M., Leamon, J., Johnson, K., Milgrew, M., Edwards, M., Hoon, J., Simons, J., Marran, D., Myers, J., Davidson, J., Branting, A., Nobile, J., Puc, B., Light, D., Clark, T., Huber, M., Branciforte, J., Stoner, I., Cawley, S., Lyons, M., Fu, Y., Homer, N., Sedova, M., Miao, X., Reed, B., Sabina, J., Feierstein, E., Schorn, M., Alanjary, M., Dimalanta, E., Dressman, D., Kasinskas, R., Sokolsky, T., Fidanza, J., Namsaraev, E., McKernan, K., Williams, A., Roth, G., and Bustillo, J. (2011). An integrated semiconductor device enabling non-optical genome sequencing. *Nature*, 475:348–352.

Rzewuski, G., Cornell, K. A., Rooney, L., Bürstenbinder, K., Wirtz, M., Hell, R., and Sauter, M. (2007). OsMTN encodes a 5′-methylthioadenosine nucleosidase that is up-regulated during submergence-induced ethylene synthesis in rice (*Oryza sativa* L.). *Journal of Experimental Botany*, 58(6):1505–1514.

Saechao, M., Richard, D., and Moffatt, B. RNAseq experiment of 14 day-old seedlings

WT, *mtn1-1mtn2-1*, and *mtn1-1mtn2-5* Arabidopsis plants with and without 100 μM spermidine treatment. Unpublished.

Saini, P., Eyler, D., Green, R., and Dever, T. (2009). Hypusine-containing protein eIF5A promotes translation elongation. *Nature*, 459:118–121.

Samartzidou, H., Mehrazin, M., Xu, Z., Benedik, M., and Delcour, A. (2003). Cadaverine inhibition of porin plays a role in cell survival at acidic pH. *Journal of Bacteriology*, 185:13–19.

Sanders, P., Bui, A., Weterings, K., McIntire, K., Hsu, Y.-C., Lee, P., Truong, M., Beals, T., and Goldberg, R. (1999). Anther development defects in *Arabidopsis thaliana* male-sterile mutants. *Plant Reproduction*, 11:297–322.

Sauter, M., Moffatt, B., Saechao, M., Hell, R., and Wirtz, M. (2013). Methionine salvage and *s*-adenosylmethionine: essential links between sulfur, ethylene and polyamine biosynthesis. *Biochemical Journal*, 451:145–154.

Sava, I., Battaglia, V., Rossi, C., Salvi, M., and Toninello, A. (2006). Free radical scavenging action of the natural polyamine spermine in rat liver mitochondria. *Free Radical Biology & Medicine*, 41:1272–1281.

Schmid, M., Sen, M., Rosenbach, M., Cerrera, C., Friedman, H., and Carson, D. (2000). A methylthioadenosine phosphorylase (MTAP) fusion transcript identifies a new gene on chromosome 9p21 that is frequently deleted in caner. *Oncogene*, 19:5747–5754.

Schreier, M., Erni, B., and Staehelin, T. (1977). Initiation of mammalian protein synthesis. i. purification and characterization of seven initiation factors. *Journal of Molecular Biology*, 116:727–753.

Schuller, A., Wu, C.-C., Dever, T., Buskirk, A., and Green, R. (2017). eIF5A functions globally in translation elongation and termination. *Molecular Cell*, 66(2):194–205.

Schwarzländer, M., Fricker, M., Müller, C., Marty, L., Brach, T., Novak, J., Sweetlove, L., Hell, R., and Meyer, A. (2008). Confocal imaging of glutathione redox potential in living plant cells. *Journal of Microscopy*, 231(2):299–316.

Seidenfeld, J., Wilson, J., and Williams-Ashman, H. (1980). Androgenic regulation of 5′-deoxy-5′-methylthioadenosine concentrations and methylthioadenosine phosphorylase activity in relation to polyamine metabolism in rat prostate. *Biochemical and Biophysical Research Communications*, 95(4):1861–1868.

Sekowska, A., Kung, H., and Danchin, A. (2000a). Sulfur metabolism in *Escherichia coli* and related bacteria: facts and fiction. *Journal of Molecular Microbiology and Biotechnology*, 2(2):145–177.

Sekowska, A., Robin, S., Daudin, J., Henaut, A., and Danchin, A. (2000b). Extracting biological information from DNA arrays: an unexpected link between arginine and methionine metabolism in *Bascillus subtilis*. *Genome Biology*, 2(6):RESEARCH0019.1–RESEARCH0019.12.

Shi, Z.-H., Zhang, C., Xu, X.-F., Zhu, J., Zhou, Q., Ma, L.-J., Niu, J., and Yang, Z.-N. (2015). Overexpression of *AtTTP* affects *ARF17* expression and leads to male sterility in Arabidopsis. *PLoS ONE*, 10(3):e0117317.

Sievers, F. and Higgins, D. (2018). Clustal Omega for making accurate alignments of many protein sequences. *Protein Science*, 27(1):135–145.

Siu, K., Asmus, K., Zhang, A., Horvatin, C., Li, S., Liu, T., Moffatt, B., Woods, Jr., V.,

and Howell, P. (2011). Mechanism of substrate specificity in 5′-methylthioadenosine/*s*-adenosylhomocysteine nucleosidases. *Journal of Structural Biology*, 173(1):86–98.

Smyth, D., Bowman, J., and Meyerowitz, E. (1990). Early flower development in *Arabidopsis*. *The Plant Cell*, 2(8):755–767.

Sprenger, J., Carey, J., Svensson, B., Wengel, V., and Persson, L. (2016). Binding and inhibition of spermidine synthase from *Plasmodium falciparum* and implications for *in vitro* inhibitor testing. *PLoS ONE*, 11(9):e0163442.

Su, Y.-H., Liu, Y.-B., and Zhang, X.-S. (2011). Auxin-cytokinin interaction regulates meristem development. *Molecular Plant*, 4(4):616–625.

Subhi, A., Diegelman, P., Porter, C., Tang, B., Lu, Z., Markham, G., and Kruger, W. (2003). Methylthioadenosine phosphorylase regulates ornithine decarboxylase by production of downstream metabolites. *Biological Chemistry*, 278:49868–49873.

Sunkara, P., Chang, C., and Lachman, P. (1985). Cell proliferation and cell cycle dependent changes in the methylthioadenosine phosphorylase activity in mammalian cells. *Biochemical and Biophysical Research Communications*, 127(2):546–551.

Tang, B., Kadariya, Y., Murphy, M., and Kruger, W. (2006). The methionine salvage pathway compound 4-methylthio-2-oxobutanate causes apoptosis independent of down-regulation of ornithine decarboxylase. *Biochemical Pharmacology*, 72(7):806–815.

Tang, B., Lee, H., An, S., Cai, K., and Kruger, W. (2018). Specific targeting of MTAP-deleted tumors with a combination of 2′-fluoroadenine and 5′-methylthioadenosine. *Cancer Research*, 78(15):4386–4395.

Tang, R., Zhao, F., Garcia, V., Kleist, T., Yang, L., Zhang, H., and Luan, S. (2015). Tonoplast CBL-CIPK calcium signaling network regulates magnesium homeostasis in Arabidopsis. *Proceedings of the National Academy of Sciences of the United States of America*, 112(10):3134–3139.

Tatematsu, K., Ward, S., Leyser, O., Kamiya, Y., and Nambara, E. (2005). Identification of cis-elements that regulate gene expression during initiation of axillary bud outgrowth in Arabidopsis. *Plant Physiology*, 138(2):757–766.

Terui, Y., Higashi, K., Taniguchi, S., Shigemasa, A., Nishimura, K., Yamamoto, K., , Kashiwagi, K., Ishihama, A., and Igarashi, K. (2007). Enhancement of the synthesis of RpoN, Cra, and H-NS by polyamines at the level of translation in *Escherichia coli* cultured with glucose and glutamate. *Journal of Bacteriology*, 189(6):2359–2368.

Tesseraud, S., Coustard, S., Collin, A., and Seiliez, I. (2009). Role of sulfur amino acids in controlling nutrient metabolism and cell functions: implications for nutrition. *British Journal of Nutrition*, 101(8):1132–1139.

The Gene Ontology Consortium, M. A., Ball, C., Blake, J., Botstein, D., Butler, H., Cherry, J., Davis, A., Dolinski, K., Dwight, S., Eppig, J., Harris, M., Hill, D., Issel-Tarver, L., Kasarskis, A., Lewis, S., Matese, J., Richardson, J., Ringwald, M., Rubin, G., and Sherlock, G. (2000). Gene Ontology: tool for the unification of biology. *Nature Genetics*, 25(1):25–29.

Thomas, D. and Surdin-Kerjan, Y. (1997). Metabolism of sulfur amino acids in *Saccharomyces cerevisiae*. *Microbiology and Molecular Biology Reviews*, 61(4):503–532.

Tiburcio, A., Altabella, T., Bitrián, M., and Alcázar, R. (2014). The roles of polyamines during the lifespan of plants: from development to stress. *Planta*, 240(1):1–14.

Tisdale, M. (1983). Methionine synthesis from 5′-methylthioadenosine by tumour cells. *Biochemical Pharmacology*, 32(19):2915–2920.

To, T. K., Saze, H., and Kakutani, T. (2015). DNA methylation within transcribed regions. *Plant Physiology*, 168(4):1219–1225.

Ubeda-Tomás, S., Federici, F., Casimiro, I., Beemster, G., Bhalerao, R., Swarup, R., Doerner, P., Haseloff, J., and Bennett, M. (2009). Gibberellin signaling in the endodermis controls *Arabidopsis* root meristem size. *Current Biology*, 19(14):1194–1199.

Waduwara-Jayabahu, C. I. (2011). *Significance of Methylthioadenosine Metabolism to Plant Growth and Development*. PhD thesis, University of Waterloo.

Waduwara-Jayabahu, I., Oppermann, Y., Wirtz, M., Hull, Z. T., Schoor, S., Plotnikov, A. N., Hell, R., Sauter, M., and Moffatt, B. A. (2012). Recycling of methylthioadenosine is essential for normal vascular development and reproduction in Arabidopsis. *Plant Physiology*, 158(4):1728–1744.

Wang, T., Lu, L., Wang, D., and Thompson, J. (2001). Isolation and characterization of senescence-induced cDNAs encoding deoxyhypusine synthase and eukaryotic translation initiation factor 5A from tomato. *The Journal of Biological*, 276(20):17541–17549.

Wang, X., Zhang, Y., Ma, Q., Zhang, Z., Xue, Y., Bao, S., and Chong, K. (2007). SKB1-mediated symmetric dimethylation of histone H4R3 controls flowering time in Arabidopsis. *The EMBO Journal*, 26(7):1934–1941.

Wang, Z., Gerstein, M., and Snyder, M. (2009). RNA-Seq: a revolutionary tool for transcriptomics. *Nature Reviews Genetics*, 10(1):57–63.

Washington, E., Mukhtar, M., Finkel, O., Wan, L., Banfield, M., Kieber, J., and Dangl, J. (2016). *Pseudomonas syringae* type III effector HopAF1 suppresses plant immunity by targeting methionine recycling to block ethylene induction. *Proceedings of the National Academy of Sciences of the United States of America*, 113(25):E3577–E3586.

Watson, N., Dunyak, D., Rosey, E., Slonczewski, J., and Olson, E. (1992). Identification of elements involved in transcriptional regulation of the *Escherichia coli* cad operon by external pH. *Journal of Bacteriology*, 174:530–540.

Winter, D., Vinegar, B., Nahal, H., Ammar, R., Wilson, G., and Provart, N. (2007). An "Electronic Fluorescent Pictograph" browser for exploring and analyzing large-scale biological data sets. *PLoS ONE*, 2(8):e718.

Wirtz, M., Droux, M., and Hell, R. (2004). O-acetylserine (thiol) lyase: an enigmatic enzyme of plant cysteine biosynthesis revisited in *Arabidopsis thaliana*. *Journal of Experimental Botany*, 55(404):1785–1798.

Wirtz, M. and Hell, R. (2007). Dominant-negative modification reveals the regulatory function of the multimeric cysteine synthase protein complex in transgenic tobacco. *THE PLANT CELL ONLINE*, 19(2):625–639.

Wittstock, U., Meier, K., Dörr, F., and Ravindran, B. (2016). NSP-dependent simple nitrile formation dominates upon breakdown of major aliphatic glucosinolates in roots, seeds, and seedlings of *Arabidopsis thaliana* Columbia-0. *Frontiers in Plant Science*, 7(1821).

Womack, M. and Rose, W. (1941). The partial replacement of dietary methionine by cystine for purposes of growth. *The Journal of Biological*, 141:375–379.

Wu, J., Wang, C., Zheng, L., Wang, L., Chen, Y., Whelan, J., and Shou, H. (2011). Ethylene

is involved in the regulation of iron homeostasis by regulating the expression of iron-acquisition-related genes in *Oryza sativa*. *Journal of Experimental Botany*, 62(2):667–674.

Xie, Q.-W., Tabor, C., and Tabor, H. (1993). Deletion mutation in the *speED* operon: spermidine is not essential for the growth of *Escherichia coli*. *Gene*, 126:115–117.

Yamaguchi, K., Takahashi, Y., Berberich, T., Imai, A., Miyazaki, A., Takahashi, T., Michael, A., and Kusano, T. (2006). The polyamine spermine protects against high salt stress in *Arabidopsis thaliana*. *FEBS Letters*, 580(30):6783–6788.

Yan, J., Niu, F., Liu, W., Zhang, H., Wang, B., Lan, W., Che, Y., Yang, B., Luan, S., and Jiang, Y. (2014). Arabidopsis CIPK14 positively regulates glucose response. *Biochemical and Biophysical Research Communications*, 450(4):1679–1683.

Yi, J., Moon, S., Lee, Y.-S., Zhu, L., Liang, W., Zhang, D., Jung, K.-H., and An, G. (2016). Defective Tapetum Cell Death 1 (DTC1) regulates ROS levels by binding to metallothionein during tapetum degeneration. *Plant Physiology*, 170:1611–1623.

Yoshida, M., Kashiwagi, K., Kawai, G., Ashihama, A., and Igarashi, K. (2001). Polyamine enhancement of the synthesis of adenylate cyclase at the translational level and the consequential stimulation of the synthesis of the RNA polymerase ω28 subunit. *The Journal of Biological*, 276:16289–16295.

Yoshida, M., Kashiwagi, K., Kawai, G., Ishihama, A., and Igarashi, K. (2002). Polyamines enhance synthesis of the RNA polymerase ω38 subunit by suppression of an amber termination codon in the open reading frame. *The Journal of Biological*, 277:37139–37146.

Yoshida, M., Meksuriyen, D., Kashiwagi, K., Kawai, G., and Igarashi, K. (1999). Polyamine stimulation of the synthesis of oligopeptide-binding protein (OppA). involvement of a

structural change of the Shine-Dalgarno sequence and the initiation codon aug in OppA mRNA. *The Journal of Biological*, 274:22723–22728.

You, Y., Sawikowska, A., Neumann, M., Posé, D., Capovilla, G., Langenecker, T., Neher, R., Krajewski, P., and Schmid, M. (2017). Temporal dynamics of gene expression and histone marks at the *Arabidopsis* shoot meristem during flowering. *Nature Communications*, 8:15120.

Yue, M., Li, Q., Zhang, Y., Zhao, Y., Zhang, Z., and Bao, S. (2013). Histone H4R3 methylation catalyzed by SKB1/PRMT5 is required for maintaining shoot apical meristem. *PLoS One*, 8(12):e83258.

Yueh, A. and Schneider, R. (1996). Selective translation initiation by ribosome jumping in adenovirus-infected and heat-shocked cells. *Genes & Development*, 10:1557–1567.

Zappia, V., Zydek-Cwick, C., and Schlenk, F. (1969). The specificity of *s*-adenosylmethionine derivatives in methyl transfer reactions. *The The Journal of Biological*, 244(16):4499–4509.

Zhang, H., Chen, Z., and Savarese, T. (1996). Codeletion of the genes for p16INK4, methylthioadenosine phosphorylase, interferon-α1, interferon-β1, and other 9p21 markers in human malignant cell lines. *Cancer Genetics and Cytogenetics*, 86(1):22–28.

Zhang, H., Tang, K., Wang, B., Duan, C.-G., Lang, Z., and Zhu, J.-K. (2014). Protocol: a beginner's guide to the analysis of RNA-directed DNA methylation in plants. *Plant Methods*, 10:18.

Zhang, W., Zhou, Y., Wang, K., Dong, Y., Wang, W., and Feng, Y. (2017). Crystral structure of a specifier protein from *Arabidopsis thaliana*. *Biochemical and Biophysical Research Communications*, 488(1):147–152.

Zhang, Z., Zhang, S., Zhang, Y., Wang, X., Li, D., Li, Q., Yue, M., Li, Q., Zhang, Y., Xu, Y., Xue, Y., Chong, K., and Bao, S. (2011). Arabidopsis floral initiator SKB1 confers high salt tolerance by regulating transcription and pre-mRNA splicing through altering histone H4R3 and small nuclear ribonucleoprotein LSM4 methylation. *Plant Cell*, 23(1):396–411.

Zhou, L., Fu, Y., and Yang, Z. (2009). A genome-wide functional characterization of *Arabidopsis* regulatory calcium sensors in pollen tubes. *Journal of Integrative Plant Biology*, 51(8):751–761.

Zhu, H., Wang, G., and Qian, J. (2016). Transcription factors as readers and effectors of dna methylation. *Nature Reviews Genetics*, 17(9):551–565.

Zierer, W., Hajirezaei, M., Eggert, K., Sauer, N., von Wirén, N., and Pommerrenig, B. (2016). Phloem-specific methionine recycling fuels polyamine biosynthesis in a sulfur-dependent manner and promotes flower and seed development. *Plant Physiology*, 170(2):790–806.

Zilberman, D. and Henikoff, S. (2007). Genome-wide analysis of DNA methylation patterns. *Development*, 134(22):3959–3965.